Mineral Sequestration for Permanent CO_2 Storage

by

Sanam Atashin

A thesis

presented to the University of Waterloo

in fulfillment of the

thesis requirement for the degree of

Doctor of Philosophy

in

Mechanical Engineering

Waterloo, Ontario, Canada, 2016

AUTHOR'S DECLARATION

I hereby declare that I am the sole author of this thesis. This is a true copy of the thesis, including any required final revisions, as accepted by my examiners.

I understand that my thesis may be made electronically available to the public.

Abstract

Mineral carbonation is one of the most appealing CO_2 emission mitigation techniques capable of storing CO_2, in the thermodynamically stable states. However, the technical mineralization process faces serious challenges, in regard to the reaction kinetics and issues with high energy intensity. Pre-activation techniques such as mechanical activation are proposed as effective strategies to enhance the kinetics of mineral carbonation processes. They however, significantly increase the total energy consumption of the processes and hence, optimizing the energy needed for pre-activation process is essential.

Mechanical activation technique was performed, using a Uni-Ball-Mill 5. The variation of determinant structural parameters such as particle size, specific surface area, pore volume, crystallite size and crystallinity was recorded as a function of injected milling energy input, using SEM, BET and XRD analysis techniques. Considering the outcomes of this research stage, the optimal level of pre-activation milling energy for the most suggested microstructure for CO_2 storage was found to be about 55 kJ/g.

Energy optimization and kinetics enhancement was then considered and expanded to the field of reactive compound extraction. Milling energy inputs of 0, 13.8, 27.6, 41.4 and 55.2 kJ/g were injected for the purpose of the reactants' pre-activation. Solid state extraction was performed under the isothermal conditions of 400, 425 and 450℃ in a combined DSC/TGA thermal analyzer device (NETZSCH STA 449F3A-0918-M Jupiter). The trend of activation energy variation vs. milling energy input was calculated and monitored to find the optimal amount of millling energy input needed to produce the structural properties with the lowest amount of activation energy for the solid state extraction process. The calculated amount of optimal milling energy input, to address the objective of this phase of study was found to be about 27.6 kJ/g. This resulted in an almost 34% reduction in the activation energy of $MgSO_4$ solid state extraction.

Complimentary to the goal of enhancing the kinetics and performance of the mineral carbonation process, the enhancement of directed anhydrous carbonation was examined as a next stage of research. Two different strategies were followed to address this objective, including the optimization and control of carbonation parameters (temperature and pressure), and the implimentation of heterogeneous precipitation, in order to promote the possibility of formation of anhydrous carbonation products during the aqueous carbonation of $Mg(OH)_2$ powders.

Carbonation reactions were performed in a 4650 Parr high-temperature high-pressure reaction vessel. Carbonation temperatures of 100, 150 and 200℃ and CO_2 pressure of 10, 20, 25 and 30 bars, were used. This stage of study confirmed the noticeable influence of carbonation temperature on the formation of anhydrous carbonates, and on the enhancement of directed carbonation. As a continution, the effects of the implimentation of preferred precipitation sites on the efficiency of directed carbonation process was figured out, by injecting two different seeding materials, in the aqueous medium. Hydrophobic activated carbon and hydrophilic alumina seeds were used to bring two different wettability properties. The combined controlling of carbonation parameters and implimentation of more efficient seeding material resulted in an improved carbonation conversion of up to 72%, with an anhydrous carbonate concentration of around 60%.

Acknowledgements

I would like to express my greatest appreciation to my co-supervisors, Prof. John Wen and Prof. Robert Varin for their incredible support, insightful advice and immense knowledge.

I sincerely acknowledge my committee members, Prof. Eric Croiset, Prof. Mustafa Yavuz and Prof. Xianguo Li for their thoughtful questions and precious comments, which encouraged me to widen my research from various perspectives. Many thanks to Prof. Charles Xu from University of Western Ontario, Canada, for his active participation in my Ph.D. committee.

I'm also thankful to Prof. Iskender Gokalp, from CNRS - National Centre for Scientific Research, France, and Dr. Jayaraman kandasamy from Veltech University, India, for their collaboration.

I would like to thank Mary Janet McPherson and Lauren LeSergent for their help with editing my manuscript and helping to develop my writing skills.

My deep gratitude goes to Jason Benninger, Martha Morales, Andy Barber, Andy Trudel and Greg Friday, for their technical support. I also acknowledge Carbon Management Canada and the Natural Sciences and Engineering Research Council of Canada, for the research funding.

I would like to extend my thanks to my incredible friends, my graduate research fellow in LEER group, Abhishek Raj, Florin Saceleanu, Hongtao Sui, John Rawlins, Dr. Jinhee Kang, Dr. Pei Zhang and Dr. Dong Zhu for their stimulating discussions, genuine friendship and scientific support. Special thanks for your understanding and support in the moments of crisis, and my gratitude for all the memorable moments you gave me.

Words are definitely inadequate in offering my thanks to my beloved mom, for her unconditional love, support and motivation. I'm also deeply thankful to my dad, for his ongoing care and support. My wholehearted thanks and love to my adorable sister and brother, Sabrine and Hossein, for their selfless love and inspiration.

And lastly, I owe my warmest gratitude to my beloved husband, Alisina, for his endless understanding, patience, care and support. Thank you for standing beside me to fulfill my dreams.

Dedication

Dedicated to:

My parents, my sister, my husband

&

The eternal memory of my beloved brother, Hossein…

Table of Contents

List of Figures

List of Tables

Abbreviations

Abbreviation	Explanation
ÅAU	Åbo Akademi University process
BET	Brunauer–Emmett–Teller theory and analysis method
BM	Ball Milling
BPR	Ball to Powder Mass Ratio in ball milling
CCS	Carbon Capture and Storage
CMM	Controlled Mechanical Milling
COP21	The 21st Conference of the Parties
CSS	Carbon Storage and Sequestration
EDX	Energy Dispersive X-Ray Spectroscopy
GHG	Green House Gas
ICCP	International Climate Change Partnership
IPCC	Intergovernmental Panel of Climate Change
JMAK	Johnson-Mehl-Avrami-Kolmogorov Theory
MC	Mineral Carbonation
QP	Energy injected to powder in ball milling process (kJ/h)
QTR	Energy injected to powder in ball milling process per unit mass (kJ/gh)
R_C	Mass ratio of rock needed to capture unit mass of C

RCO_2	Mass ratio of rock needed to capture unit mass of CO_2
SEM	Scanning Electron Microscope
SI	Saturation Index
SSA	Specific Surface Area
WD	Working Distance (distance between magnet and vial in magneto ball mill)
XRD	X-Ray Diffraction

Chapter 1
Introduction

1.1 Problem Statement and Thesis Overview

Greenhouse gases (GHG) are the major cause of global warming through their ability to trapping heat in the atmosphere. Energy production and use lead to almost two-thirds of global greenhouse gas emission [1]. CO_2 is known as the greenhouse gas with the greatest contribution to global warming and the global CO_2 emission is used as a clear indicator of the world's fossil energy consumption [2-8]. Therefore, CO_2 capture is an essential approach to control the global temperature increase [9-14].

Since the mid-1970s approximately 168.5 billion metric tons of carbon has been emitted from fossil fuels consumption and cement production [15]. According to the International Climate Change Partnership (ICCP), continuing the current rate of emission would cause CO_2 concentration of as high as 1000 ppmv by 2100 [16], resulting in the global temperature increase of 3.6 ℃ [16-18]. The goal of limiting the global temperature increase to within 2℃ by 2100, as set in 2015 at the 21st Conference of the Parties (COP21) 5 [1], necessitates effective controlling of the global CO_2 level. Considering an accelerating rate of worldwide energy use, several methods have been suggested to reduce CO_2 emissions. Carbon storage and sequestration techniques (CSS) has drawn much attention, as well as the development of other emission controlling strategies such as renewable energy replacement and energy efficiency improvement [2, 4-6, 19].

Mineral carbonation (MC) is viewed as the safest approach in order to reduce the level of atmospheric CO_2 emission, and is applied to capture and store CO_2 in geological formations. Mineral carbonation offers the advantage of permanent CO_2 storage, in the form of thermodynamically stable and environmentally friendly carbonates [2, 4-6], along with the beneficial exothermic nature and raw materials availability [8]. With this technique, minerals react with CO_2 and form a thermodynamically stable carbonates. This prevents CO_2 emission in the atmosphere, while permanent CO_2 sequestration is achieved [3, 9, 10, 14]. In current research, mineral carbonation of olivine $(Mg, Fe)_2SiO_4$) was investigated as a prototype

feedstock, considering the storage capacity and abundancy of olivine for the sake of CO_2 storage.

Although MC based CCS is thermodynamically favorable, the slow kinetics of this process has greatly challenged its feasibility. Much effort has been made, in order to address the challenges in regard to the energy consumption and kinetics of the MC process. Pre-activation techniques are of the most recommended remedies to enhance the kinetics of mineral carbonation. Several different activation methods have been studied and investigated previously, such as mechanical activation, chemical activation, thermal activation, etc. [20-22]. Haug et al. [23, 24] performed a comprehensive study on the effect of mechanical activation via wet/dry high energy ball milling in a planetary mill, in order to improve the Mg-extraction potential of olivine samples in an HCl solution.

This addressed the optimal amount of mechanical activation energy for the most enhanced rate of olivine dissolution. Chemical activation [25] and thermal activation [9, 26] are the other major types of activation processes which have been shown to enhance the conversion rate of carbonation through the structural modification of raw materials. As an example, thermal activation of serpentine feedstock has been extensively evaluated through the method called "Shell thermal activation" [27, 28], which includes heating up the serpentine feedstock for the duration of one hour at 650℃, for the latter purpose of direct flue gas CO_2 capture. Also, the effect of thermal activation on the dissolution of serpentine in acidic medium, has been evaluated by Hariharan et al. [26].

Although the activation process enhances the kinetics of mineral carbonation, it consumes extra energy and affects the energy balance of the entire carbonation process. Therefore, the optimization of the pre-activation energy is still an essential gap in developing MC based CCS approaches. The level of activation energy must be carefully considered and an optimized activation energy level needs to be extensively sought.

In the first stage of this Ph.D. work, the optimal amount of pre-activation mechanical energy to achieve the most enhanced structural properties for carbon sequestration was studied. This task was done by monitoring the variation in the dominant factors affecting the microstructure

of the mineral, such as particle size, specific surface area, pore volume, crystallite size and crystallinity percentage, as a function of applied pre-activation mechanical energy.[1]

As another remedy to design and optimize the MC process, indirect carbonation was suggested to enable a better control of the factors affecting the kinetics, along with a higher possibility of process optimization [3, 29-31]. In an indirect carbonation process, the two highlighted steps of mineral carbonation including the extraction of reactive compounds and the carbonation of extracted products are performed in separate stages. Hence, the individual processes could be optimized and kinetically enhanced separately. ÅAU (Åbo Akademi University) process is of the most reputed and practical techniques proposed for indirect mineral carbonation of Mg-silicates. In this process, the extraction of magnesium hydroxide ($Mg(OH)_2$) is achieved through the reaction of ammonium sulfate ($(NH_4)_2SO_4$) and Mg-silicate feedstock [13, 32-36]. The kinetic enhancement of the solid state reaction between ammonium sulfate and Mg-silicate is still a limiting barrier in the way of the industrial development of this well-reputed technique.

The acceleration of the aforementioned solid state process via mechanical activation of reactive compounds was implemented in this thesis, using a controlled amount of milling energy. The optimal amount of pre-activation milling energy input for the most modified structural parameters and consequent enhanced kinetics of extraction was also addressed[2].

In another attempt to improve the efficiency of mineral sequestration, a directed mineral carbonation process was developed. The goal was to promote the formation of anhydrous carbonated precipitates, with higher storage density and thermodynamic stability compared to more kinetically favorable hydrous carbonates. Although a noticeable amount of research has been performed so far on the mechanism and kinetics of anhydrous carbonates [37-41], a comprehensive study on the effect of carbonation controlling factors, such as temperature and pressure is still lacking. Therefore, the optimization of carbonation parameters, besides

[1] The detailed justification of research gap and goal of this investigation, are presented in Chapter 3.

[2] The detailed justification of research gap and goal of this investigation, are presented in Chapter 4.

enhancing the kinetics and efficiency of aqueous carbonation of $Mg(OH)_2$ was investigated in this thesis, and the optimal value of temperature and pressure were achieved, through monitoring the trend of carbonation conversion percentage and anhydrous carbonate percentage changes with applied carbonation temperature and pressure.

As a continued attempt to promote the process of directed carbonation, in the later phase of this study, heterogeneous precipitation (seeding) of carbonated products was followed and evaluated. The technique of preferred seeding has been applied by others as well, in different aspects of studies, to control the kinetics of precipitates formation [42-45]. However, quantitative study of the effects of heterogeneous precipitation on the carbonation efficiency, and specifically the enhancement of directed anhydrous precipitation during mineral carbonation process is still needed. In this thesis, an expanded effort was performed on the estimation and evaluation of the possible effects of varied surface properties of injected precipitation sites during the directed carbonation process. This was examined under different temperature and pressure conditions, during the carbonation process, with the hope of achieving the most favorable type of seeding materials for anhydrous carbonated products formation.[3]

1.2 Research Objectives

The primary objective of this Ph.D. study is to develop a MC process with enhanced kinetics of optimized CO_2 storage capacity, where olivine is implemented as a carbonation feedstock. The specific goals of individual projects are shown below.

1. Determination of the optimal amount of pre-activation milling energy input, to achieve the most enhanced structural properties for mineral sequestration. This goal is achieved through the following approaches.[4]

[3] The detailed justification of research gap and goal of investigation, are presented in Chapter 5.

[4] This objective is achieved, as presented in Chapter 3.

I. Evaluation of the effect of milling energy input on the structural variation of processed olivine powders, for CO_2 sequestration.

II. Determination of the correlation between the amount of pre-activation milling energy input and the controlling structural properties, to form the most modified structure for CO_2 storage.

III. Determination of optimal amount of pre-activation milling energy input needed to achieve the most modified structural parameters for CO_2 storage.

2. Enhancement of the kinetics of $Mg(OH)_2$ extraction, as an essential stage of Mg-silicate carbonation, through pre-activation of reactant material with the optimal level of energy. The kinetics of solid state extraction of $MgSO_4$, as a rate limiting process has been the focus. The main research activities are as follow.[5]

    I. Pre-activation of reactant material and determination of the effects of milling energy input, on the microstructural properties of activated materials, in order to enhance the kinetics of extraction process.

    II. Seeking the optimal amount of required pre-activation energy for enhancing the kinetics of the solid-state reaction in the proposed extraction stage.

3. Directed precipitation of anhydrous magnesite during mineral carbonation of magnesium hydroxide ($Mg(OH)_2$), as a reactive extracted compound, for indirect mineral sequestration of Mg-silicates. This objective is achieved through the two critical strategies of controlling the carbonation parameters and the implementation of heterogeneous carbonation. This following tasks are included.[6]

    I. Controlling and optimizing of the carbonation temperature and pressure, in order to promote the process of directed anhydrous carbonation, during aqueous carbonation of $Mg(OH)_2$.

[5] This objective is achieved, as presented in Chapter 4.

[6] This objective is achieved as presented in Chapter 5.

II. Enhancing the kinetics and efficiency of $Mg(OH)_2$ directed precipitation, via implementation of preferred sites for the precipitation of favorable anhydrous carbonates.

III. Investigation of the effect of different surface properties of precipitation sites, under varied temperature and pressure conditions, during the mineral carbonation process.

1.3 Research Approach

This thesis is categorized into five chapters. Chapter 1 includes the research statement, gaps and motivation, proposed objectives and research structure and approach. This chapter presents a brief introduction to the research field and flow of thesis.

A comprehensive literature review is performed in preliminary stages of research, as presented in Chapter 2, in order to give a clear view of basic and fundamental knowledge in the current field of interest, while expanding to show the actual flow of current studies. Research objectives and approaches are also defined considering the current knowledge gaps, as determined through an expanded literature study.

Chapters 3, 4 and 5 present the details of research studies that were performed to address the defined research goals and objectives. The content of the presented chapters includes: a) a summary of proposed research and outcomes, b) an introduction to the research study, literature study, detailed research gaps and objectives, c) an experimental approach, presenting the research methodology, instrumental and analysis procedures and, d) the specific outcomes and results of the proposed research, while referring to the pre-defined goals.

In Chapter 3, the correlation between the amount of pre-activation mechanical energy input and the structural properties of olivine powders is evaluated, in order to form the most enhanced microstructural properties, for CO_2 storage purposes. The calculation of the actual amount of milling energy input is based on the pre-build model by Parviz and Varin [22]. The investigation of the effect of milling energy input on the variation of structural properties,

including particle size, specific surface area, pore volume, crystallinity percentage and crystallite size, during milling process is highlighted. The preliminary goal of this research task was to enhance the microstructural properties of olivine powders with an optimized level of milling energy input for the later task of direct carbonation. This task was not successful in further assessment. The activated samples didn't show any successful carbonation conversion as compared to non-activated ones, under dry direct carbonation ran at atmospheric CO_2 pressure and temperature range of 100-200 ºC. However, structural enhancement methodology that was achieved in this stage was implemented in next research task as is explained in Chapter 4.

In Chapter 4, the procedure to enhance the kinetics of the extraction stage, as an initial stage of the indirect mineral carbonation process is deliberated. Solid state extraction of $MgSO_4$ as a rate limiting stage of $Mg(OH)_2$ formation during ÅAU indirect mineral carbonation of Mg minerals is addressed. The optimization of crystal structure (particle size, specific surface area, pore volume, crystallite size and crystal strain) with mechanical milling is carried out by monitoring the trend of intended structural parameter variation vs. milling energy input. Also, the variation of activation energy of solid state extraction reaction is recorded as a function of pre-activation milling energy.

Chapter 5, presents the attempts on enhancement of directed carbonation of the $Mg(OH)_2$ process through the formation of anhydrous carbonates in order to improve the efficiency and stability of the aqueous mineral carbonation process. In this phase, two different strategies, controlling of the carbonation parameters, and impelimenting hetrogeneous precipitation using different seeding sites, are attempted. The main aspects of this phase of research includes the investigation of the effects of carbonation temperature and pressure on conversion percentage and anhydrous carbonate concentration, in directed carbonation. The effects of hetrogeneous precipitation on carbonation conversion percentage and anhydrous carbonate concentration, as a scale of directed carbonation progress are also evaluated.

Finally, the key outcomes of the current Ph.D study, research limtation and future work suggestions and directions are presented as Chapter 6, which is itemized based on the major research topics that are evaluated in this study.

Chapter 2
Literature Review

2.1 Global Warming and CO_2 Emission Reduction Technologies

Fossil fuels are still the world's primary source of energy, producing almost 80–85% of the world's total energy requirements [5, 6, 46, 47]. Besides all their advantages such as high energy density, abundance, ease of use and storage, and low cost, their application is facing global challenges, and their emission of CO_2 into the atmosphere is known to be one of the major sources of global warming [48]. CO_2 is of the primary types of greenhouse gases, and is mostly emitted to the atmosphere by human activates such as fossil fuel combustion for energy production.

The growing energy demand has led to increasing fuel consumption, which releases a huge amount of CO_2 into the atmosphere [11]. As reported by the International Energy Agency, 13.1 gross tonnage of CO_2 was emitted from the combustion of coal between 2009 and 2010 [49]. CO_2 is also released by natural activities such as the respiration of living species, plants, and microorganisms; the decay of organic material; plus, volcanic outgassing and forest fires [12]. Because the rate of CO_2 emission is growing noticeably, the establishment and development of CO_2 emission mitigation techniques, such as carbon capture and storage (CCS) technology has become crucial to controlling the global carbon footprint. Improved energy efficiency and replacing fossil fuels with alternative options are the suggested strategies for reducing CO_2 emissions. The option of CO_2 capture and storage (CCS) in geological formation is offered as one promising method, by which emitted CO_2 will be stored in the form of thermodynamically stable and environmentally friendly carbonates [2, 5, 6, 14, 50-55]. CCS referrers to a variety of technologies that capture CO_2 from processes such as, combustion power plants, iron and steel making, natural gas treatment, etc. It pressurizes the captured CO_2 to the level of over 100 bars and transfers the pressurized gas through pipelines or tankers to sites for long-term storage in a stable geological formation [27]. CO_2 removal from the gas stream, called

capturing process, could take several promising approaches such as pre-combustion, post combustion and oxy-fuel combustion techniques [56].

CCS was initiated in the 1960s and is reported to be capable of storing almost 90% of CO_2 emissions produced by fossil fuel combustion, electricity generation, and other industrial processes [57]. It has been offered as the most immediate solution that can reduce the effect of emissions from huge industrial emitters such as the power plants and refineries that are responsible for 40 to 60% of total global CO_2 emission [58]. Geological storage indicates trapping of CO_2 in geological structures. The injection of CO_2 into underground storage sites, such as saline aquifers, depleted oil and gas fields, deep coal seams, is one method that has been tried for storing CO_2 in geological formations. The idea of underground injection of CO_2 for storage purposes has been initiated based on the natural capability of underground spaces to store thousands of naturally occurring gases, including naturally occurring CO_2. The proposed technique is designed to take advantage of natural barriers that have already stored varied types of gases underground for millions of years, thereby helping CO_2 reduction [59]. However, this technique has been debated because of the high risks of leakage [60]. Thus, mineral carbonation has been proposed as an alternative strategy for storing CO_2 in geological formations, with safer conditions.

2.2 Mineral Carbonation

"*Mineral carbonation is the fixation of CO_2 as stable carbonate minerals, such as calcite ($CaCO_3$), dolomite ($Ca\ Mg(CO_3)_2$), magnesite ($MgCO_3$), siderite ($FeCO_3$) and Mg–Fe carbonate solid solutions [4].*"

Carbon mineralization, also known as "enhanced natural weathering", is an accelerated type of natural geological weathering, defined as the sequestration of CO_2 by the reaction of alkaline-earth-metal-bearing silicates with CO_2, to store CO_2 in the form of stable carbonates [6, 9, 61]. The idea was initiated by Seifritz in 1990 [62], further studied by Dunsmore [63], and expanded by Lackner et al. [20] The process was termed mineral carbonation. Later on,

the technique was extended to other feedstock rather than minerals, such as industrial wastes and slags, and found a more general name of carbon mineralization [9]. The MC process has been developed and conducted through different routes and approaches including, an aqueous scheme suggested by Kojima [64]; an underground injection scheme proposed by Gunter et al. [65]; a process via mineral derived $Mg(OH)_2$ suggested by Lackner et al. [66]; and a carbonic acid process using olivine and serpentine by O'Connor et al. [67, 68].

Figure 2-1 presents a total overview of the carbonation process [9, 67]. CO_2-containing exhaust gas from power plant and mineral carbonation feedstock are transferred to a mineral carbonation reactor. Upon the reaction in the mineral carbonation reactor, CO_2 is stored, and carbonated compounds are formed as mineralization reaction products. The carbonated products of mineral sequestration will then be stored, disposed of or reused in other industrial applications.The most important advantages of the mineral carbonation process can be summarized as follows:

1) Mineral carbonation results in the formation of thermodynamically stable carbonate, insuring permanent fixation of CO_2.
2) Raw materials exist in vast quantity and are quantitatively enough to capture all emitted CO_2 from fossil fuel combustion.
3) Value-added by products can be formed and used to compensate for a part of the process cost. On the other hand, the total process is exothermic, and the released heat can be used to provide some portion of the energy required for process enhancement [67].

Addressing this third advantage of the MC process, this technology can be considered as a multipurpose carbonation approach, with the capability of both storing and utilizing CO_2, and with the carbonated materials being utilized in latter applications such as construction building materials or as filler materials in paper and plastic products [69, 70]. However, MC demands a high level of costly energy consumption and suffers from a slow conversion rate [3, 34].

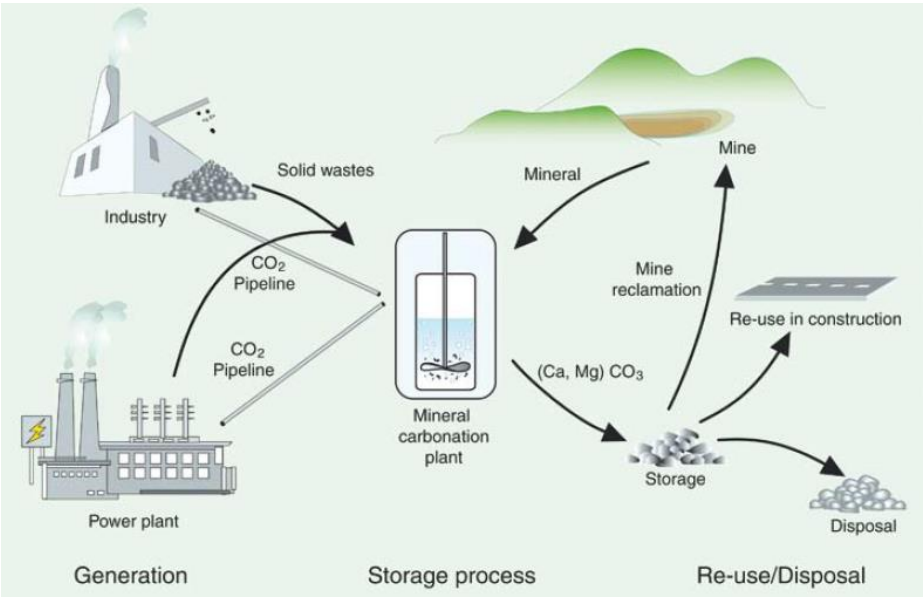

Figure 2-1. Total overview of carbon sequestration process, Energy Research Centre of the Netherlands (ECN) [9, 71].

The process of mineral carbonation can be operated under either in-situ or ex-situ conditions. During in-situ carbonation, CO_2 is injected underground to accelerate the chemical reaction between subsurface alkaline minerals and CO_2. Ex-situ activities occur above ground, requiring mineral processing and mining, as well as feedstock communication [71]. Mineral carbonation has currently the potential of storing over 10000 Gt of carbon, due to the high abundancy of mineral carbonation feedstock [27]. Carbonation reactions typically require around 2 tons of silicate feedstock per ton of captured CO_2, and thus require huge levels of mining. As an example, a 100 kt per day mining operation is capable of storing about 18 Mt CO_2 per year which is enough to store the CO_2 emitted by five 500 MW coal fire power stations [72, 73]. In order to express the feasibility of a carbonation process, in regard to the availability of mineral sources, we may consider two selected reservoirs in the United States. Twin Sisters, Washington, and Wilbur Springs, California, which are capable of sequestering the globally

emitted carbon dioxide for 2 and 5 years respectively [9]. In other research, Lackner [66, 74] has indicated that Oman, by having 30,000 km^3 magnesium silicates is capable of storing most of the CO_2 generated by coal combustion in the world.

2.2.1 Sources of Mineral Carbonation

During mineral carbonation, CO_2 must be combined with metals to form carbonate minerals. In general, metals are the source of divalent cations, including Ca^{2+}, Mg^{2+}, and Fe^{2+}. Silicates are the most abundant sources for these cations in nature [4, 8]. Among silicate rocks, mafic and ultramafic rocks are suggested for carbonation, as they contain high amounts of magnesium and calcium. Although molar abundances of magnesium and calcium silicates in the earth's crust are similar, the application of magnesium based silicates is more favorable for mineralization, due to their higher concentration of metal oxide. Magnesium silicates contain a high concentration of magnesium oxide (up to 50% by weight, equal to a theoretical CO_2 storage capacity of 0.55 kg CO_2/kg rock). This concentration is obviously higher than that in the rocks containing calcium silicates, such as basalts, which have a CaO content of about 10% by weight (equal to theoretical CO_2 storage capacity of 0.08 kg CO_2/kg rock) [3, 6]. On the other hand, the amount of oxide required to bind one ton of carbon is 3.3 ton in MgO compared to 4.7 ton CaO [9, 71], which presents the higher storage density of magnesium based silicates, as compared to calcium containing ones. The largest quantity of magnesium silicate is found in the forms of olivine $(Mg, Fe)_2 SiO_4$, forsterite (Mg_2SiO_4) and serpentine $Mg_3Si_2O_5(OH)_4$ [6, 75, 76]. Earth's serpentine deposits alone are enough to sequester all the carbon associated with known coal reservoirs [5]. Dunites and peridotites are the main candidate magnesium-rich rocks that could be mined for olivine and serpentine production.

Table 2-1 compares some of the most-significant candidates used as mineral carbonation feedstock, based on RCO_2 (the mass ratio of rock needed for capturing unit mass of CO_2 [6, 77]) and Rc (mass ratio of rock needed to capture a unit mass of C [6, 9]). As this table shows, olivine offers the best carbon storage properties, due to its highest storage density and metal

oxide concentration. Olivine is a solid solution of forsterite (Mg_2SiO_4) and fayalite (Fe_2SiO_4) [6, 9, 71]. It has been mined for most of the past century as a refractory material, and is used extensively in the metal foundry industry for sand mold castings [68, 78].

Table 2-1. Comparison of capability of different mineral feedstock for CO_2 sequestration [6, 9].

Rock	MgO wt%	CaO wt%	Rc (kg/kg)	RCO_2 (kg/kg)
Olivine	49.5	0.3	6.8	1.8
Serpentine	Around 40	Around 0	Around 8.4	2.3
Wollastonite	-	35	13.0	Around 3.6
Talc	44	-	7.6	2.1
Basalt	6.2	9.4	26	7.1

On the other hand, considering the exothermic nature of mineral carbonation reactions, feedstock with the chemical capacity to release more heat during mineralization reactions would be more practical, since the released heat could be stored and recovered to compensate for a portion of the total process' energy requirement. In this regard, the amount of energy released during the carbonation reaction of typical feedstock in mineral carbonation is compared and presented in Table 2-2 [79]. In this table. Magnesium-bearing minerals are capable of releasing highest levels of energy through exothermic reactions, and forsterite olivine, as an abundant and naturally available Mg-silicate, could be an appealing candidate, in this sense.

2.2.2 Chemistry of Mineral Carbonation and Mineral Carbonation Routes

In general, during mineral carbonation divalent metal oxide (Fe, Mg or Ca oxide) bearing compounds react with CO_2 to form carbonate, according to Eq.(2-1) [6, 79].

$$MgO + CO_2 \longrightarrow MgCO_3 + Heat \quad \text{2-1}$$

This reaction is exothermic, and the heat of reactions is reported per mole of CO_2. In nature, calcium and Mg exist in the form of silicates. The carbonation reaction of silicates is also exothermic. Mg and Ca minerals are the best candidates for mineralization, since they form stable carbonate products upon reaction with CO_2. These carbonates have very low solubility and emit minimum water contamination as a result of leaching [73].

Eq.(2-2) illustrates the general carbonation reaction of Mg and Ca silicates [6]. In the same way, the general carbonation reaction of forsterite olivine is as in Eq.(2-3) [6, 62, 66, 80, 81].

$$(Mg,Ca)_x Si_y O_{x+2y+z} H_{2z} + xCO_2 \longrightarrow x(Mg,Ca)CO_3 + ySiO_2 + zH_2O + Heat \quad \text{2-2}$$

$$Mg_2SiO_4 + 2CO_2 \longrightarrow MgCO_3 + SiO_2 + 90kJ/mol \quad \text{2-3}$$

Table 2-2. Enthalpy of carbonation reaction, for different mineral feedstock [79].

Mineral	Enthalpy of reaction (kJ/mol)
Calcium oxide (CaO)	179
Magnesium oxide (MgO)	118
Forsterite olivine (Fe_2SiO_4)	89
Wollastonite ($CaSiO_3$)	87
Serpentine($(Mg, Fe)_3Si_2O_5(OH)_4$)	64

The carbonation process occurring as a result of silicate/CO_2 reaction is exothermic and thermodynamically favorable. Addressing to the exothermic nature of reactions in (Eq.(2-1) to Eq. (2-3), Gibbs free energy of carbonation reaction also increases, by temperature increment. Hence, in the case of olivine, the thermodynamic tendency of carbonation decreases with an

increase in temperature and the applicable thermal range of the mineral carbonation process would be limited, thermodynamically. However, at the thermal range below 200°C (473K), the negative value for ΔS (T) of carbonation could be compensated for the large negative ΔH(T) value of the reaction, leading to a negative ΔG(T) of carbonation and spontaneous mineralization [82].

The decomposition temperature of carbonated products adds another limitation to the thermal range definition of the mineral carbonation process. Thus, exceeding the carbonation temperature over 900ºC for calcium carbonate and 300 ºC for magnesium carbonates may lead to the thermal decomposition of carbonated products [6]. As reported by other researchers, the optimal reaction temperature range for olivine carbonation is 150–200 °C at atmospheric pressure [6, 71, 80]. Table 2-3 summarizes the maximum temperature allowance for the mineral carbonation of typical mineralization feedstock [6, 66].

Table 2-3. Maximum allowance reaction temperature for different mineralization feedstock [6, 66].

Mineral	Max carbonation temperature allowance (K)	Carbonation pressure (bars)
Calcium oxide (CaO)	1161	1
Calcium oxide (CaO)	1670	200
Magnesium oxide (MgO)	680	1
Magnesium oxide (MgO)	930	200
Wollastonite ($CaSiO_3$)	554	1
Forsterite olivine (Mg_2SiO_4)	515	1
Serpentine ($Mg_3Si_2O_5(OH)_4$)	680	1

2.2.3 Mineral Carbonation Approaches

The MC process may be implemented through either direct or indirect approaches, upon the separation or combination of two critical MC stages of extraction and carbonation, in either dry or aqueous media [6, 83-85]. Each route brings specific chemistry, technical advantages and drawbacks that are discussed in the following sections.

2.2.3.1 Direct Carbonation Routes

2.2.3.1.1 Direct Dry Carbonation

In direct-dry carbonation reactions, gaseous CO_2 reacts directly with solid minerals or alkaline wastes, in a non-aqueous medium. This process is the most straightforward mineralization approach (Eq.(2-1)), and was first studied by Lackner et al. [66, 74]. However, direct-dry carbonation suffers from very slow reaction rates. Many technical studies have been performed on enhancing the kinetics of this process [6, 66, 86-88] as will be discussed more in section. (2.2.5.1). This approach can be conducted through a reaction with either gaseous or supercritical CO_2 gas. In spite of the simplicity and thermodynamic favorability, the major concern related to the slow kinetics of the reaction is still unsolved, which has limited the process' practical feasibility. Zevenhoven et al. [22, 72, 84, 85, 89-92] have performed a comprehensive study, in order to promote the kinetics of direct dry carbonation.

2.2.3.1.2 Direct Aqueous Carbonation

In direct-aqueous carbonation, CO_2 gas directly reacts with mineralization feedstock in an aqueous medium to form stable carbonates. The aqueous approach is mainly followed through three important stages. In the first step, CO_2 gas is dissolved in water to form an acidic medium and bicarbonate (HCO_3^-) ion, as Eq.(2-4). This reaction liberates protons, causing a pH reduction in the carbonation solution, where the pH of the solution depends upon the partial pressure of the CO_2, and the temperature, alkalinity, and salinity of the water. Thereafter, Ca

and Mg ions are leached from the mineral matrix in the acidic medium (Eq.(2-5)). Finally, magnesium or calcium carbonates are precipitated in the solution based on (Eq.(2-6)) [6, 9, 79, 93-97].

$$CO_{2(g)} + H_2O_{(l)} \longrightarrow H_2CO_{3(aq)} \longrightarrow H^+_{(aq)} + HCO_3^-{}_{(aq)} \quad 2\text{-}4$$

$$(Ca, Mg) - Silicates_{(s)} + 2H^+_{(aq)} \longrightarrow (Ca, Mg)^{+2}_{(aq)} + SiO_{2(s)} + H_2O_{(l)} \quad 2\text{-}5$$

$$(Ca, Mg)^{+2}_{(aq)} + HCO_3^-{}_{(aq)} \longrightarrow (Ca, Mg)CO_{3(s)} + H^+_{(aq)} \quad 2\text{-}6$$

In the same way, the reaction of forsterite (Mg_2SiO_4) with aqueous CO_2 to yield the final products of magnesite ($MgCO_3$) and quartz (SiO_2) starts with the dissolution of CO_2 in water, as Eq. (2-4) [4, 48], and then proceeds based on Eq. (2-7) [98]. In this reaction, the rock is firstly dissolved in an acidic medium, releasing divalent ions. Then, the dissolved metal reacts with CO_2 to produce carbonates, according to Eq.(2-6).

$$Mg_2SiO_4 + 4H^+ \longrightarrow 2Mg^{+2} + 2H_2O + SiO_{2(aq)} \quad 2\text{-}7$$

2.2.3.2 Indirect Carbonation

Indirect carbonation is a process in which the overall carbonation is divided into two or more stages. For example, in the case of wet (aqueous) carbonation, the dissolution of CO_2, extraction of metallic ions and precipitation of carbonates take place in different reactors. During indirect carbonation, the reactive compounds such as MgO or $Mg(OH)_2$ are initially extracted from the silicate minerals and then are carbonated to store CO_2. Figure 2-2 compares the direct and indirect carbonation approaches for Mg-silicates [6]. The studies on carbonation of MgO and $Mg(OH)_2$ as reactive compounds, to be extracted from Mg-silicates, were started in 1990 by Zevenhoven et al. [83] with the purpose of accelerating Mg-silicate mineralization. Eq. (2-8) represents the general extraction formula in indirect Mg silicate carbonation [8, 83,

90-93, 99, 100]. The extracted compound is then carbonated, based on Eq. (2-1). However, Mg-hydroxides are much more favorable than oxide compounds and offer a much more noticeable degree of reactivity for mineral carbonation.

$$xMgO.ySiO_2.zH_2O(s) \longrightarrow xMgO(s) + ySiO_2 + zH_2O \qquad 2\text{-}8$$

2.2.3.2.1 Indirect Dry Carbonation

As discussed in section (2.2.3.1.1) the carbonation of naturally available silicate minerals is almost not feasible, as a result of the significantly slow reaction rate of silicates in dry condition. To addressing this point, the process of indirect dry carbonation has been proposed and advances, and includes the extraction of reactive compounds from unreactive silicate structures prior to the actual carbonation reaction. One of the most primitive advantage of the indirect carbonation route is that it can expand the range of thermodynamic stability. Figure 2-3 illustrates the thermodynamic-defined applicable range of CO_2 sequestration for olivine as well as some other Mg silicates [92, 101], where the carbonate products are thermodynamically stable in the range, defined by the corresponding curves in Figure 2-3 [92, 101].

The thermodynamic equilibrium lines for each reaction are plotted considering the general equation of free energy change. For example, in the case of the carbonation of forsterite olivine (Mg_2SiO_4) (Eq.(2-3)), free energy variation can be formulated, as in Eq. (2-9) and Eq. (2-10) [21, 22, 102-104].

$$\Delta G = \Delta G^0 + RTLn(K_p) \qquad 2\text{-}9$$

$$K_p = \frac{[MgCO_3]^2 \times [SiO_2]}{[Mg_2SiO_4] \times [CO_2]^2} \qquad 2\text{-}10$$

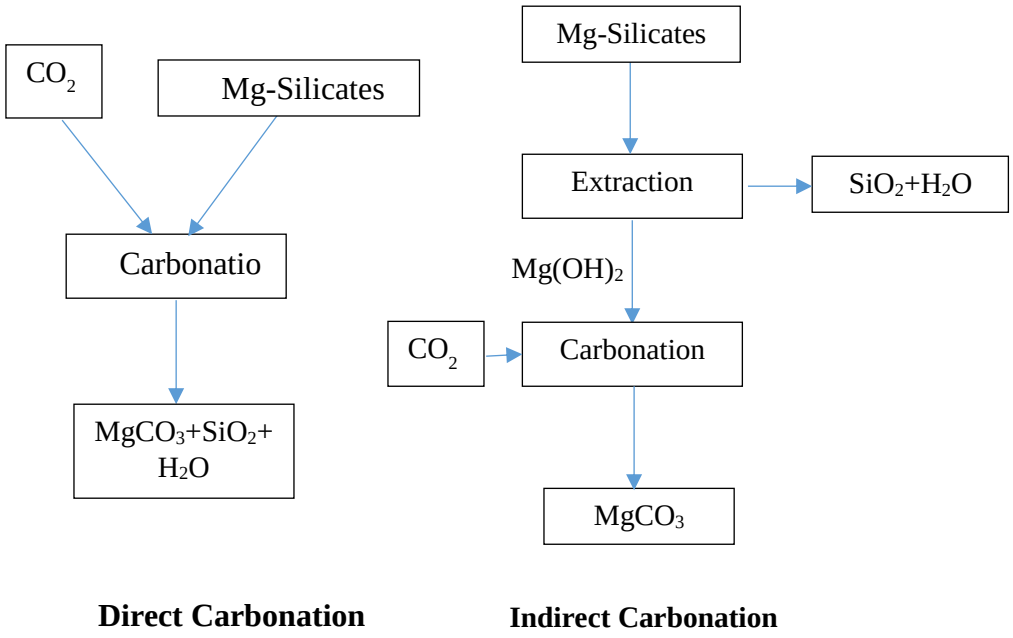

Figure 2-2. Schematic comparison of direct and indirect carbonation approaches, modified from [6].

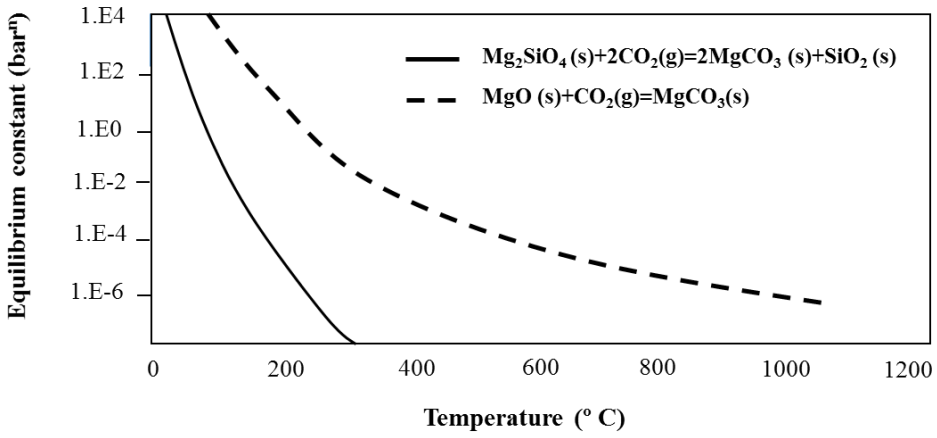

Figure 2-3 Thermodynamic equilibrium constant vs temperature for carbonation of Mg_2SiO_4 and MgO, modified from [92, 101].

ΔG^0: Standard free energy of reaction (The free energy of reaction at standard state conditions, where the partial pressures of any gas involved in the reaction is 0.1 MPa and the concentrations of all aqueous solutions are 1 M [102])

K_p: Equilibrium constant of reaction

T: absolute temperature in K

R: Universal gas constant

The terms in brackets show the thermodynamic activity of chemical species. Assuming that the chemical activity of solid compounds is equal to unity under dry condition, K_p is equal to $(\frac{1}{[P_{CO_2}]^2})$. Hence, the range of thermodynamic stability for the direct dry carbonation of olivine increases, as a function of CO_2 pressure and, the process can be speeded up by CO_2 pressure increment, thus enabling the implementation of higher carbonation temperatures. However, the increase in the maximum allowed carbonation temperature for forsterite, by CO_2 pressure is not noticeable and will not noticeably improve the kinetics of dry forsterite carbonation, as is also reported in previous studies [21, 22].

As is seen in Figure 2-3, MgO offers a higher range of thermal allowance for mineral carbonation than forsterite [92], which means that carbonation of MgO could be performed at higher temperatures, with more enhanced kinetics, compared to forsterite. Hence, indirect carbonation of forsterite (decomposition of forsterite to MgO and then MgO carbonation) is one applicable method to promote the carbonation process, as it ends up with higher range of thermodynamic stability for CO_2 sequestration. The maximum range of $MgCO_3$ stability in MgO carbonation (Eq.(2-1)) can be calculated as in Eq. (2-11) [105], which is formulated based on the free energy change in the MgO carbonation reaction.

$$T_{eq}(K) = \frac{13636}{\ln(\frac{1}{P_{CO_2}(bars)}) + 20.01} \quad \text{2-11}$$

Also based on Eq.(2-1), the range of $MgCO_3$ stability in MgO carbonation can be increased, through the increase of CO_2 pressure, which is also shown in Figure 2-3. $Mg(OH)_2$ is also proposed as another candidate compound, to be extracted from Mg- silicates during indirect carbonation, with the goal of more desirable carbonation properties (Eq.(2-12)). Similar to MgO, $Mg(OH)_2$ can also offer a wider thermal range of $MgCO_3$ thermodynamic stability compared to forsterite. The equilibrium temperature of $Mg(OH)_2$ for carbonation as a function of CO_2 pressure can be calculated based on Eq. (2-13), with the same method explained for MgO [105].

$$Mg(OH)_2 + CO_2 \longrightarrow MgCO_3 + H_2O \quad \text{2-12}$$

$$T_{eq}(K) = \frac{4796.3}{\ln(\frac{P_{H_2O}(bars)}{P_{CO_2}(bars)}) + 3.538} \quad \text{2-13}$$

Another significant benefit of indirect carbonation is that, as the total carbonation process is divided into two separate sections, liberation of SiO_2 from the structure can be performed in the extraction stage, resulting in better carbonation efficiency than with the original feedstock. Also, since the silicate layer acts as a kinetics barrier during carbonation, the overall kinetics of mineralization can be speed up by removing the silica layer prior to the carbonation step [20, 106].

2.2.3.2.2 Indirect Wet Carbonation

To explain the benefits of indirect wet carbonation compared to the direct process, one may consider that the aqueous carbonation process faces two big challenges. The first challenge is that, during wet carbonation of minerals, more CO_2 can be dissolved into the aqueous phase, under low temperature conditions (Eq.(2-4)), where both the dissolution of the raw material (Eq.(2-5)) and the precipitation of carbonates (Eq.(2-6)) are favored at elevated temperature levels. Secondly, an acidic environment (low pH) would accelerate the Mg and Ca-leaching through proton exchange reaction, but high precipitation levels with respect to the Mg/Ca-carbonates are reached at alkaline conditions (high pH). It would then be a big challenge to find optimal conditions to satisfy all considerations. However, if the whole carbonation process could be staged into different sections through indirect approach, each step could be conducted in separate reactors, under its own favorable condition [8, 23, 79], and parameter optimization and control could be significantly facilitated.

2.2.4 Extraction Techniques in Mineral Carbonation

The process of MgO or $Mg(OH)_2$ extraction from Mg silicates structure has been categorized, based on the most reported techniques of extraction, as either thermal or chemical.

2.2.4.1 Thermal extraction

Thermal extraction is performed on some Mg and Ca silicates to extract MgO or $Mg(OH)_2$ from silicates, followed by carbonation [84]. Serpentine minerals ($Mg_3Si_2O_5(OH)_4$) are studied more than any other Mg-silicate in thermal extraction [19, 101]. The process of thermally extracting MgO from serpentine is referred to as thermal activation and are suggested by Zevenhoven et al. [85]. As they showed, serpentine activation through this method is not effective, so they suggested a process for extracting $Mg(OH)_2$ as a substitute [6, 83, 85]. This process will be discussed in more detail, in section (2.2.5.1). After finding the feasibility of improving the Mg silicates carbonation process through the extraction of reactive compounds

such as MgO and $Mg(OH)_2$ and carbonation of extracted compounds (indirect carbonation), the effective thermal range for the decomposition of olivine/ forsterite to more reactive compounds (either MgO or $Mg(OH)_2$) needs to be estimated from thermodynamics of the decomposition reaction, as in Figure 2-4.This figure shows the equilibrium temperature of decomposition, as a function of an equilibrium constant for different decomposition reactions [92, 101].The applicable temperature for MgO extraction from Mg_2SiO_4 structure (Eq. (2-14)) is calculated based on Eq. (2-15) to Eq. (2-16). Obviously, the calculated temperature (37387 ºC) is too high to be applicable in an experimental process, and the direct thermal extraction of MgO from forsterite does not seem to be feasible under atmospheric pressure.

$$Mg_2SiO_4 \longrightarrow 2MgO + SiO_2 \qquad 2\text{-}14$$

$$\Delta G^0 = \Delta H^0 - T\,\Delta S^0 \qquad 2\text{-}15$$

$$T_{eq}(^{\circ}C) = \frac{\Delta H^0}{\Delta S^0} - 273 = 37387 \qquad 2\text{-}16$$

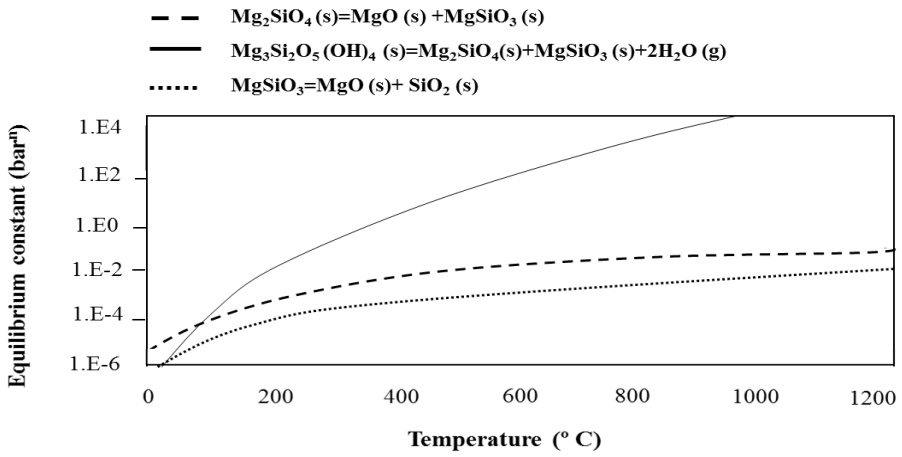

Figure 2-4. Thermodynamic equilibrium constant vs temperature for decomposition of Mg_2SiO_4, $MgSiO_3$ and $Mg_3Si_2O_5(OH)_4$, modiied from [92, 101].

2.2.4.2 Chemical Extraction

Two methods are offered by Lackner et al. [66], for the chemically extraction of $Mg(OH)_2$ from olivine or serpentine, in hydrochloric acid and carbonic acid [9, 81, 87, 107]. The HCl route of extraction is suggested by Lackner et al. in 1995 [66, 79], for the extraction of $Mg(OH)_2$ reactive compounds from serpentine mineral. In this process, at the initial stage, serpentine reacts with HCl (Eq. (2-17)) to leach Mg ions at a temperature of about 100ºC for one hour [6, 9]. Then $Mg(OH)_2$ as an intended compound is extracted, and HCl is recovered by heating the solution to 250 ºC to dehydrate $MgCl_2.6H_2O$ to MgCl(OH) through Eq. (2-18). And finally, $Mg(OH)_2$ is formed, based on Eq. (2-19), by thermal transition of MgCl(OH) to $Mg(OH)_2$.

$$Mg_3Si_2O_5\left(OH\right)_{4(s)} + 6HCl_{(l)} + H_2O_{(l)} \rightarrow 3MgCl_2.6H_2O_{(aq)} + 2SiO_{2(s)} \quad \text{2-17}$$

$$MgCl_2.6H_2O_{(aq)} \rightarrow MgCl\left(OH\right)_{(l)} + HCl_{(l)} + 5H_2O_{(l)} \quad \text{2-18}$$

$$MgCl\left(OH\right)_{(l)} \rightarrow Mg\left(OH\right)_{2(s)} + MgCl_{2(s/l)} \quad \text{2-19}$$

Acetic acid (CH_3COOH) extraction is another route of reactive compound extraction that is suggested by Lackner et al. [9, 66, 108] as a part of wollastonite ($CaSiO_3$) carbonation. Where, wollastonite reacts with acetic acid to leach Ca ions as Eq. (2-20). Later on, the extracted Ca ion reacts with CO_2 in presence of acetate ion (CH_3COO^-) to form calcium carbonate ($CaCO_3$), while recovering acetic acid as in Eq. (2-21).

$$CaSiO_{3(s)} + 2CH_3COOH_{(l)} \rightarrow Ca^{+2}\left(aq\right) + 2CH3COO^-_{(aq)} + H_2O_{(l)} + SiO_{2(s)} \quad \text{2-20}$$

$$Ca^{+2}_{(aq)} + 2CH_3COO_{-(aq)} + CO_{2(g)} + H_2O_{(l)} \rightarrow CaCO_{3(s)} + 2CH_3COOH_{(aq)} \quad \text{2-21}$$

2.2.4.3 Thermo-Chemical Extraction

The process of $Mg(OH)_2$ chemical extraction from serpentine is explained by Zevenhoven et al. [89, 90]. In this method, $Mg(OH)_2$ is formed from a solid-solid reaction of serpentine and ammonium sulfate as a part of an integrated ÁAU carbonation process suggested by Nduagu et al. [13, 34-36, 109, 110]. In the first step, serpentine rock is thermally treated with ammonium sulfate at about 400 – 500 °C and atmospheric pressure as (Eq. (2-22)) [6, 111].

$$Mg_3Si_2O_5(OH)_4(s) + 3(NH_4)_2SO_4(s) \longrightarrow 3MgSO_4(s) + 2SiO_2(s) + 5H_2O(l) + 6NH_3(g) \qquad 2\text{-}22$$

Magnesium content in the rock is converted to $MgSO_4$, which is highly soluble in water and will react with ammonia at PH 9-10 to separate silica and iron. The range of 60%-66% Mg extraction is reported by this method [6, 111, 112]. Then, $MgSO_4$ reacts with ammonium hydroxide (NH_4OH) and converts to $Mg(OH)_2$ in an aqueous solution, at a pH of 10-12. Ammonium sulfate is also produced as a side product of the reaction [6]. The produced $Mg(OH)_2$ is then separated, and ammonium sulfate is slurred in water, leaving behind unreacted mineral and insoluble reaction products, such as silica [13, 21, 90, 91, 105]. Figure 2-5 provides a schematic overview of the process [6, 89, 90, 105][7].

[7] More comprehensive explanation of process is offered in Chapter 4. The suggested extraction process is implemented for extraction purpose of $Mg(OH)_2$ from olivine mineral using mechanical pre-activation with an optimal energy level.

2.2.5 Kinetics of Mineral Carbonation and Technical Approaches to Enhance the Kinetics

Although carbonation is thermodynamically favorable, it suffers from slow kinetics of reaction [86]. Several strategies have been applied so far to speed up the rate of carbonation, in both dry and wet conditions. Process optimization and the implementation of specified kinetic enhancement techniques are among the best approaches to dealing with this issue.

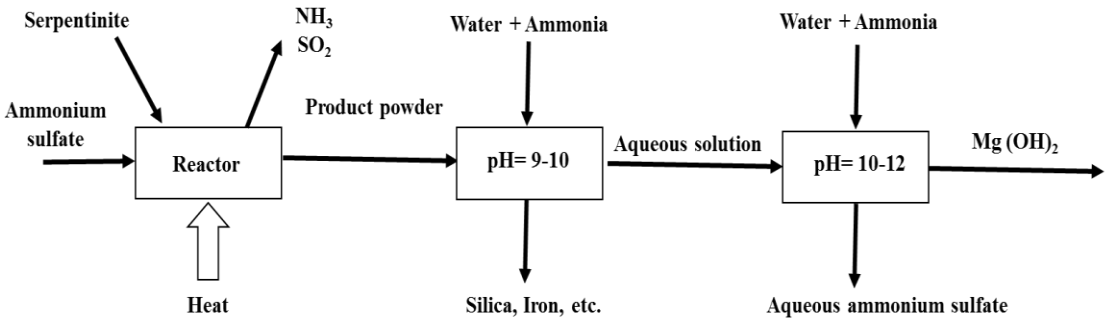

Figure 2-5. $Mg(OH)_2$ production process from serpentine, modified from [111].

2.2.5.1 Kinetics Enhancement in Dry Carbonation

The kinetics of the direct dry carbonation of silicate minerals is mostly limited due to the formation of a diffusion barrier silica shell, which inhibits the carbonation process. Researchers have tried to enhance the kinetics of dry carbonation, using supercritical CO_2 gas [66, 81, 87, 92, 101, 107]. (The critical point of CO_2 is 7.38 MPa at 31.1 °C).]. However, the value of achieved carbonation conversion percentage is still negligible.

The thermal activation of reactants is another suggested strategy used to improve the overall rate of direct dry reaction. This process removes chemically banded water and increases porosity and specific surface area in the structure of reactants. Thermal activation has mostly been tried on serpentine to remove water from the structure and form an open structure, thus

improving the kinetics of reaction by providing more reactive sites for carbonation [9, 91, 113]. Pre–activation of feedstock through heat treatment was also attempted by Zevenhoven and Kohlmann in 2002 [72], to speed up the rate of reaction but their suggested technique was found to be infeasible, as a result of its high energy consumption [92].

The addition of steam to the gaseous medium is the other suggested technique to promote the rate of dry carbonation [114, 115]. In a study by Thompson et al. [116] on forsterite carbonation under supercritical CO_2 (35℃ and 100 bars), it was shown that water has an essential role in the carbonation of metal silicates under supercritical CO_2 conditions. Thus, in a water-free condition, no carbonation was observed after 24h, but when water steam was added in the system, a thin water layer was formed on the surface. Hence, carbonation extent increased from 54% to 116% [116]. Also, the effect of water seam on the carbonation of MgO was confirmed by Fagrlaund et al. [105], who reported that the injection of 5% steam during carbonation of MgO, under a total of 20 bar atmosphere of CO_2, can result in carbonation, at 300 ºC. The same run, without water, showed no noticeable carbonation [61]. The enhanced kinetics of direct dry carbonation, in the presence of water steam, is attributed to the key role of water steam in converting the unreactive oxide compounds to reactive hydroxides [12, 27, 80].

The higher reactivity and better performance of magnesium hydroxide in carbonation process, as compared to magnesium oxide, was also shown by Zevenhoven et al. [85, 89] through the comparison of two different carbonation routes for mineralization of serpentine feedstock. In the first route, MgO was extracted at a temperature of about 600 ºC and came into reaction with CO_2. The second route was performed through the hydroxylation of extracted MgO; the extracted MgO was hydroxylated to $Mg(OH)_2$ by the reaction with water steam, under high temperature of 270-450 ºC and CO_2 pressure of 1-75 bars. Finally, it was brought into a carbonation reaction. The outcome of carbonation though these separate routes was compared and the results suggested that the carbonation of $Mg(OH)_2$ was much more efficient than that of MgO, which was formed through a two-stage process. The hydration of MgO to $Mg(OH)_2$ has also been addressed in other studies promoting carbonation behavior

[85]. However, the hydration of MgO to $Mg(OH)_2$ is very slow and there is always a chance that during the first thermal heating (MgO extraction), serpentine may be converted to olivine, water and quartz rather than MgO [83]. Moreover, a high energy consumption remains a big challenge with this process [6, 9].

Investigation of the mechanism behind steam effect enhancement, free energy calculation of the initial adsorption of water onto forsterite surface by Kirsch et al. [10], indicates that the formation of a water film, up to three-monolayers thick, could be exothermic. H_2O was found to displace CO_2 at the surface and therefore, CO_2 can not penetrate below a two-monolayer hydration layer formed by water. The simulations suggested that, in the presence of sufficient water, carbonation occurs in the water films and not via a direct reaction of CO_2 with the forsterite surface [10]. Water also plays an essential role in the chemistry of indirect dry mineralization of CO_2 with magnesium silicates. H_2O reduces the rate of dehydroxylation, although at the comparatively low H_2O partial pressures, the influence of water on carbonation, is small.

Some P_{H2O} is needed in the carbonation of $Mg(OH)_2$ to prevent rapid calcination of $Mg(OH)_2$ to MgO [105]; thus, in an experiment run on $Mg(OH)_2$ samples that were first calcined to MgO before carbonation, no significant carbonation was recorded [19, 117]. On the other hand, water improves the carbonation extent, in that the dependence of carbonation on H_2O content is higher at lower temperatures. However, there is still a temperature limitation and the maximum carbonation temperature should be kept below the $MgCO_3$ to MgO calcination temperature [19].

Fricker et al. [19] stated that, the presence of water vapor in $Mg(OH)_2$ carbonation which is released from solid structures of $Mg(OH)_2$ may facilitate the formation of an aqueous thin film leading to the carbonation of MgO sites. They also attributed the effect of water steam during $Mg(OH)_2$ carbonation to preventing rapid dehydroxylation and reported a noticeable increase in $Mg(OH)_2$ carbonation conversion, under steam condition. Based on their reported results, the carbonation conversion of $Mg(OH)_2$ to $MgCO_3$ under (T=473K, P_{H2O} around 1.5 Mpa and P_{CO2}=1.03 Mpa) and (T=573K, P_{H2O} around 3.5 Mpa and P_{CO2}=1.24 Mpa) showed respectively

33 and 58 times increase compared to the same condition without steam, which had offered negligible amounts of carbonation conversion.

In other research, Shih et al. [118] studied the kinetics of $Ca(OH)_2$ carbonation in the presence of humid low temperature CO_2. $Ca(OH)_2$ carbonation was assumed to show behavior similar to that of $Mg(OH)_2$ carbonation, and they found that, high humidity promotes the final conversion degree, by thickening the water layer that covers the reacting particles. In a similar study, Wu et al. [119] noted that the CO_2 sorption capacity of $Ca(OH)_2$ was enhanced in the presence of steam, as gaseous steam maintains the pores open in $Ca(OH)_2$ carbonation.

To add more to the steam concept, it worth mentioning that, gas flow rate in $Mg(OH)_2$ carbonation needs to be kept at an optimum value, as in a higher flow rate condition, the formed water vapor is carried away so quickly by the flowing CO_2 stream that the steam does not have time to interact with the CO_2 to form the carbonate. In the case of near-static conditions, Butt et al. [120, 121] argued that the reduced reactivity could be the result of increased H_2O pressure around the particles hindering both further dehydroxylation and CO_2 penetration. This effect is confirmed by the carbonation of $Mg(OH)_2$ under close to optimal carbonation condition at high temperature and in a high pressure medium (565 ºC and 57.2 bar CO_2, respectively) and slow flow rate, which offered 90% conversion in 30 min [105]. H_2O can enhance the carbonation of MgO by forming a region of dense water vapor around the reacting MgO particles in accordance with Eq. (2-23) [105, 122].

$$MgO + H_2O \longrightarrow MgO.H_2O \longrightarrow Mg(OH)_2 \qquad 2\text{-}23$$

Based on the research by Fagerlaund et al. [105], CO_2 can interact with water to form carbonate ions and H^+ ions (Eq.(2-4)). Then, the released Mg^{2+} ions come into reaction with the carbonate ions to form $MgCO_3$. A dense H_2O region can generate more ions and thus, increases both the yield and rate of carbonation.

The same mechanism can be also considered for $Mg(OH)_2$ carbonation, with the difference that, in the case of $Mg(OH)_2$, H_2O is provided intrinsically from inside the particle [105]. There

is an optimal value at which water vapor has the best kinetics of carbonation [105]. A small amount of steam (around 2.5%) is not found to influence the rate of carbonation significantly, but a higher concentration of steam in gaseous medium, can reduce the rate of dehydroxylation and enhance the carbonation, accordingly [105, 123].

Besides the effect of water steam, it is noted that high external gas pressure can increase H_2O pressure at the surface by slowing down the dehydroxylation process [105]. An experiment on the dry carbonation of $Mg(OH)_2$ under a CO_2 atmosphere showed the maximum conversion of 17.6% under 1.45 MPa CO_2 and 673K [19, 84, 90]. The influence of CO_2 pressure is mainly two sided. On one hand, it reduces the rate of dehydroxylation, which evidently influences the carbonation of $Mg(OH)_2$ by preventing a dehydroxylation stage, an initial step of $Mg(OH)_2$ carbonation. On the other hand, it increases the conversion rate during the $Mg(OH)_2$ to $MgCO_3$ reaction (Eq. (2-12)) [105].

In an experiment on $Mg(OH)_2$ carbonation under 585 ºC and 27.2 atm CO_2, there was an increase in the carbonation conversion to 26.1% compared to the 1.4% that occurred at the same temperature and a CO_2 pressure of 10 atm [117]. As the pressure of CO_2 increases, the calcination of $MgCO_3$ is suppressed and $MgCO_3$ is stable at higher temperatures. Thus, a carbonation process may be designed for higher temperatures, with an accelerated kinetics of reaction. At CO_2 pressures of 1 bar, $MgCO_3$ is just stable, up to temperatures of around 400°C, where, at 35 bar $MgCO_3$ is stable up to around 550°C.Since the carbonation of $Mg(OH)_2$ must be performed in the thermal range below the calcination temperature of $MgCO_3$, as the calcination temperature increases, $Mg(OH)_2$ carbonation could be done at higher temperatures with an enhanced kinetics of reaction. Moreover, at higher pressures, equilibrium shifts toward $Mg(OH)_2$ carbonation, in accordance with the general $Mg(OH)_2$ carbonation reaction (Eq. (2-12)) [117].

With the same effect as in highly humid systems, over pressure of CO_2 may decrease the extent of $Mg(OH)_2$ carbonation, by total hindering the dehydroxylation process, through slowing down the outward diffusion of $H_2O_{(g)}$ from the dehydroxilating lattice sites [117].

However, it has been shown that, increased pressure levels do not end up with an expected increment in the magnesium oxide (MgO) carbonation rate [90].

Temperature can also improve the kinetics of carbonation, due to faster reaction kinetics or by changing in the thermodynamic stability of different Mg-bearing phases in the system [19]. At low temperatures, carbonation is quickly limited by diffusion and a high conversion degree (assuming sufficient porosity) is never achieved [105]. On the other hand, at high temperatures, where the rate of dehydroxylation is much higher than that of carbonation, MgO would be the final product, and offers a very slow rate of carbonation. Thus, at higher temperatures, diffusivity increases and enables higher conversion degrees, assuming that excessive dehydroxylation is prevented and that the thermodynamic limit for $MgCO_3$ stability is not exceeded. In this regard, the highest conversion extent for $Mg(OH)_2$ carbonation is reported by Fricker and Park [19] to be around 70%, under a temperature of 673K, a steam pressure of 5.5 Mpa and CO_2 pressure of 1.45 Mpa.

Surface area and porosity can influence on the kinetics of $Mg(OH)_2$ carbonation, as well. The higher the surface area, the smaller the effect of intra-particle diffusion limitation. Hence, less severe reaction conditions need to be implemented [105, 117]. The initial porosity needs to be sufficiently high so as to prevent $MgCO_3$ from completely filling the pre-available porosities [89, 105]. Additionally, dehydroxylation becomes faster with increasing surface area [105]. In one study by Assima et al. [124], the dehydroxylation rate of brucite is attributed to its particle size.

High carbonation extent of serpentine-derived $Mg(OH)_2$ proves the importance of high surface area and porosity, as serpentine-derived $Mg(OH)_2$ particles are not limited by pore space availability, during carbonation [89, 105, 117]. In an experiment by Bearat et al. [117], it is shown that serpentine-derived $Mg(OH)_2$ presents a higher rate of conversion under supercritical CO_2 pressure, compared to synthesized commercial $Mg(OH)_2$, due to higher SSA and larger porosity of serpentine-derived $Mg(OH)_2$. (The pore volume of commercial $Mg(OH)_2$: 0.024cm^3/g, pore volume of serpentine-derived $Mg(OH)_2$: 0. 24cm^3/g, SSA of commercial $Mg(OH)_2$: 5m^2/g, SSA of serpentine-derived $Mg(OH)_2$: 40-50m^2/g) [2, 89, 90].

The maximum conversion degree, or final conversion degree reached for MgO carbonation, is dependent upon particle porosity as well. Carbonation of MgO is accompanied by a significant volume increase, which fills pores available for carbonation [105]. The effect of porosity on the carbonation of MgO is also referred to in a study by Zevenhoven et al. As they reported, MgO particles that are formed by $Mg(OH)_2$ calcination at high temperatures (more than 700 ºC), are very unreactive, when subjected to different pressures and 1% H_2O.

The fact is attributed to the high temperature at which the particles are calcined in, which reduces both porosity and SSA. In other research, by Fagerlund et al. [105], the carbonation of $Mg(OH)_2$ is modelled as a function of pore volume. According to their carbonation model, it may be speculated that the maximum achievable conversion is determined by the initial porosity of the particle in accordance with Eq. (2-24).

$$\frac{1-\varepsilon}{1-\varepsilon_0} = Z + (1-Z)(1-X) \qquad 2\text{-}24$$

Where, ε and ε_0 are porosity and initial porosity, respectively. Z is the volumetric ratio between product and reactant, and X is the conversion degree, towards $MgCO_3$.

The maximum conversion degree for a specific initial pore volume is obtained when ε reaches zero, so the maximum conversion degree is formulated as a function of the initial pore volume and the volumetric ratio between product and reactants. However, the maximum X is gained, when all other conditions (e.g., temperature and pressure) are favorable [105]. A research task on the effect of steam concentration and carbonation temperature is presented as Appendix C.

2.2.5.2 Kinetics Enhancement in Aqueous Carbonation

Both carbonation temperature and pressure can significantly influence the carbonation process. As an example, O'Connor et al. [68, 125, 126] investigated the effect of temperature increment, as well as pressure raise, on the carbonation process of olivine samples in wet condition. The

results of investigating temperature effect show that at 115°C and P_{CO2} = 80 atm, no discernable reaction had occurred after six hours. However, increasing the temperature to 185°C while holding a constant $P_{CO2,}$ resulted in an over 65% extent of reaction for a similar duration of six hours [68, 125, 126]. Also based on their investigation, the extent of reaction was improved to nearly 85%, by increasing the CO_2 pressure to 11.5 atm, while holding the temperature constant at 185°C. In regard to the pressure effect, in other research, it has also been shown that a supercritical CO_2 pressure, combined with a carbonation temperature of above 150°C, is likely necessary to achieve effective mineral dissolution rates [68, 125, 126][8].

It is generally accepted that, silicate dissolution is the rate limiting step during aqueous carbonation processes [31, 127], and as a result, efforts have focused on improving the kinetics of silicate dissolution, using a wide range of additives and by varying and controlling the operating conditions such as the temperature, pressure, CO_2 concentration, solid to liquid ratio, and particle size [4, 6, 8, 29, 30].

Table 2-4 has gathered some of the results achieved through different studies by O'Connor et al. [68, 113, 126, 128] showing the effect of particle size on the carbonation conversion percentage of forsterite. Based on Table 2-4, carbonation conversion percentage increases with particle size reduction, under constant temperature and CO_2 pressure. This effect is attributed to the higher kinetics of forsterite dissolution upon particle size reduction [68, 113, 126, 128].

Different activation processes can be applied to speed up the rate of mineral carbonation. Pretreatment is a critical step in carbonation; however, it increases the cost of the process. In most pretreatment processes, mineral dissolution would be improved by the creation of disorder in the mineral structure and increment of SSA [9]. With this background, mechanical activation (pre-treatment) is among the most addressed and appealing pre-treatment technologies suggested for improving the rate of aqueous carbonation, via structural modification.

[8] Temperature and pressure optimization, is implemented in Chapter 4.

Table 2-4. Effect of particle size reduction on carbonation conversion percentage of forsterite in aqueous carbonation [68, 113, 126, 128].

Particle Size (µm)	Time (h)	Temperature (◦C)	P_{CO2} (atm)	Carbonation Solution	Conversion Percentage
106-150	24	185	11.5	Distilled water	10
75-106	24	185	11.5	Distilled water	Around 50
37-57	48	185	11.5	Distilled water	56.1
37	24	185	11.5	Distilled water	91.5

Mechanical activation results in size reduction, amorphization and lower crystallite size. It also causes imperfections in the structure and influences the ion-liberation rate and carbonation rate accordingly [25, 125]. A study on the effect of crystallinity on the dissolution rate of SiO_2 shows that the rate limiting factor in the dissolution of SiO_2 is breaking the Si–O bond. Thus, amorphization can improve the kinetics of minerals dissolution (e.g. olivine), as it causes disordering, which weakens the Si–O bond, hereby lessening in less resistance to dissolution [129]. Research by Connor et al. [128] investigated the effect of mechanical activation on the carbonation of olivine particles. They tried both dry and wet milling of olivine in an attrition mill, and recorded structural change as in Table 2-5.

The reaction kinetics of the carbonation process was then reported as a function of structural changes. For this purpose, the extent of carbonation was considered as the extent of mass change due to carbonation, as a percent of the theoretical extent of the mass change in carbonation. Comparison of wet and dry mechanical milling results showed that the extent of carbonation depends mostly on SSA and, as wet milling can increase SSA dramatically, it leads to a higher extent of carbonation [128]. Connor et al. [68, 113, 126] reported that particle size

is a major factor determining the reaction rate and extent of reaction, since most of the mineral dissolution reactions are surface controlled. The extent of a reaction increased dramatically with decreasing particle size, to over 90% for the test conducted on 37-micron olivine feed material. In contrast, the carbonation extent was 10% under the same condition, for olivine particles with a particle size of 106-150 microns [68, 94, 113, 126]. Several other researchers have also evaluated the influence of milling conditions on structural properties. Details of the progress in mechanical activation are presented as section (3.2).

Table 2-5. Structural change of olivine as a result of attrition milling [51].

Measurement	Olivine (75µm)	Attritted olivine (1h)	
		Dry	Wet
Mean (µm)	25.85	10.15	5.228
Mode (µm)	35.48	4.217	3.981
Median (µm)	19.46	4.335	1.915
BET SSA (m^2/g)	4.600	5.092	46.293
Pore volume (Angstrom)	0.0118	0.0375	0.1213
Pore diameter (Angstrom)	102.587	294.474	104.748

Another technique for enhancing the reaction rate in wet carbonation processes is of the use of special additives such as sodium bicarbonate ($NaHCO_3$) in the solution, to improve the dissolution rate of mineral feedstock [73, 79, 113]. As is obvious from the dissolution equations of CO_2 (Eq.(2-4)), leaching reaction of minerals (Eq. (2-5)) and precipitation reaction of carbonates (Eq. (2-6)), dissolution of CO_2 and precipitation of carbonates are more likely to occur under high pH (basic) conditions, whereas mineral leaching tends to proceed in an acidic medium (Low pH). Consequently, the optimal value of pH must be maintained in the solution, to satisfy both criteria [6, 23, 24, 79, 130, 131].

A common process, known as “pH sewing technique” is capable of varying the pH in the solution to achieve an optimal and fixed condition, thereby satisfying the dissolution of CO_2

in solution (Eq. (2-4)), mineral leaching to extract divalent ions (Eq. (2-5)) and precipitation stage (Eq. (2-6)). Dissolution of additives results in an increment in the concentration of bicarbonate ions ($HCO3^-$) in the solution. Bicarbonate ions would be consumed through the reaction with intended minerals (e.g., forsterite) to form a carbonate product, while releasing OH^- ion (Eq. (2-25))[68, 93, 132].

2-25

$$Mg_2SiO_{4(s)} + 2HCO_3^-{}_{(aq)} \rightarrow 2MgCO_{3(s)} + SiO_{2(s)} + 2OH^-{}_{(aq)}$$

However, bicarbonate will be regenerated through the reaction of CO_2 and OH^- as Eq. (2-26).

$$OH^-{}_{(aq)} + CO_{2(g)} \rightarrow HCO_3^-{}_{(aq)} \qquad 2\text{-}26$$

Thus, the bicarbonate concentration and pH of the solution would be remained constant, through the buffered role of additives. A chemical pre-activation technique is also suggested, prior to aqueous carbonation for kinetics enhancement. In this process, the Mg bond within the Mg silicate structure is weakened by changing the solution chemistry, and the liberation of metal ions would be enhanced accordingly [9]. O'connor et al. [126] provided an example of this activation technique through modifying the solution chemistry with (0.5 M $NaHCO_3$, 1 M NaCl), which dramatically increased the rate of olivine wet carbonation.

The kinetics of aqueous carbonation can be enhanced by thermal pre-treatment. As an example, a thermal pretreatment with the goal of enhancing the kinetics of serpentine and olivine feedstock aqueous carbonation, was designed by Shell, and named Shell's pure direct and flue gas technology [27, 28, 133]. In this technology, serpentine feedstock was activated under a high temperature of over 600 ºC for one hour, then was ground to increase the surface area and reduce the particle size of reactive powders. Finally, the powders were carbonated through reaction with pure CO_2 gas. In a variation of same technique, pre-ground and activated serpentine was milled under the flue gas medium, at moderate temperature. The flue gas was

dissolved in an aqueous solution, and then the reactants were directed to the precipitation chamber for the final carbonation reaction.

2.2.6 Products of Mineral Carbonation

Various types of carbonated products can be formed during the mineral carbonation process, including both hydrous and anhydrous carbonates. Anhydrous carbonates are much more appealing than hydrous ones, as a result of their higher storage capacity and thermodynamic stability making possible the goal of long term CO_2 storage [3, 6, 75]. However, whether the carbonation process proceeds to the formation of hydrous or anhydrous carbonate is controlled by the carbonation conditions, including carbonation temperature and pressure. It may also be affected by the kinetics of the precipitate phase formation [79, 134-136][9].

2.2.7 Analysis of Carbonated Products

2.2.7.1 Structural Analysis

The products of carbonation reaction can be analyzed using structural analysis techniques as follows [137-139][10].

X-Ray diffraction (XRD): A non-destructive technique, designed based on the constructive interference of monochromatic X-rays and a crystalline sample, which is capable of detecting crystalline phases, levels of crystallinity, crystallite size, etc.

[9] A comprehensive study on directed carbonation process and formation of precipitates is presented as Chapter 5.

[10] The application of analytical methods and the analytical calculation equations are explained in more detail, in Chapter 3, Chapter 4 and Chapter 5, where the intended analysis technique is applied in the flow of research.

Scanning Electron Microscopy (SEM): An electron microscopy technique, designed based on the interaction of atoms and a high-energy focused electron beam, to investigate the morphology, particle size, etc.

Brunauer–Emmett–Teller (BET): An analytical technique, based on the theory of physical adsorption of gas on the surface of adsorbent materials, where the amount of adsorbate gas corresponding to a monomolecular layer on the surface is measured to calculate surficial parameters such as specific surface area, pore size, pore volume, etc.

2.2.7.2 Thermal Analysis

Carbonated materials can be tested in a DSC/TGA device in the thermal range that exceeds the decomposition temperature of carbonated products, while the decarbonation properties achieved in DSC and TGA (decarbonation peak in DSC and mass change as a result of decarbonation in TGA) are monitored for calculation of the carbonation extent or kinetics of carbonation. As will be discussed in Chapter 5, the products of the carbonation process may be either hydrous or anhydrous magnesite, depending upon the carbonation condition (temperature and pressure) and, reaction pathway and also water steam availability [19, 105, 117]. The thermal properties of two commonly forming hydrous magnesite (hydromagnesite ($3MgCO_3.Mg(OH)_2.3H_2O$) and nesquehonite ($MgCO_3.3H_2O$)), that form during $Mg(OH)_2$ carbonation, are addressed as

Table 2-6 [140]. The possibility of formation of either hydrous carbonated compound is determined by considering the reaction parameters and barriers. Decarbonation reaction of $MgCO_3$ (Eq. (2-27)) is of the most important reactions that needs to be considered, in order to measure the performance of directed precipitation, as is discussed in chapter 5 . Thermal analysis of carbonated products is capable of defining the carbonation reaction efficiency and mass concentration of different formed products during the process[11].

[11] The calculation methods and analysis approaches are discussed in Chapter 5.

$$MgCO_3(s) \longrightarrow MgO(s) + CO_2(g) \qquad 2\text{-}27$$

Table 2-6. Thermal reaction of hydrous Mg-carbonates (hydromagnesite and nesquehonite)[140].

Hydromagnesite ($3MgCO_3.Mg(OH)_2.3H_2O$)						
References	Temperature interval					
	200-300	300-400	400-500	500-600	600-700	Other reactions
Beck (1950)		375	440	565	600	510
		Dehydration	Dehydroxylation	Decarbonation	Decarbonation	Crystallization of MgO
Lauer et al. (2000)	296	-	426	548	-	511
	Dehydration	-	Dehydroxylation	Decarbonation	-	Crystallization of magnesite
Monioya et al. (2001)		320	420	530	-	-
Nesquehonite ($MgCO_3.3H_2O$)						
References	Temperature interval					
	200-300	400-500	500-600	600-700	Other reactions	
Beck (1950)	210-235	425	535-585	-	510	
	Dehydration	Dehydroxylation	Decarbonation	-	Crystallization of MgO	
Isveikov et al.(1964)	210-235	425	535-585	-	-	
	2 moles of water	1 mol of water	Decarbonation	-	-	
Queralt et al. (1997)		455	-	630	-	
		Dehydroxylation	-	Decarbonation	-	

Chapter 3

Investigation of Milling Energy Input on Structural Variation of Processed Olivine Powders for CO_2 Sequestration[12]

3.1 Overview

This part of research identifies the correlation between microstructure of mechanically processed olivine powders and the milling energy input, for an ultimate purpose of optimizing the ball milling approach for achieving the best CO_2 sequestration characteristics. Powders were processed in a high energy magneto ball mill. A variety of instrumental techniques such as scanning electron microscopy (SEM), Brunauer–Emmett–Teller (BET) and X-Ray diffraction (XRD) were utilized to characterize the particle size, specific surface area, pore volume, crystallinity and crystallite size of processes powders obtained with different levels of milling energy input. In each case, the variation of microstructural parameters with milling energy was compared for different milling devices extracted from the literature. Structural parameters of activated powders were correlated as a function of milling energy input, regardless of the ball mill type. The optimal range of milling energy input, expected to achieve the most suggested microstructure for CO_2 sequestration was found to be about 55 kJ/g.

3.2 Introduction

As discussed before, the ultramafic minerals are promising candidates for mineral sequestration because they are very rich in magnesium oxides which are bound with other

[12] The content of this chapter is published as:

Atashin, S., Wen, J.Z., Varin. R.A. (2015). Investigation of milling energy input on structural variation of processed olivine powders for CO_2 sequestration. *Journal of Alloys and Compounds*, 618:555-561.

oxides in a silicate matrix [11]. Among these ultramafic minerals, olivine (magnesium silicate) is known to be one of the most ideal reactants for investigating CO_2 sequestration as it is an abundant natural mineral with a high carbonation efficiency [3, 12]. Although the CO_2 mineralization process is thermodynamically favorable, the rate of reaction is usually very slow and it is not industrially feasible without pretreatment [12, 13, 86]. Direct carbonation of solid olivine can be performed in dry CO_2 gas. In a dry process direct gas/solid reaction occurs as described by Eq. (2-3) [9, 23]. This reaction could be accelerated in the presence of water steam, as it activates the olivine surface by producing $Mg(OH)_2$ as an intermediate product which reacts with CO_2 to produce $MgCO_3$ (Eq. (2-12)) [12].

Alternatively, carbonation of olivine can also be carried out through wet (aqueous) processes. Wet carbonation includes dissolution of CO_2 in water and creation of carbonic acid (H_2CO_3) which reduces the pH of medium (Eq.(2-4)). Olivine is dissolved in an acidic medium and Mg^{+2} is liberated from the mineral matrix by H^+ (Eq.(2-7)). Subsequently, the Mg^{+2} ions react with bicarbonate (HCO_3^-) and precipitate as magnesite ($MgCO_3$) (Eq. (2-6)) [9, 23]. Dissolution of olivine (magnesium silicate) (Eq.(2-7)) is known to be an important step that determines the reaction rate and improves the total kinetics of carbonation process [9, 23, 31]. Structural parameters of minerals can also control the dissolution rate of minerals. As an example, the dissolution rate of forsterite could be affected by specific surface area (SSA) as well as its reactive surface sites [25]. Also, another research on the effect of crystallinity on the dissolution rate of SiO_2 shows that the rate limiting factor in dissolution of SiO_2 is breaking the Si-O bond and thus amorphization can improve the kinetics of dissolution of minerals (e.g. olivine) as it causes disordering which weakens the Si-O bond resulting in less resistance to dissolution [129].

In the literature several pretreatment methods have been developed to accelerate the rate of mineralization including the thermal activation, chemical activation, use of additives, combined high temperature – high pressure processes, and mechanical milling [23]. Mechanical milling (or ball milling) improves the kinetics of mineralization, by modifying the structure and reactivity of minerals [3, 8-10, 13, 14, 23, 25, 31, 54, 58, 134, 141]. It changes

the microstructural parameters of minerals such as the particle size, specific surface area, crystallinity and crystallite size, resulting in a high level of structural disordering which facilitates CO_2 sequestration [54, 86]. Thus, the investigation of the effect of milling parameters on the microstructure of minerals is necessary to optimize the activation process.

Several researchers have evaluated the influence of milling conditions on structural properties. Haug [23] investigated the effect of mechanical milling on olivine microstructural characteristics such as the particle size, specific surface area and crystallinity. It was reported that the effect of different milling processes on the carbonation properties of olivine samples are significant when a planetary mono mill, laboratory ball mill, Hicom 15 mill, and attritor mill were utilized. In particular, Haug [23] compared the conversion percentage after direct wet carbonation for 2h of olivine samples that were initially ball milled in a Fritsch Pulverisette 6 mill. The conversion percentage was calculated by considering the molar ratio of precipitated carbonate ((Mg, Fe) CO_3) to available Mg and Fe (Fe, Mg) in olivine. They reported that the conversion percentage increased from 25 to 32% with the increase of milling time from 10 to 60 min. They suggested a correlation between the amount of amorphization and dissolution rate.

In another study by Kleiv and Thornhill [141], the effect of structural changes on reactivity of mechanically milled olivine powders was evaluated. Mechanical milling was performed by a planetary mono mill and the effect of structural disordering on the increase of olivine powders reactivity was analyzed using XRD analysis [141]. Based on this study, relative to the samples that were milled for 1 min, the 60 min milling duration increased the dissolution rate by a factor of 9.0 [141]. The authors claimed that the observed dissolution rate was correlated to SSA. The influence of ball milling was also investigated in a planetary mono mill running at 450 rpm and the reactivity of samples was compared after 6h carbonation under ambient temperature and 60 bar pressure. In that study, the effect of mechanical milling on the increase of material's affinity for CO_2 sequestration was identified by Turianicová et al. [142]. They investigated both dry milled and unmilled samples after wet carbonation and reported no trace of carbonation on unmilled samples while the samples that were mechanically milled for 30 min

before carbonation showed a clearly visible carbonate peaks as evidence of CO_2 sequestration [142]. Unfortunately, Turianicová et al. [142] did not provide any specific correlation between the enhanced wet carbonation and microstructural parameters brought about by ball milling. Other researchers also reported [130, 131] that the wet/dry carbonation rate was increased by mechanical milling. Although a number of investigations have been performed to study these structural variations occurring as a result of mechanical milling, a comprehensive study which correlates this variation with the milling energy input is still lacking.

In this phase of research study, the olivine powders were processed in a magneto ball mill and structural changes were studied as a function of milling energy input. The ball milled olivine powders were characterized using scanning electron microscopy (SEM), X-ray powder diffraction (XRD) and the Brunauer–Emmett–Teller analysis (BET) methods to evaluate the particle size, specific surface area, pore volume, crystallinity (%) and crystallite size. The main purpose of this research was to identify a quantitative correlation between the milling energy input and structural variations. This was expected to be used as a comprehensive factor for most mechanical activation processes, regardless of the milling type, considering that, for a specific milling mode and ball to powder mass ratio, milling energy input per unit mass of powder is the single factor that includes all the other effective parameters such as mill geometry, milling time etc. For this purpose, structural changes in the milled samples were examined as a function of milling energy input. The derived trend of each property's variation was then used, by comparison with other reported milling types, to find the correlation between milling energy input and microstructural parameters of processed olivine samples.

The outcome of this study can result in determining critical parameters as the process controlling factors for optimizing olivine structural activation and estimating the milling energy input range which could be applied for CO_2 sequestration experiments in the future experiments.

3.3 Experimental

As received olivine powders were supplied by READE Advanced Materials, China. The bulk chemical composition of the olivine samples, before ball milling, was analyzed by means of energy-dispersive X-ray spectroscopy (EDX) using a Zeiss ULTRA Plus Scanning Electron Microscope equipped with a calibrated Pegasus 1200 energy-dispersive X-ray Spectroscopy (EDX) analyzer which revealed the olivine formula of (Mg1.842, Fe0.158) SiO_4 with approximately 92 mol% forsterite (Mg_2SiO_4) and 8 mol% fayalite (Fe_2SiO_4).

Mechanical processing (ball milling) of olivine powders was implemented by controlled mechanical milling (CMM) in the magneto ball mill (Uni-Ball-Mill 5 manufactured by A.O.C. Scientific Engineering Pty Ltd., Australia) [143-145]. In this particular ball mill the milling modes with varying milling energy input can be achieved by using one or two strong NdFeB magnets, changing their angular positions and changing the number of hard steel balls in a milling vial. Milling experiments were conducted in a stainless steel vial, operating under the impact mode at 200 rpm.

Four 25 mm steel balls of 65 g mass each were used for grinding. The total mass and the radius of the vial were 4030 g and 75 mm, respectively. Milling energy was adjusted by controlling milling time, while the other milling parameters such as the ball to powder mass ratio, number of balls, milling mode, RPM and mass of powder were fixed. Details of milling energy variation as a function of milling time are explained in section (3.4.1). Figure 3-1, shows the actual image of ball milling device that was used, in the current research.

The SEM micrographs were obtained with the secondary electron detector using Zeiss ULTRA Plus Scanning Electron Microscope with the voltage of 10 kV. Samples were sputter coated with a thin layer of gold prior to SEM imaging to provide a conductive surface. Gold sputtering was performed via a UHV sputter system with the current of 20 mA and the duration of 139 s. SEM images were examined using an image processing and analysis program (Image J, Version 1.47 V, developed at the National Institutes of Health, USA) [146]. The procedure of particle size measurement using SEM micrographs is explained in Appendix A.

The X-ray diffraction (XRD) patterns were collected by a Bruker D8 diffractometer using a monochromated CuKa1 radiation (k = 0.15406 nm) with the accelerating voltage of 40 kV and current of 30 mA. Diffraction data were recorded in the range of $15^\circ < 2\Theta < 70^\circ$ with a step size of 0.02 and the rate of 1.2° min^{-1}. A custom made brass holder with a Cu plate for powder support containing an X-ray transmittable Kapton window was used for XRD studies. An XRD pattern of LaB_6 sample, which was used to eliminate the instrumental peak broadening, was obtained in the same way as other samples with the identical XRD facility and method of analyzing.

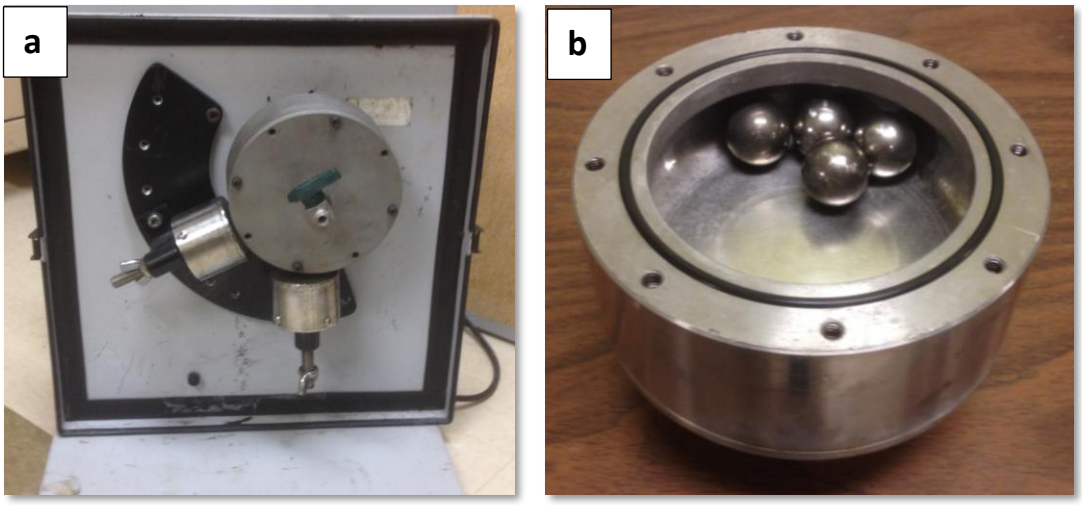

Figure 3-1. a) Magneto ball mill (Uni-Ball-Mill 5 manufactured by A.O.C. Scientific Engineering Pty Ltd, Australia). b) Stainless steel vial with radius of 75 mm containing steel balls with radius of 12.5mm.

This approach is suggested by the National Institute of Standards and Technology as a standard for powder diffraction [147, 148]. The XRD patterns were further fitted to the Pseudo–Voigt line shape function as a convolution of Cauchy (Lorentz) and Gaussian functions [148, 149] and were analyzed using the Materials Data Inc. Jade v.5 software.

The specific surface area (SSA) of powders was determined through nitrogen adsorption at 77 K based on the Brunauer–Emmett–Teller (BET) method using the surface area and pore size analyzer from Micromeritics ASAP 2020 Accelerated Surface Area and Porosimetry Analyzer. The measurements were performed after a degassing treatment at 50 ˚C. The reported SSA data were calculated based on 5 points BET method.

3.4 Results and Discussions

3.4.1 Calculation of Milling Energy Input

Milling energy is known as one of the most effective parameters to control structural properties of materials [130, 131, 150]. In order to investigate the effect of milling energy input on the microstructural parameters of mechanically processed olivine powders, four different milling energy levels were applied during ball milling and the microstructural characteristics of as processed powders were examined.

The total amount of energy input which was transferred to olivine powders during ball milling was calculated using the model proposed by Parviz and Varin [151] who analyzed the shear and impact energies for the magneto ball mill used in this study. The milling energy was formulated to be a function of the working distance (WD), ball-to-powder mass ratio (BPR), milling mode, number of balls and positions of the magnets. All experiments in this study were completed with the impact mode applied using two magnets, located at the six and eight o'clock positions, and four balls which is designated as IMP68-4B [151]. The working distances were 10 and 2 mm for magnets at six and eight o'clock, respectively, and the ball to powder mass ratio was 50. For the employed IMP68-4B milling mode [151] with BPR = 50 the corresponding mass of olivine powder was equal to 5.2 g. For this particular milling mode, according to the model presented in [151], the amount of energy input that was injected into the powders (designated QP in [151]) was calculated to be 143.4 kJ/h. The milling energy input per gram hour (gh), designated QTR in [151], was 27.6 kJ/ gh. Thus the milling time was the only variable for obtaining a desired amount of milling energy input. Four different milling

durations, namely, 0.5, 1.0, 2.0 and 6 h, respectively, were applied in this study and the respective milling energy inputs were calculated following the model reported in [151]. Table 3-1 summarizes the total amount of energy input which was injected into the olivine powders as a function of milling time.

3.4.2 Effect of Milling Energy Input on Particle Size

Figure 3-2 illustrates the SEM images of as received and ball milled olivine samples. The former (Figure 3-2-a) were characterized by a bigger average particle size and irregular shapes while the milled powders (Figure 3-2-b to e) were mostly fine and rounded which resulted from extensive fracture and erosion during milling.

Table 3-1 summarizes the results of particle size measurements with standard deviations (±std) which were obtained through analysis of SEM images using the image processing software. One SEM image contained about 100 particles whose sizes were analyzed. Since in the previous studies [23, 24, 152] their authors used a median D50 as a measure of particle size, that value was also calculated and is shown in Table 3-1.

Although the average size of particles is generally reduced with an increase in the milling energy input (increasing milling time), the extent of agglomeration slightly increases and becomes noticeable after one hour of milling (27.6 kJ/g energy input) in Table 3-1. This rather mild agglomeration effect is in agreement with the observation of other researchers, who investigated the effects of milling on the particle size or shape of olivine powders, using different types of milling facilities such as planetary [142] and attritor mills [152].

The average particle size data from Table 3-1, obtained in this work, are plotted in Figure 3-3 as a function of milling energy input. For comparison, the D50 results reported in the literature [23, 24, 152] for other type of mills are also included in the plot. The D50 median size data for planetary mill and Hicom 15 nutating batch were estimated using the cumulative distribution curve, suggested by Haug et al. [23, 24]. The milling energies reported in the

literature were originally presented in different scales in the corresponding papers so we converted them to a uniform unit of (kJ/g) for easier comparison.

It is clearly seen in Figure 3-3 that as a result of intense particle fracturing, the particle size (average or median) initially decreases rapidly to about 4 μm with milling energy input increasing to 13.8 kJ/g and then slightly increases to 13±6 μm due to agglomeration. A comparison with the data collected from the literature in Figure 3-3 shows the same particle size vs. energy trend as obtained in this study which clearly confirms the dependency of particle size on the milling energy input, regardless of the type of mill used.

Table 3-1. Summary of milling energy input and microstructural parameters for ball milling with the milling energy input QTR=27.6 kJ/gh [151].

Sample number	Milling time (h)	Injected milling energy input (kJ/g)	Mean particle size±std (μm)	Median particle size D50 (μm)	SSA±std (m^2/g)	Total pore volume±std (cm^3/g)	Crystallite size ±std (nm)		Structural strain (Williamson –Hall)
							Scherer	Williamson-Hall	
1	0	0.0	92 ±41	82	1.12 ±0.05	0.003 ±0.000	56.50 ±7.1	144.76 ±0.00	1.25×10^{-3}
2	0.5	13.8	4 ±1	4	8.69 ±0.57	0.037 ±0.002	33.08 ±3.42	72.38 ± 0.00	2.00×10^{-3}
3	1.0	27.6	13 ±6	13	8.16 ±1.16	0.034 ±0.001	25.77 ±4.95	72.38 ±0.00	3.50×10^{-3}
4	2.0	55.2	6 ±3	6	6.59 ±0.04	0.029 ±0.002	20.71 ±5.13	24.13 ±0.01	1.20×10^{-3}
5	6.0	165.6	8 ±4	6	7.07 ±0.02	0.025 ±0.001	15.56 ±3.55	9.52 ±0.01	0

So, neglecting the type of mill, milling energy acts as a determining factor and controls the particle size. According to Figure 3-3, the optimal value of milling energy input resulting in the minimum particle size which could be favorable for CO_2 sequestration is around 13.8 kJ/g as shown by an arrow. In this range of milling energy (0 to 13.8 kJ/g), particle size decreases continuously with milling energy.

Specific surface area (SSA) was measured from the BET analysis as described earlier and the results are included in Table 3-1. In order to identify the effect of milling energy input on

SSA the graph of SSA vs. milling energy input is plotted in Figure 3-4 which also includes the data reported from different types of milling experiments (Fritsch Pulverisette planetary ball mill 1 [23], Fritsch Pulverisette planetary ball mill 2 [152], Hicom 15 nutating mill [24], Molinex PE 075 nutating mill [152], laboratory ball mill [24] and attrition milling [152]).

As can be seen, regardless of the mill type, in all reported cases, SSA initially increases with increasing milling energy, reaches a maximum value and then decreases to a varying extent depending on the mill type. The optimum range of milling energy input which results in the maximum SSA value is marked by the dashed line at the energy value of 13.8 kJ/g and seems to be consistent for all types of mills. In general, SSA increases within this range of milling energy. Ball milling in a magneto mill in the present work is apparently very effective because the SSA values increase from the initial value of 1.12 m^2/g to reach about 8.7 m^2/g for the energy input of 13.8 kJ/g (Table 3-1). Also the slight drop in SSA for milling energies larger than about 13.8 kJ/g in the magneto mill is relatively shallow and the SSA values are much larger than those for any other type of mill. This behavior is very beneficial for offering the desired characteristics for dry CO_2 sequestration by olivine.

Since one would expect that SSA is directly proportional to the particle size both parameters should behave in a similar manner vs. milling energy input. However, if one compares Figure 3-3 and Figure 3-4 a slight drop in SSA for milling energies larger than about 13.8 kJ/g is observed in Figure 3-4 for SSA which is not observed in Figure 3-3 for particle size. That means that SSA is not the sole function of particle size but also depends on another factor which influences its behavior as a function of milling energy input.

In order to find a quantitative factor responsible for a SSA decrease after reaching a milling energy of 13.8 kJ/g, as observed in Figure 3-4, the total pore volume was estimated from the BET measurements [153] as a single point adsorption total volume of pores, less than 1855.565 Å width at P/P_0= 0.989470121 where P is the partial vapor pressure of adsorbate gas in equilibrium with the surface at 77.4 K (b.p. of liquid nitrogen) and P_0 is the saturated pressure of adsorbate gas.

The calculated values are included in Table 3-1 and plotted in Figure 3-5 as a function of the milling energy input. It is clearly seen that the total pore volume increases quite dramatically with increasing milling energy input up to 13.8 kJ/g and then slightly decreases for the larger milling energy inputs. This behavior is identical to the behavior of SSA as a function of milling energy input in Figure 3-4. Therefore, the second microstructural parameter that influences the SSA behavior vs. milling energy, besides the particle size variation, is the total pore volume that starts decreasing above the energy input up of 13.8 kJ/g most likely due to enhanced compaction of agglomerated powder particles. A lower porosity makes the powder particles surfaces "smoother" reducing their SSA. In other words, for the powders which were ball milled employing the milling energies larger than 13.8 kJ/g, their surface roughness decreased and SSA dropped as a result.

3.4.3 Effect of Milling Energy Input on Crystallinity/Amorphization

XRD patterns related to different milling energies show a general reduction in a peak height and broadening of the peaks with increasing milling time (Figure 3-6). The same effect of milling on XRD curves was also observed by Kleiv and Thornhill who investigated the influence of planetary milling time on XRD peaks of olivine powders [141].

In order to characterize the micro-structural characteristics developed during the mechanical processing of powder samples, the changes in the crystallinity (%) and crystallite size were investigated with varying milling energy input. Milling energy influences the XRD peaks through the reduction of peak intensity and increase peak broadening and background level. Crystallinity is a factor which presents the combined effect of these parameters [23, 24, 148, 152] as shown Eq. (3-1).

$$Crystallinity(\%) = \left(\frac{U_O}{I_O} \times \frac{I_x}{U_x}\right) \times 100 \qquad 3\text{-}1$$

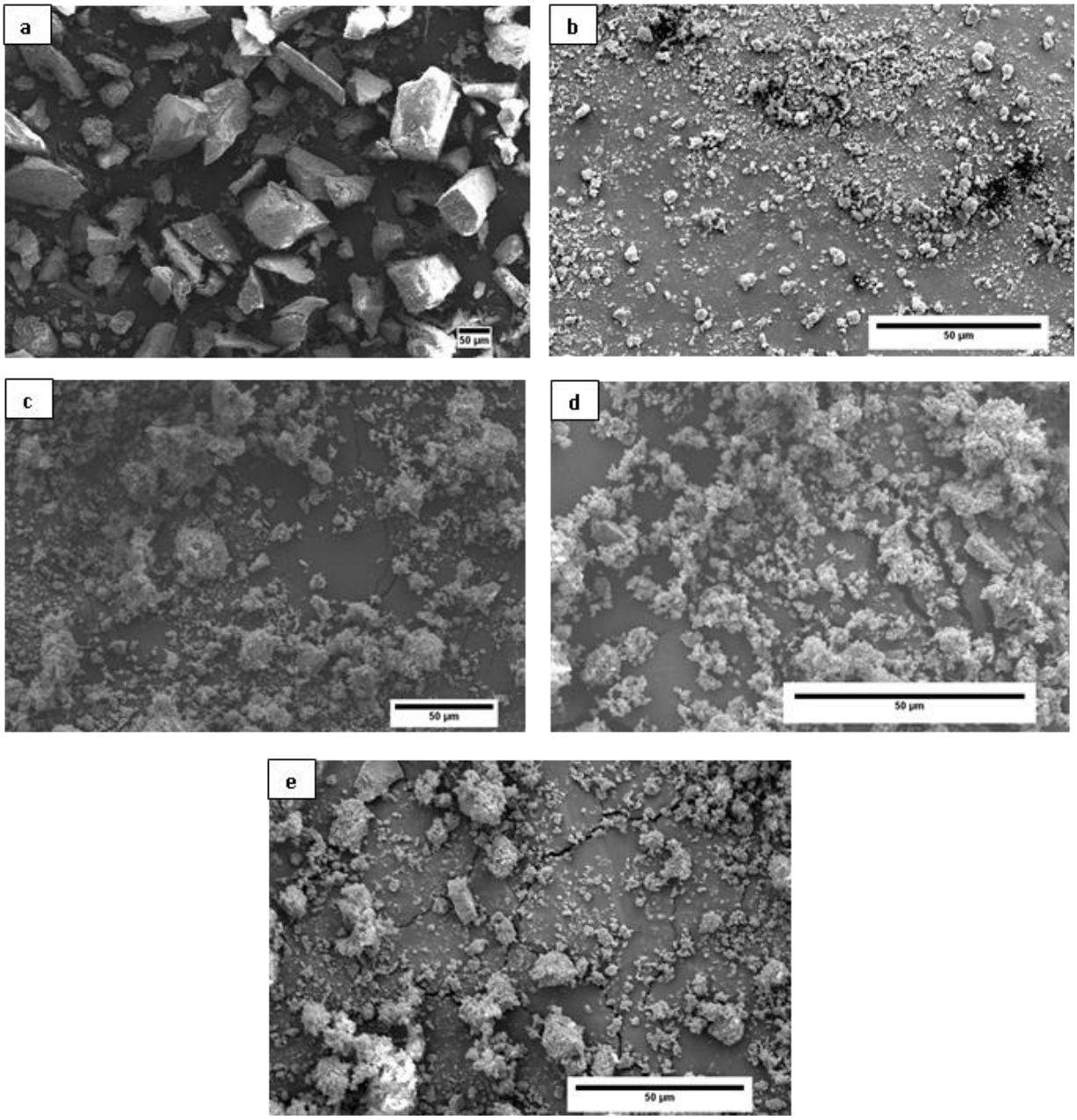

Figure 3-2. SEM micrograph of olivine. a) Non activated olivine powder, b) olivine powder after 30 min of BM, c) Olivine powder after 60 min of BM, d) olivine powder after 120 min of BM and e) olivine powder after 360 min of BM.

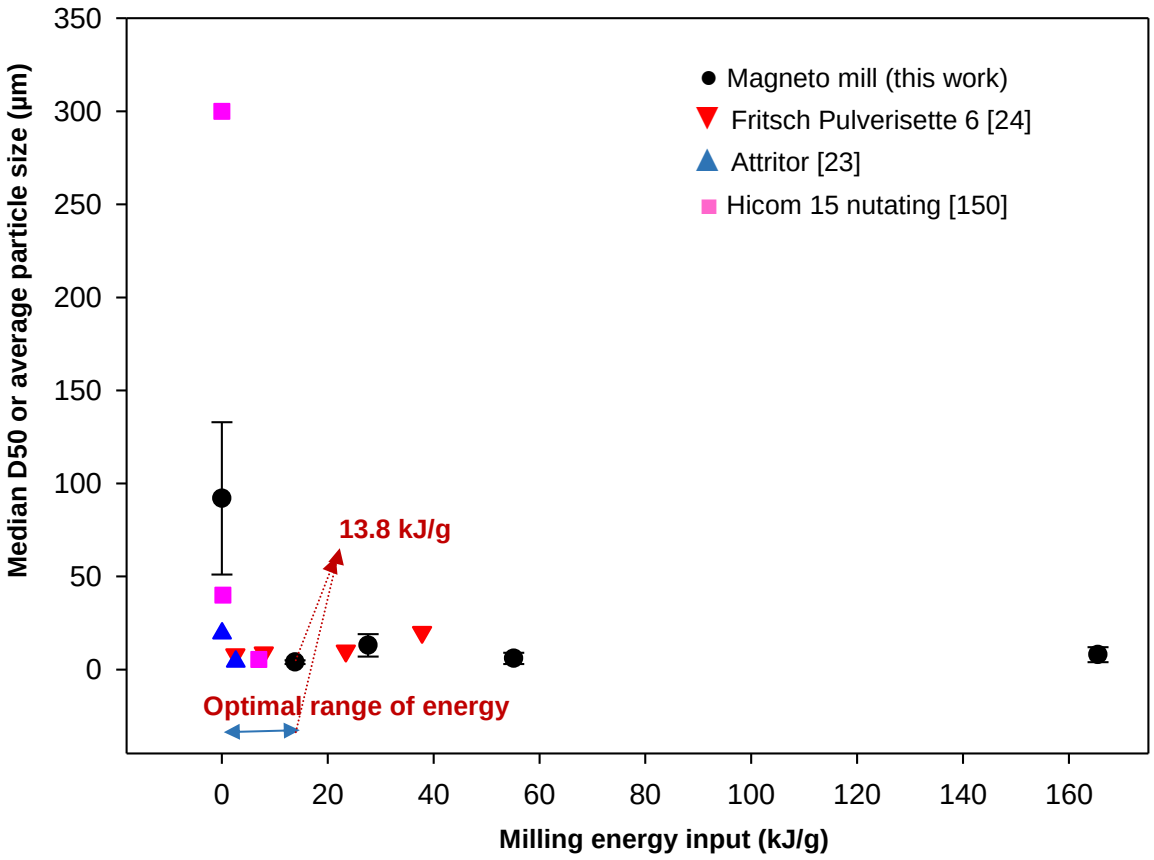

Figure 3-3. Particle size variation as a function of milling energy input. The data points for a magneto ball mill in this work are presented as the average values with corresponding standard deviations. The median data point for the Fritsch Pulverisette 6 is from [24], for Hicom 15 nutating batch mill from [23] and for attritor from [150].

In the same way, the amount of amorphous phase (amorphization) could be calculated using Eq. (3-2).

$$Amorphization(\%) = 100 - crystallinity(\%) \qquad 3\text{-}2$$

U_0 and U_x are background values of the reference and activated samples at the intended peak, respectively. I_0 and I_x are the integral peak area above the background of intended peak in reference and activated sample, respectively. In both cases, non-activated olivine powder is taken as a reference.

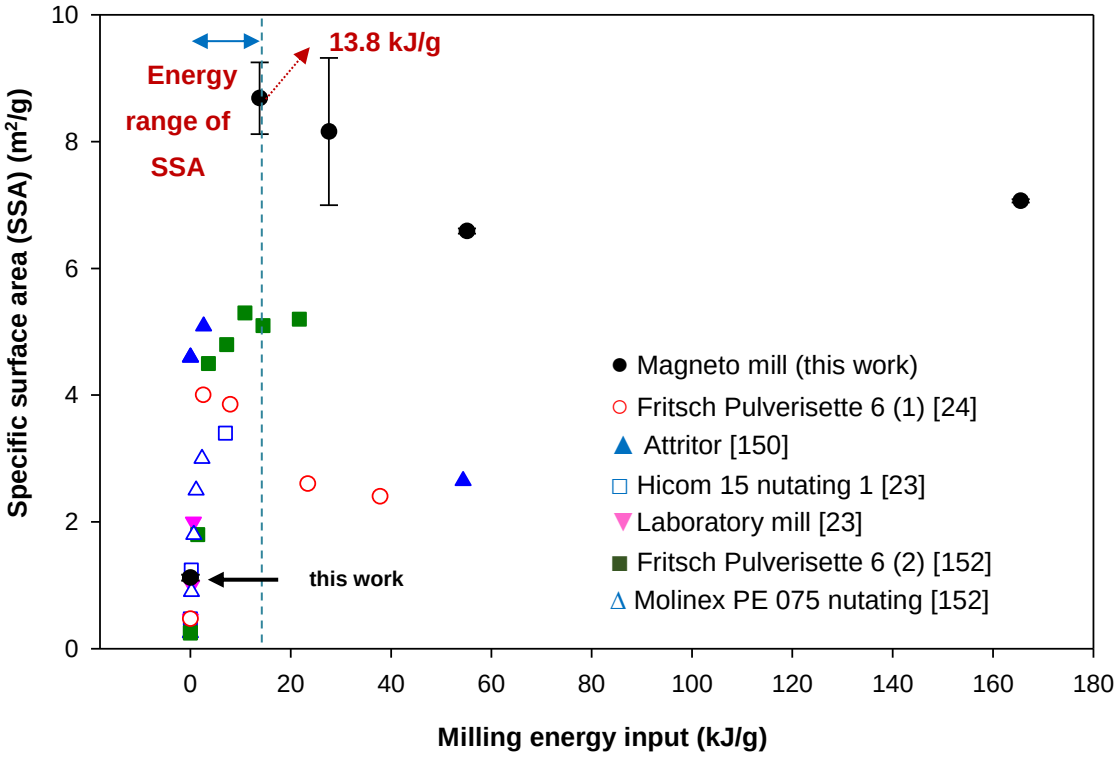

Figure 3-4. Specific surface area (SSA) variation as a function of milling energy input. The data points for a magneto ball mill in this work are presented as the average values with corresponding standard deviations. The data for the Fritsch Pulverisette 6 (1) is from [24], for Hicom 15 nutating is from [23], for Fritsch Pulverisette 6 (2) is from [152], for Molinex PE 075 nutating mill is from [152], for attritor mill from [150] and for laboratory mill from [23].

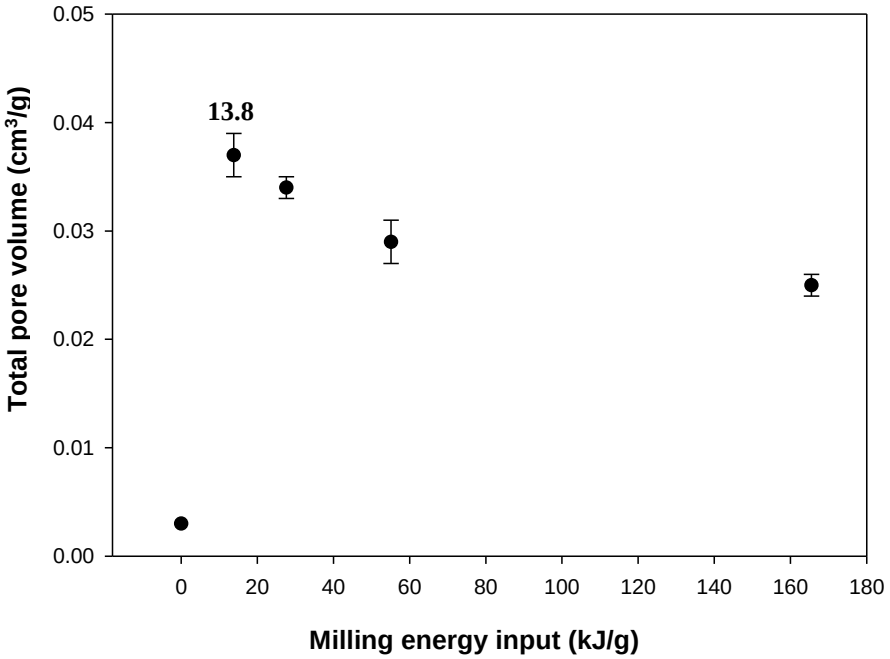

Figure 3-5. Total pore volume as a function of milling energy input for olivine powders milled in a magneto ball mill in this work.

Since the previous studies reported in the literature [23, 24, 152] used the sole peak at $2\theta=17.2^{o}$ (020) to estimate crystallinity we used the same peak in the present work for estimating crystallinity. Crystallinity change as a function of energy input for the magneto mill used in the present work, as compared to other types of mills reported in the literature, is presented in Figure 3-7.

The trend of crystallinity vs. milling energy input that is achieved in a magneto ball mill is compatible with the data that were collected from the literature which confirms the controlling role of milling energy on the crystallinity variation, regardless of the mill type. According to Figure 3-7, there is not much obvious variation in crystallinity beyond milling energy of 27.6 kJ/g. This point is marked by an arrow in Figure 3-7.

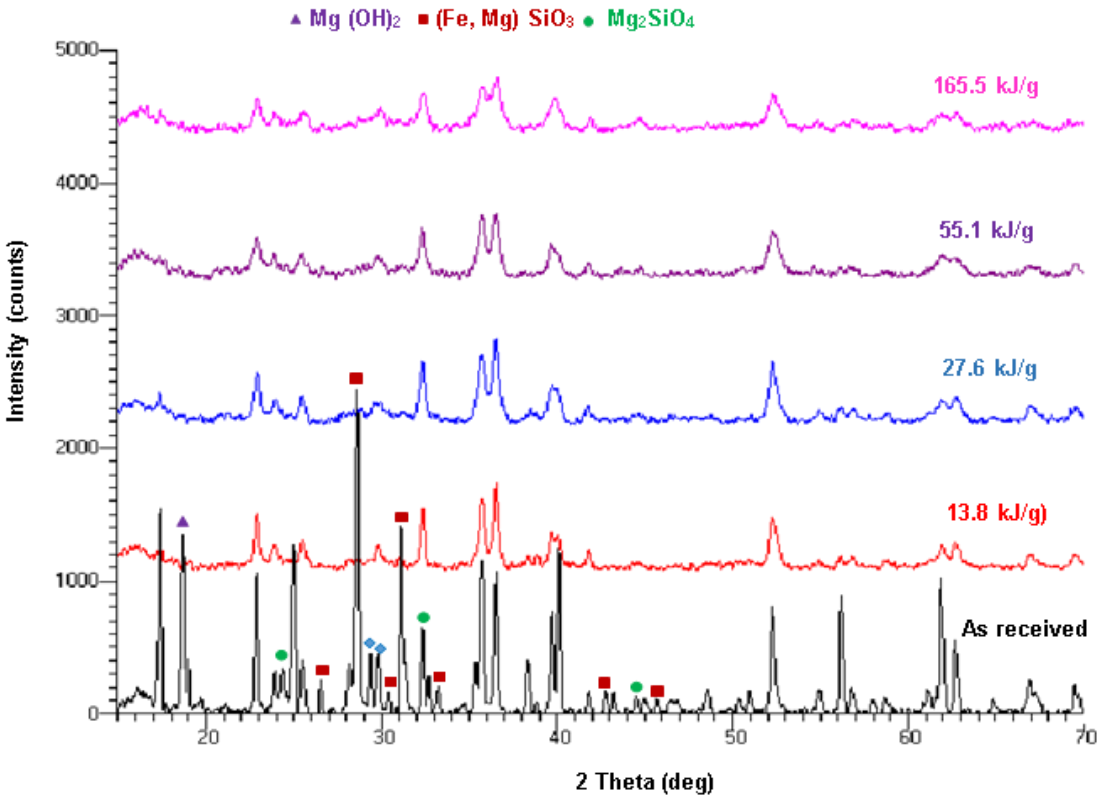

Figure 3-6. XRD patterns of olivine samples ball milled at different milling energy input.

3.4.4 Effect of Milling Energy on Crystallite Size

Crystallite size for as received and mechanically processed samples was calculated from XRD peaks through two separate methods of Scherrer and Williamson-Hall [154, 155], respectively. In both cases, the 2θ peaks of 22.9° (021), 32.3° (130), 35.7° (131) and 36.5° (112) were considered in calculations and crystallite size was measured by the analysis of XRD profiles based on the peak broadening as a full width at a half- maximum (FWHM) factor. According to the Scherrer method, crystallite size is directly related to the XRD peak width of diffracted crystalline structure and this method is capable of accurately estimating the crystallite size of less than 100 nm [155]. Eq. (3-3) was used for the calculation of crystallite size by the Scherrer method [154, 155].

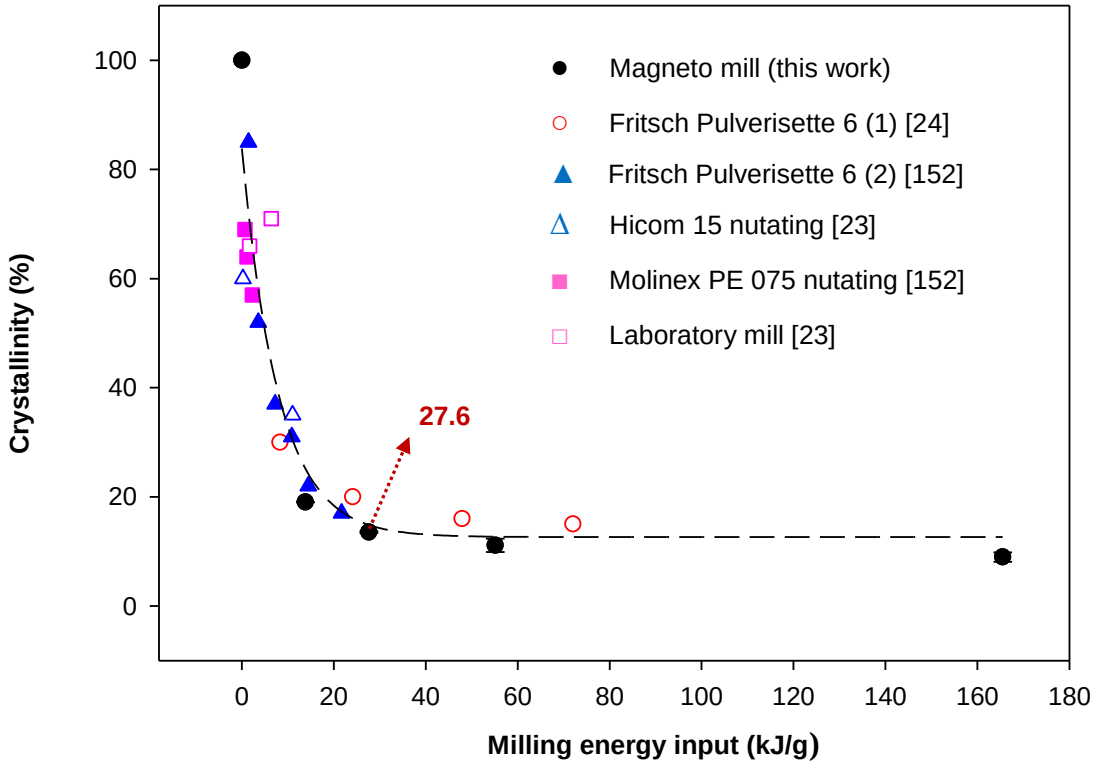

Figure 3-7. Crystallinity as a function of milling energy input. Data of Fritsch Pulverisette planetary ball mill 1 by Haug et al. [24], Hicom 15 nutating mill by Haug et al. [23], Fritsch Pulverisette planetary ball mill 2 by Balaz et al. [152], Molinex PE 075 nutating mill by Balaz et al. [152]and laboratory ball mill by Haug et al. [23] are presented.

$$L = \frac{0.94\lambda}{\beta(2\theta)\times\cos(\theta_0)} \qquad 3\text{-}3$$

Where, L is the average crystallite size, θ is a Bragg angle of the (hkl) diffraction plane, β(2θ) is the instrumental broadening-corrected 'pure' peak breadth obtained from the full width at a half maximum intensity (FWHM) of a diffraction peak and λ is the wavelength of X-ray radiation.

For the purpose of improving accuracy, the crystallite size was calculated using Eq. (3-4) for all five early observed 2θ peaks and the average values were compared. The crystallite size was also estimated using the Williamson-Hall method, which is a simplified integral breadth calculation method to evaluate both strain-induced broadening and size-induced broadening, using Eq. (3-4)[155].

$$\beta(2\theta)\mathrm{Cos}(\theta_0) = \frac{0.94\lambda}{L} + 4eSin(\theta_0) \qquad 3\text{-}4$$

Based on the Williamson-Hall equation (Eq.(3-4)), the crystallite size (L) was obtained from the intercept of "$\beta(2\theta)\mathrm{Cos}(\theta_0)$" vs. "$Sin(\theta_0)$". All of these 2θ peaks were considered in calculations of crystallite size for each milled sample, as well as the non-activated powder. Figure 3-8 presents the average crystallite size of specimens determined by both Scherrer and Williamson-Hall methods as a function of milling energy input.

Both methods predict the reduction of crystallite size with increasing milling energy, although the Scherrer estimate provides smaller crystallite sizes at lower energy levels. The main difference between the Williamson-Hall and Scherrer estimations originates from the structural strain, since the Williamson-Hall method considers the strain in the estimate while the Scherrer method doesn't [154, 155].

The Williamson-Hall and Scherrer curves start converging after 120 min of milling time (55.1 kJ/g). As the main difference in these methods is the inclusion of the milling strain in the Williamson-Hall method, the observed compatibility of these curves when the milling energy is above 55.1 kJ/g shows a negligible effect of milling strain for higher milling energies. Table 3-1 shows the crystallite size and amount of structural strain for as processed materials which were calculated based on the Williamson-Hall equation (Eq.(3-4)). According to Figure 3-8 there is not much variation in the crystallite size at the range of milling energies higher than 55.1 kJ/g and the structural strain is also negligible.

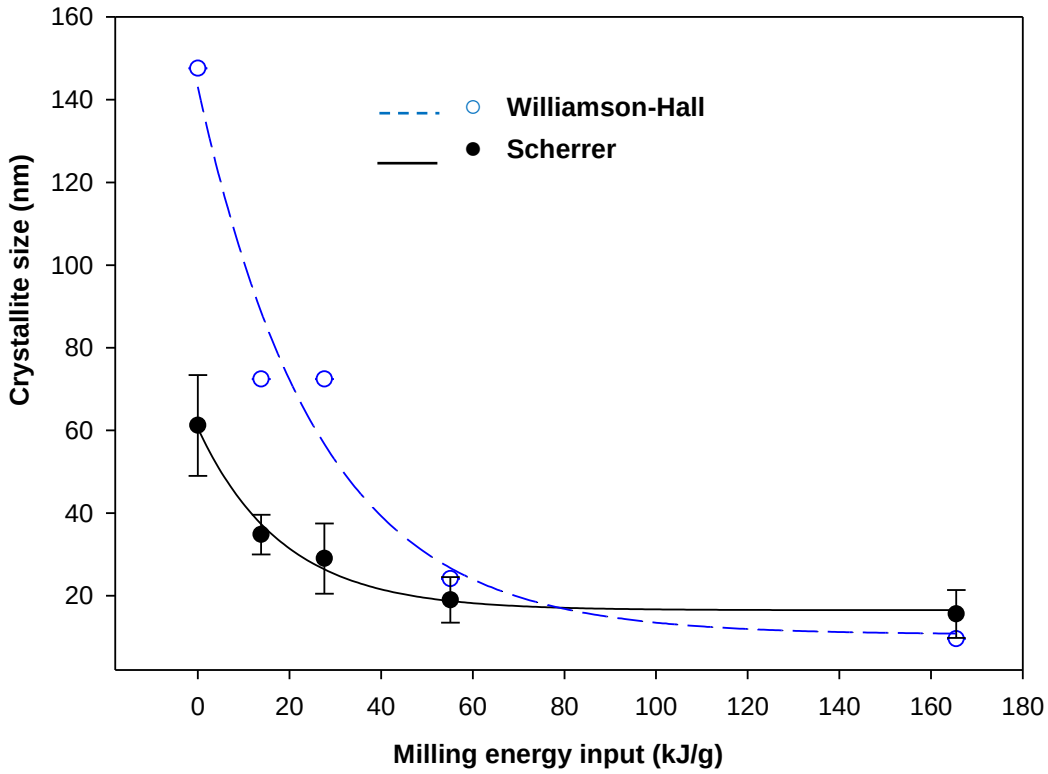

Figure 3-8. Crystallite size variations as a function of milling energy input in a magneto ball mill in this work. Fit lines are passed through the Scherrer and Williamson-Hall data points with R^2 of 0.954 and 0.989, respectively.

3.5 Summary

The following conclusions are made based on the correlations between the milling energy and the produced material properties.

1. Regardless of milling type, milling energy is found to be the determining factor controlling the structural parameters of ball milled olivine powders such as particle size, specific

surface area (SSA), pore volume, crystallinity percentage (amorphization) and crystallite size. These properties are known as the most essential parameters for CO_2 absorption capability of olivine. Hence, milling energy can control the CO_2 storage properties of activated olivine powders.

2. The particle size variation of activated olivine powders vs. milling energy input is found to be controlled by the competing events of fracture and agglomeration during ball milling. The optimal amount of energy (of those tested) to achieve the minimum particle size is around 13.8 kJ/g.
3. The SSA of olivine powders increases with increasing milling energy up to 13.8 kJ/g (of those tested) and subsequently slightly decreases most likely as a result in decreasing total porosity volume.
4. The total pore volume of milled samples increases with increasing milling energy up to the energy level of 13.8 kJ/g and subsequently slightly decreases, most likely, as a result of milling compaction and resulting reduction in surface porosity.
5. The crystallinity percentage of mechanically activated powders decreases with increasing milling energy input while the crystallinity percentage doesn't not show a considerable variation beyond the energy of 27.6 kJ/g.
6. The crystallite size shows a decreasing trend vs. milling energy input up to 55.1 kJ/g. In addition, the effect of structural strain on materials disorder is found to be negligible above this energy.
7. In summary, considering the optimal energies estimated from the behavior of all investigated structural parameters (particle size, SSA, total pore volume, crystallinity and crystallite size), the optimal range of milling energy input for the most suggested material characteristics for CO_2 sequestration via olivine powders is suggested to be in the vicinity of 55 kJ/g. Although SSA slightly decreases beyond this energy value due to decreasing pore volume (likely at the surface), it is still much larger than SSA values for any other type of ball mill reported in the literature.

Chapter 4

Optimizing Milling Energy for Enhancement of Solid State Magnesium Sulfate ($MgSO_4$) Thermal Extraction for Permanent CO_2 Storage[13]

4.1 Overview

Mineral carbonation of Mg-silicates via the indirect-dry route is among the most appealing technical approaches for permanent CO_2 storage. It brings about the possibility of recycling heat released during exothermic carbonation and it offers a higher rate of conversion through two separate stages: producing of reactive compounds, mainly $Mg(OH)_2$, through solid reactions between Mg-silicates and ammonium sulfates and subsequent carbonation of reactive compounds. Milling is essential to enhance the solid-state reaction rate and increase the conversion percentage. The milling energy, being the major energy consumption of the entire carbonation process, needs to be minimized without sacrifice of its activation purpose. This study was focused on enhancing the kinetics of solid-state magnesium sulfate ($MgSO_4$) thermal extraction from the solid-solid reaction of olivine ($(Fe, Mg)_2SiO_4$) and ammonium sulfate ($(NH_4)_2SO_4$), with optimized milling energy input. This process constitutes the first stage of $Mg(OH)_2$ production for indirect CO_2 storage purposes. The mechanical activation of reactants was achieved via a high-energy magneto ball milling with a controlled energy input. The variation of structural parameters such as the particle size, specific surface area (SSA), pore volume, and crystallite size and strain were characterized as a function of milling energy input and the correlation between stuructural factors and activation energy of extraction was

[13] The content of this chapter is published as:

Atashin, S., Wen, J.Z., Varin. R.A. (2016). Optimizing milling energy for enhancement of solid-state magnesium sulfate ($MgSO_4$) thermal extraction for permanent CO_2 storage, RSC Advances, 6: 68860 - 68869.

investigated. In addition, the variation in the apparent activation energy of solid-state extraction was examined as a function of milling energy. The optimal amount of milling energy input for increasing the reaction kinetics of $MgSO_4$ extraction was estimated to be about 27.6 kJ/g which causes around 34% reduction in the activation energy of $MgSO_4$ solid-state extraction.

4.2 Introduction

The indirect dry carbonation approach has been comprehensively studied which brings the advantage of storing the energy released during exothermic process to compensate a portion of total energy of carbonation, including the activation stage and utilizing the enhanced kinetics of indirect carbonation process [3, 29-31]. Mg-silicate mineral carbonation proposed by Nduagu et al. [32] is one of the most interesting and well referred indirect processes that is perceived as a closed loop, suitable for developing practical approaches of dry carbonation. The proposed carbonation approach, known as the ÅAU (Åbo Akademi University) process, includes extraction of magnesium hydroxide ($Mg(OH)_2$) for the later carbonation process, through the reaction of ammonium sulfate ($(NH_4)_2SO_4$) and Mg-silicate feedstock [13, 34-36]. Figure 4-1 shows a schematic representation of the ÅAU carbonation process, including the dry solid-state magnesium sulfate ($MgSO_4$) extraction, $Mg(OH)_2$ precipitation and subsequent $Mg(OH)_2$ dry carbonation [13, 33-36, 110].

Eq. (4-1) presents the extraction reaction of $MgSO_4$ from the mixture of solid (s) ammonium sulfate ($(NH_4)_2SO_4$(s)) and solid olivine (Mg_2SiO_4(s)) powders. This reaction usually occurs at elevated temperatures.

$$Mg_2SiO_4(s) + 2(NH_4)_2SO_4(s) \rightarrow 2MgSO_4(s) + SiO_2(s) + 2H_2O(g) + 4NH_3(g) \qquad 4\text{-}1$$

Solid-state (s) extraction of $MgSO_4$ in Eq. (4-1) is the rate limiting step in the process of $Mg(OH)_2$ formation. In order to accelerate this process, the mixture of ammonium sulfate and

olivine can be mechanically activated. The energy input for this activation, which should be minimized, corresponds to the optimal composition and microstructure of the ammonium sulfate and olivine mixture that results in the highest kinetics of $MgSO_4$ extraction and, subsequently, the largest production rate of $Mg(OH)_2$.

This research was complementary to our previous study on mechanical activation of olivine powders for CO_2 sequestration [156]. As indicated in Figure 4-1 the focus of this study was on optimizing the extraction of $MgSO_4$ as expressed by Eq. (4-1). The main objectives of this study were as follows:

1. To find the effect of milling energy input on structural parameters of the milled powders and to estimate the optimal milling energy input that results in the most suitable crystal microstructure, which improves the kinetics of desired solid-state extraction process.
2. To establish the optimal amount of milling energy for the enhancement of the kinetics of $MgSO_4$ solid-state extraction as a part of the ÅAU carbonation process.

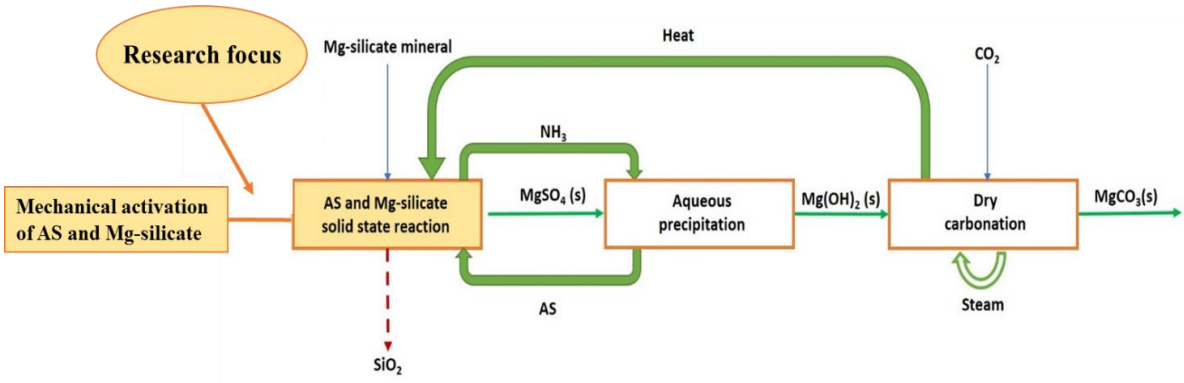

Figure 4-1. The ÅAU indirect carbonation approach, adapted from ref [110]. AS-Ammonium sulfate ($(NH_4)_2SO_4$); (s)-solid.

4.3 Experimental

Ammonium sulfate ($(NH_4)_2SO_4$) powders (AX 1385-1; 99.0% assay), supplied by EMD Millipore, and olivine ($(Fe, Mg)_2SiO_4$) powders, supplied by READE Advanced Materials, China, were used in this research. The chemical composition of olivine mineral was investigated prior to mechanical activation using energy dispersive X-Ray spectroscopy (EDX) with a Zeiss ULTRA Plus Scanning Electron Microscope equipped with a calibrated Pegasus 1200 EDS analyzer. The exact chemical formula olivine was $(Mg_{1.842}, Fe_{0.158})\ SiO_4$, showing an approximate combination of 92 mol% forsterite (Mg_2SiO_4) and 8 mol% fayalite (Fe_2SiO_4). Particle size distribution of olivine powders was obtained through the analysis of SEM images, using image processing software. SEM image containing about 100 particles was considered in particle size calculation, which resulted in the a d50 size of 82 μm (average particle size of 92±41 μm) as was also reported in Ref [156]. The particle size value of ammonium sulfate sample powder was calculated with the same method, which comes to d50 of 111 μm (average particle size of 117±22 μm).

Mechanical activation was performed using a high-energy magneto ball mill Uni-BallMill 5 [143-145] (manufactured by A.O.C. Scientific Engineering Pty Ltd., Australia). In this particular type of milling device, the milling modes with varying amount of milling energy were achieved using either one or two NdFeB magnets, as well as changing angular position and number of steel balls in the vial. All the experiments in this study were performed at the IMP68-4B setup representing impact mode using two magnets at 6 and 8 o'clock position. The working distance of six and eight o'clock magnets were 10 and 2 mm, respectively. All the milling runs were performed at approximately 200 rpm, by using four 25 mm steel balls of 65 g each and ball-to-powder mass ratio (BPR) of 50. The diameter and mass of vial was 75 mm and 4030 g respectively. The total amount of milling energy that was transferred to powders during ball milling process was calculated via Parviz and Varin model [151]. In this model, the value of injected milling energy was formulated as a function of BPR, milling time, milling mode, working distance (WD), number of balls and position of magnets. The readers can be referred to the reference [151] for more details. Varying milling times of 0, 30, 60, 90 and 120

min were applied with corresponding milling energy inputs of 0, 13.8, 27.6, 41.4 and 55.2 kJ/g, respectively.

The SEM micrographs were obtained via the secondary electron detector of LEO 1550 Zeiss SEM at 10 kV. All the samples were coated with a thin gold layer via a UHV spotter system with current of 20 mA for 139 seconds, to provide a sufficient connectivity. SEM images were analyzed using Image J, version 1.47 V, developed at the National Institutes of Health, USA, [146] for the particle size analysis. The procedure of particle size measurement using SEM micrographs is explained in Appendix A.

X-ray diffraction was performed using INEL XRG 3000 Powder Diffractometer XRD device. X-ray patterns were collected using monochromic Cu Kα1 radiation with the wavelength of 0.15406 nm, generated by accelerating voltage of 30 kV and current of 30 mA. Specific surface area (SSA) and total pore volume of the powders were measured using a Micromeritics ASAP 2020 Accelerated Surface Area and Porositometry Analyzer through nitrogen adsorption at 77 K. XRD patterns were utilized to calculate both crystallite/grain size and structural strain parameters using Williamson-Hall method (Eq.(3-4)) [155], which considers both strain-induced and size-induced broadening.

Based on Eq. (3-4) crystallite/nanograin size (L) and crystal strain (e) could be estimated from the intercept and slope of $B(2\theta)\cos(\theta_0)$ vs. $\sin(\theta_0)$ graph, respectively. The 2θ peaks at 23.1, 36.1, 39.2 and 62.6° were used for calculation of crystallite size and crystallinity. For the sake of comparison, crystallite size was also calculated via Scherrer method using Eq.(3-3) [154, 155] for all 2θ peaks as shown above.

Both SSA and pore volume parameters were measured via Brunauer–Emmett–Teller (BET) method [153]. The total pore volume was estimated using single point adsorption model and it represents the total volume of pores with a width size below 1855 Å at $P/P_0=0.99$ (P: Partial vapor pressure of adsorbate gas; P_0: Standard pressure of adsorbate gas in equilibrium with the surface at boiling point of liquid nitrogen).

The process of solid-state extraction of $MgSO_4$ from the mixture of olivine and ammonium sulfate was performed in a combined DSC/TGA thermal analyzer device (NETZSCH STA 449F3A-0918-M Jupiter), under argon atmosphere (Figure 4-2).

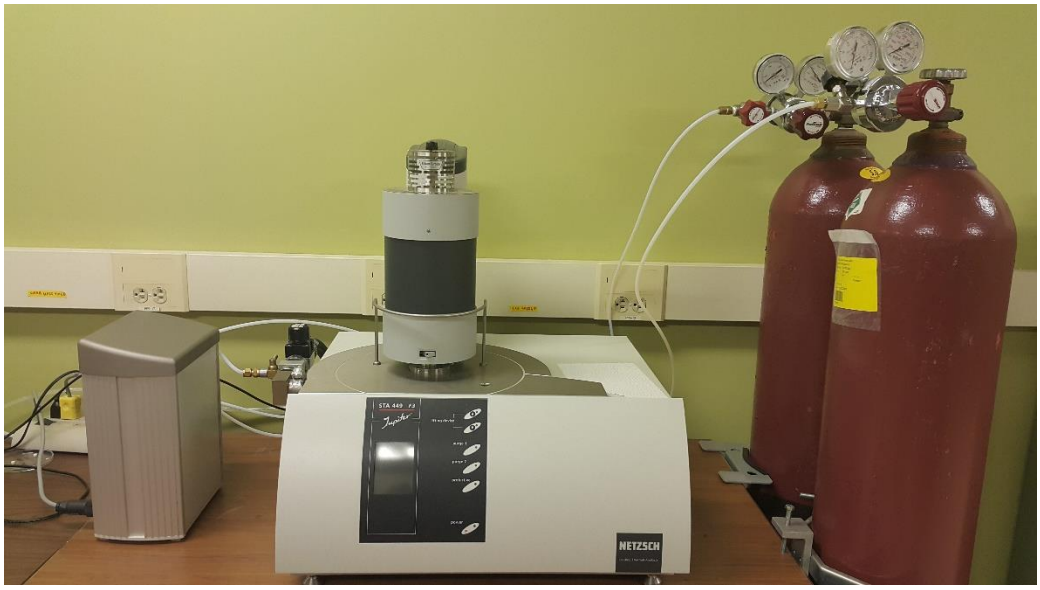

Figure 4-2. (NETZSCH STA 449F3A-0918-M Jupiter) DSC/TGA thermal analyzer.

An alumina crucible was used as a sample container. The molar ratio of olivine to ammonium sulfate in the mixture was adjusted based on the stoichiometric molar ratio of olivine to ammonium sulfate in Eq. (4-1) i.e. 1 mol olivine to 2 moles ammonium sulfate (1mol Mg:1mol S), resulting in the olivine to ammonium sulfate mass ratio of about 0.55.

Isothermal conditions of 400, 425 and 450℃ were applied for the duration of 120 min, for calculation of apparent activation energy of solid-state extraction process (Eq. (4-1)). The specimens were heated from room temperature to the desired extraction temperature with the heating rate of 10 $deg.min^{-1}$. Then, the samples were heated under constant temperatures of 400, 425 and 450°C, for 120 min. The temperature values were selected based on the reported

applicable temperature range for solid-state extraction of $MgSO_4$ from the reaction of Mg-silicate and ammonium sulfate by Nduagu et al. [36].

In order to investigate the kinetics of solid-state $MgSO_4$ extraction, the order of Avrami (m) and kinetics constant were evaluated using Johnson-Mehl-Avrami (JMAK) approach (Eq. (4-2)) [145, 157-159] which is reported to be able of characterizing the kinetics of solid-state reactions [157-160]. The derivation and considerations of JMAK kinetics model are explained in Appendix B.

$$\ln(-\ln(1-\alpha)) = m\ln(t) + m\ln(k) \quad (4\text{-}2)$$

The Arrhenius equation [160-162] was applied (Eq. (4-3)) to calculate the amount of activation energy of extraction process, based on the variation of kinetic constant (k) vs. temperature, during isothermal extraction reactions.

$$k = A \exp(-E_A/RT) \quad (4\text{-}3)$$

Where, k is the kinetic constant (s^{-1}, for the first order reactions), E_A is the apparent activation energy ($J.mol^{-1}$), A is the frequency factor (s^{-1}, for first order reactions), R is the universal gas constant ($J.mol^{-1}. K^{-1}$) and T is absolute temperature (K).

4.4 Results and Discussion

4.4.1 Optimization of Structural Parameters via Mechanical Activation

The rate of solid-state extraction of $MgSO_4$ from olivine ($(Fe, Mg)_2 SiO_4$) and ammonium sulfate ($(NH_4)_2 SO_4$) expressed by Eq. (4-1), is reported to be controlled by solid-state diffusion mechanism [13, 33]. Hence, the optimization of the most important diffusion controlling structural parameters, such as the particle, pore and crystallite size, specific surface area (SSA) and crystal strain was implemented for the ultimate purpose of enhancing the rate

of solid-state extraction process given by Eq. (4-1). Issues related to the effect of mechanical activation on the structural parameters and the minimum amount of milling energy input for structural optimization were also addressed in this section.

4.4.2 The Effect of Milling Energy Input on Particle Size

Figure 4-3-a presents the SEM micrographs of the non-activated mechanically/unmilled ammonium sulfate ($(NH_4)_2SO_4$) and olivine ($(Fe,Mg)_2SiO_4$) mixture. Figure 4-3-b shows the EDS elemental distribution of sulfur (S) and magnesium (Mg), as the indicators of the presence of ammonium sulfate and olivine, respectively. The elemental map in Figure 4-3-b corresponds to the SEM micrograph in Figure 4-3-a.

For particle size measurements three repeated runs were performed using an image processing software for SEM images. The average particle size along with the related error bar were estimated. The trend of average particle size variation vs. milling energy is presented as Figure 4-4. The average particle size initially decreases to about 19 μm as a result of particle fracturing by injecting the milling energy of 27.6 kJ/g and then starts increasing, most likely, due to particle agglomeration. Considering the trend in Figure 4-4, the milling energy of about 27.6 kJ/g (1 h) results in the minimum particle size, which is expected to enhance the kinetics of intra particle diffusion, for a solid-state extraction purpose.

4.4.3 The Effect of Milling Energy Input on the Specific Surface Area and Pore Volume

The trends of SSA and total pore volume vs. milling energy input are illustrated in Figure 4-5. Both SSA and total pore volume increase as a function of milling energy input until they reach 27.6 kJ/g. Comparing Figure 4-4 and Figure 4-5 it is apparent that injecting milling energy input up to 27.6 kJ/g results in the particle size reduction and an increase in SSA. The particle shape irregularities that are created during milling process, due to fracture, result in increased value of both SSA and the total pore volume.

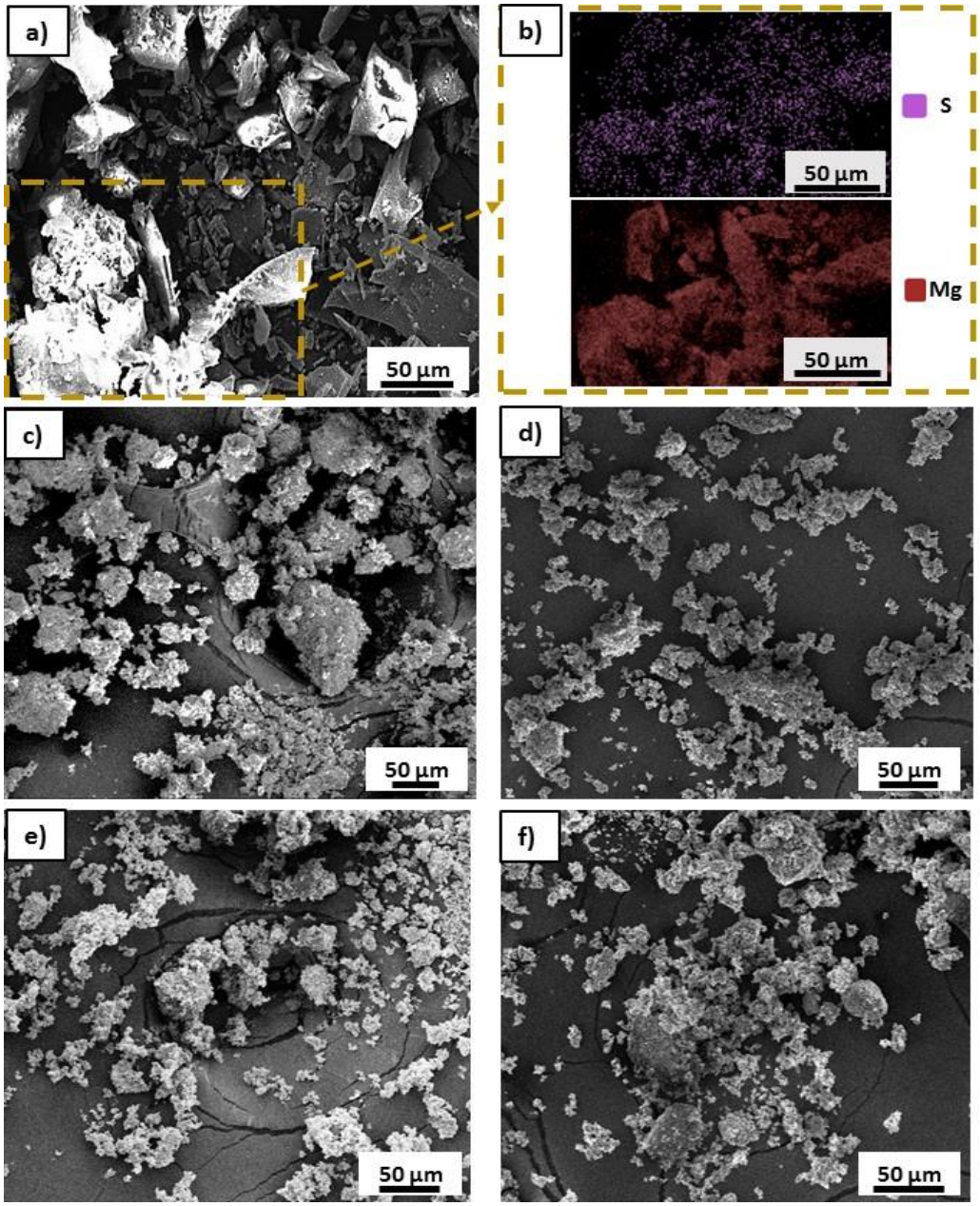

Figure 4-3. SEM micrographs of ammonia sulfate ($(NH_4)_2SO_4$) and olivine mixtures. a) Non activated/unmilled mixture and b) EDS elemental distribution map of S and Mg as the indicators of the presence of $(NH_4)_2SO_4$ and olivine, respectively. Mixtures after c) 30 min of BM (13.8 kJ/g), d) 60 min of BM (27.6 kJ/g), e) 90 min of BM (41.4 kJ/g) and f) 120 min of BM (55.1 kJ/g).

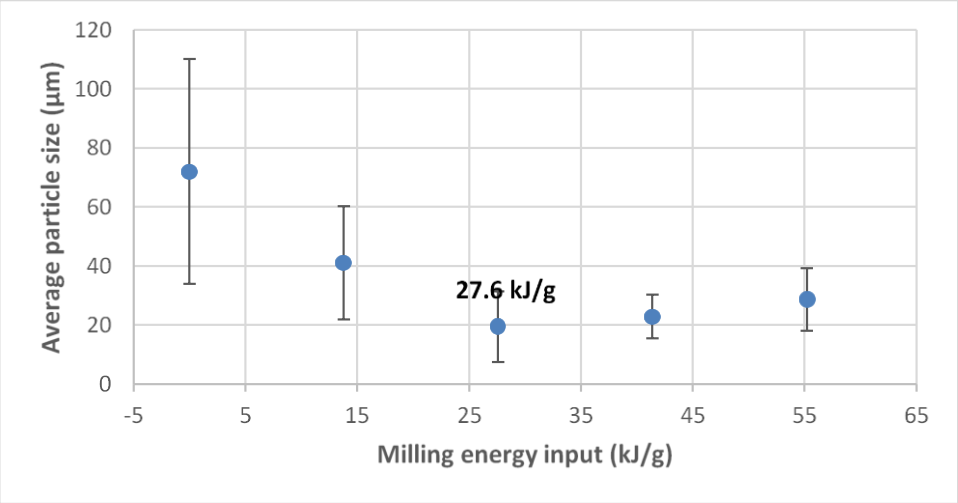

Figure 4-4. Particle size variation as a function of milling energy input.

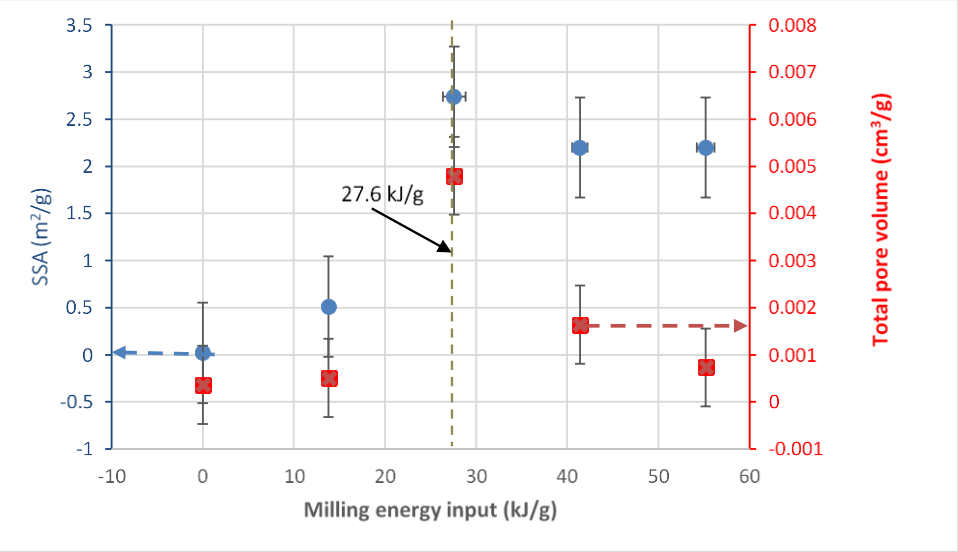

Figure 4-5. SSA and total pore volume variations as a function of milling energy input.

Above the milling energy input of 27.6 kJ/g, particles get more compacted and consequently pore volume is reduced. No measurable change in SSA is observable for a milling energy input higher than 27.6 kJ/g.

4.4.4 The Effect of Milling Energy Input on the Crystallite/Nanograin Size and Crystal Strain

Figure 4-6 shows the XRD patterns for the non-activated/unmilled and ball milled powder mixtures. The trends of crystallite size, calculated from both Williamson-Hall and Scherrer methods (Eq. (3-4) and (3-3)) and crystal strain vs. milling energy input are plotted in Figure 4-7. Both methods show the reduction in crystallite/nanograin size with increasing milling energy input until the value of energy input reaches 27.6kJ/g. In contrast, the crystal strain shows an opposite trend with increasing the milling energy. This general trend is related to the common influence of milling process on the crystallite/nanograin size refinement due to localized deformation phenomena. The detailed mechanism of this process is thoroughly discussed by Fecht et al. [163, 164] through a comprehensive TEM study of atomic structure variations during milling process. Based on his model, localized deformation in shear bands results in the formation of high density of dislocations in those bands. Based on the results on the stability of dislocations in olivine structure reported in [165-167] under the applied conditions in this work, the dislocations are expected to be very stable. In addition, consequent annihilation and recombination of dislocations that are formed at the site of shear bands, result in the formation of sub-grain structure and crystallite size reduction [163, 168-170]. This mechanism is in a good agreement with the behavior of crystallite/nanograin size and crystal strain in Figure 4-7 as a function of increasing milling energy input up to 27.6 kJ/g.

The slight increase of crystallite/nanograin size and decrease of crystal strain for milling energy inputs larger than 27.6 kJ/g in Figure 4-7 could be attributed to the strain induced grain boundary (SIGB) migration phenomena, which usually results in the grain growth where the applied mechanical energy makes the dislocations aligned in a unique direction. The grain boundary migration leaves a low dislocation region behind the migrating boundaries, with a similar orientation to the old grain. At the same time, cancelation of opposite strain fields of annihilated dislocations during grain boundary alignment could be the reason of crystal strain reduction [171-173].

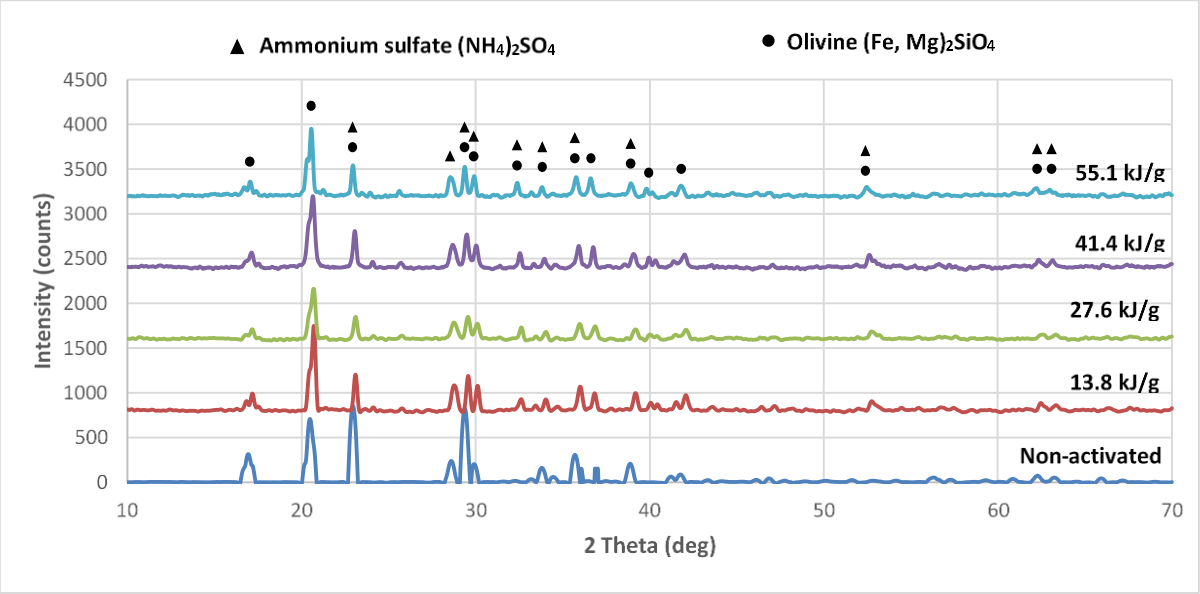

Figure 4-6. XRD patterns of olivine and $(NH_4)_2SO_4$ mixtures, ball milled with varying milling energy inputs.

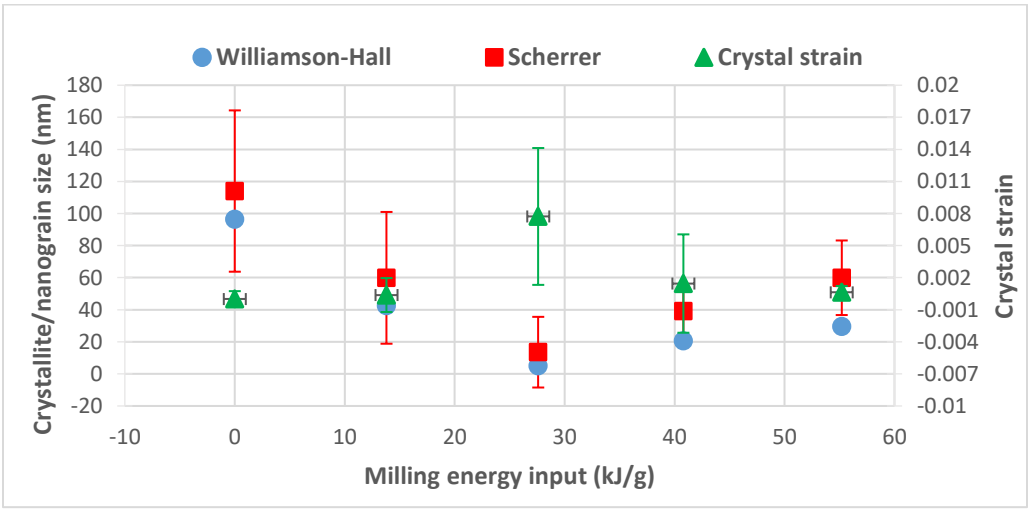

Figure 4-7. Crystallite size (Scherrer and Williamson-Hall) and crystal strain variations as a function of milling energy input.

4.4.5 The Effect of Mechanical Activation on the Apparent Activation Energy of Extraction

The apparent activation energy of extraction process was estimated via the Arrhenius method, which gives the activation energy according to the temperature dependency of reaction rate. To calculate the amount of the apparent activation energy, the amount of mass variation vs. extraction time was recorded via TGA analysis, under three different pre-defined constant temperatures (400, 425 and 450°C). Figure 4-8 presents the TGA graphs for the non-activated/unmilled and activated ammonium sulfate/olivine mixtures under the applied isothermal extraction processes. With increasing temperature, the total mass of the sample decreases due to release of steam H_2O, as shown in Eq. (4-1).

The trend of conversion factor of reaction vs. extraction time was calculated at each applied condition. For this purpose, TGA plots presented in Figure 4-8 were converted to fraction transformed graphs, by measuring the ratio of the actual mass loss at each time to the maximum mass loss, reached by the end of extraction reaction [160, 161] as shown in Eq. (4-4).

$$\alpha = (m_0 - m_t) / (m_0 - m_f) \qquad 4\text{-}4$$

Where, m_0 is the initial mass of tested specimen in TGA device, m_t is the actual mass of specimen at time t and m_f is the final mass of specimen.

The total mass loss, achieved at the end of each isothermal extraction process was assumed as 100% transformation (α=1). Figure 4-9 shows the JMAK plots of ln(-ln(1-α)) vs. ln(t) at each temperature for the non-activated/unmilled and mechanically activated mixtures of ammonium sulfate and olivine through isokinetic region, which was used for calculation of order of Avrami (m), based on Eq. (4-5).

The rate determining kinetic mechanism and reaction rate function were estimated using the rate models which were chosen in accordance with the n values for the applied specific extraction conditions [157, 158, 160, 174]. All the values of m (slope of fitted lines), recorded in Figure 4-9, are close to unity which corresponds to the first order reaction (n). So, the Avrami

order (m) is almost identical to reaction order (n) and hence, the mathematical model of reaction rate can be written as Eq. (4-5).

$$\ln(1-\alpha) = (k\,t)^n \qquad 4\text{-}5$$

Where, k is the kinetic constant and n is order of reaction.

Considering Eq. (4-5), the value of the kinetic constant (k) at each temperature, was estimated from the intercept of ln(-ln(1-α)) vs. ln(t) plots that are presented as Figure 4-8. The apparent activation energy of reaction was calculated from the slope of ln(k) vs. 1000/RT plot (Figure 4-10), based on Eq. (4-3) [175]. The trend of apparent activation energy of solid-state $MgSO_4$ extraction as a function of applied milling energy is presented in Figure 4-11. As can be clearly seen, the activation energy of extraction process decreases (about 34%) as the milling energy input increases until the energy level reaches 27.6 kJ/g and afterwards the apparent activation energy increases.

In the same way, as discussed previously, this amount of milling energy input (27.6 kJ/g) creates the optimal structural parameters for diffusion kinetics enhancement. Thus, this value of milling energy input is the optimal level of milling energy, which can optimize the structural parameters with the purpose of enhancing of rate of solid-state diffusion process and the overall rate of solid-state extraction. For example, in regard to the particle size parameter, the milling energy input of around 27.6 kJ/g results in the minimum size of particles on the order of 19 μm. As the particle size decreases the diffusion length also decreases and consequently, it results in a higher rate of diffusion.

With regard to the SSA and pore volume parameters, the minimum amount of milling energy input (27.6 kJ/g) that corresponds to a minimum quantity of activation energy of extraction, results in the maximum SSA and total pore volume.

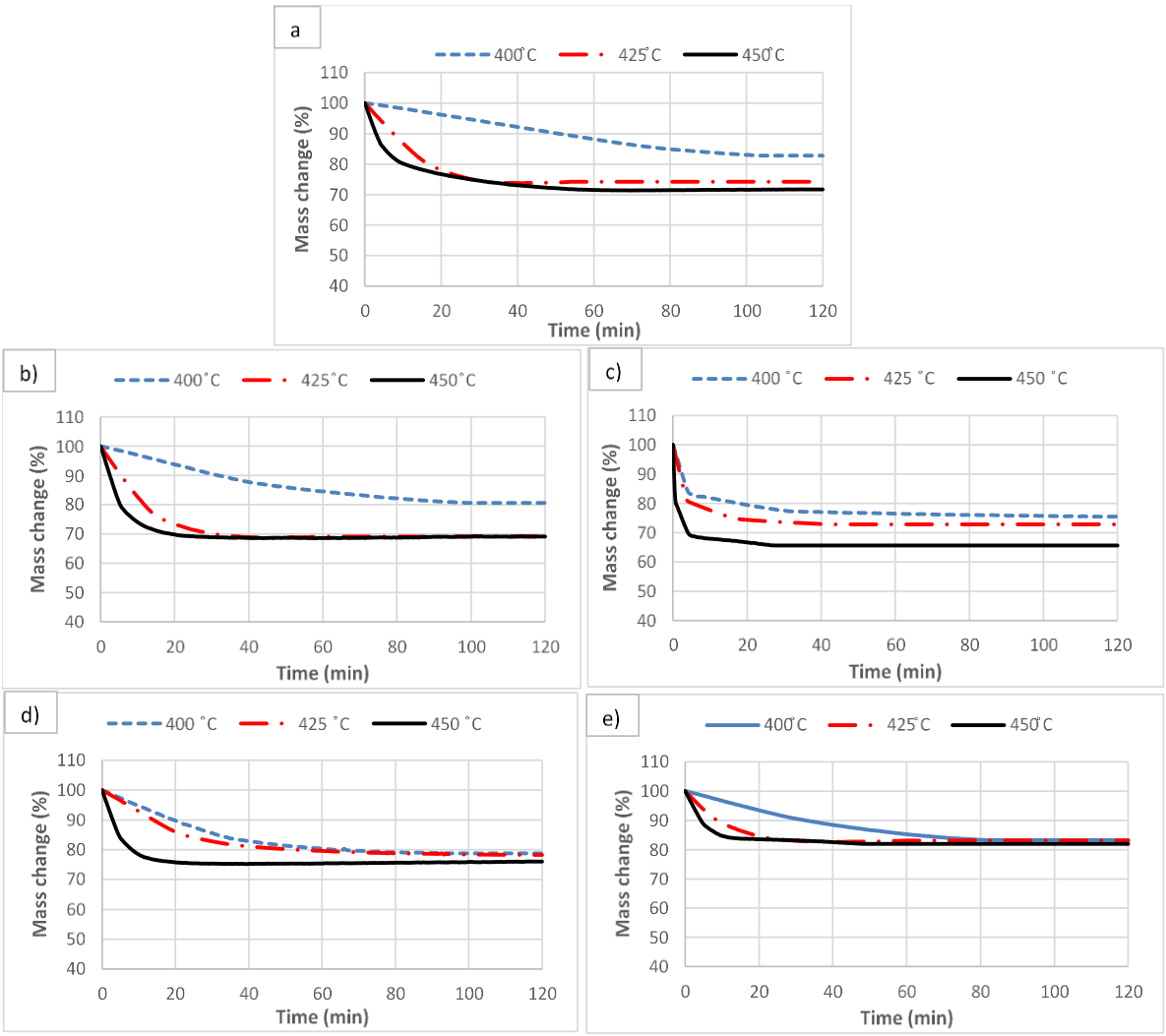

Figure 4-8. TGA mass change vs. time graphs of extraction process. a) Non activated/unmilled mixture. b) Mixtures after b) 30 min of BM (13.8 kJ/g), c) 60 min of BM (27.6 kJ/g), d) 90 min of BM (41.4 kJ/g) and e) 120 min of BM (55.1 kJ/g).

The increment of both total pore volume and SSA is related to the particle shape irregularity, which can be varied during ball milling. The irregular particles have both a larger SSA and a total volume of surface pores compared to the spherical particles, which provide the shorter diffusion length for enhancing the diffusion process. Finally, when it comes to the

crystallite/nanograin size, the milling energy of 27.6 kJ/g results in the smallest crystallite/nanograin size for the investigated range of energy.

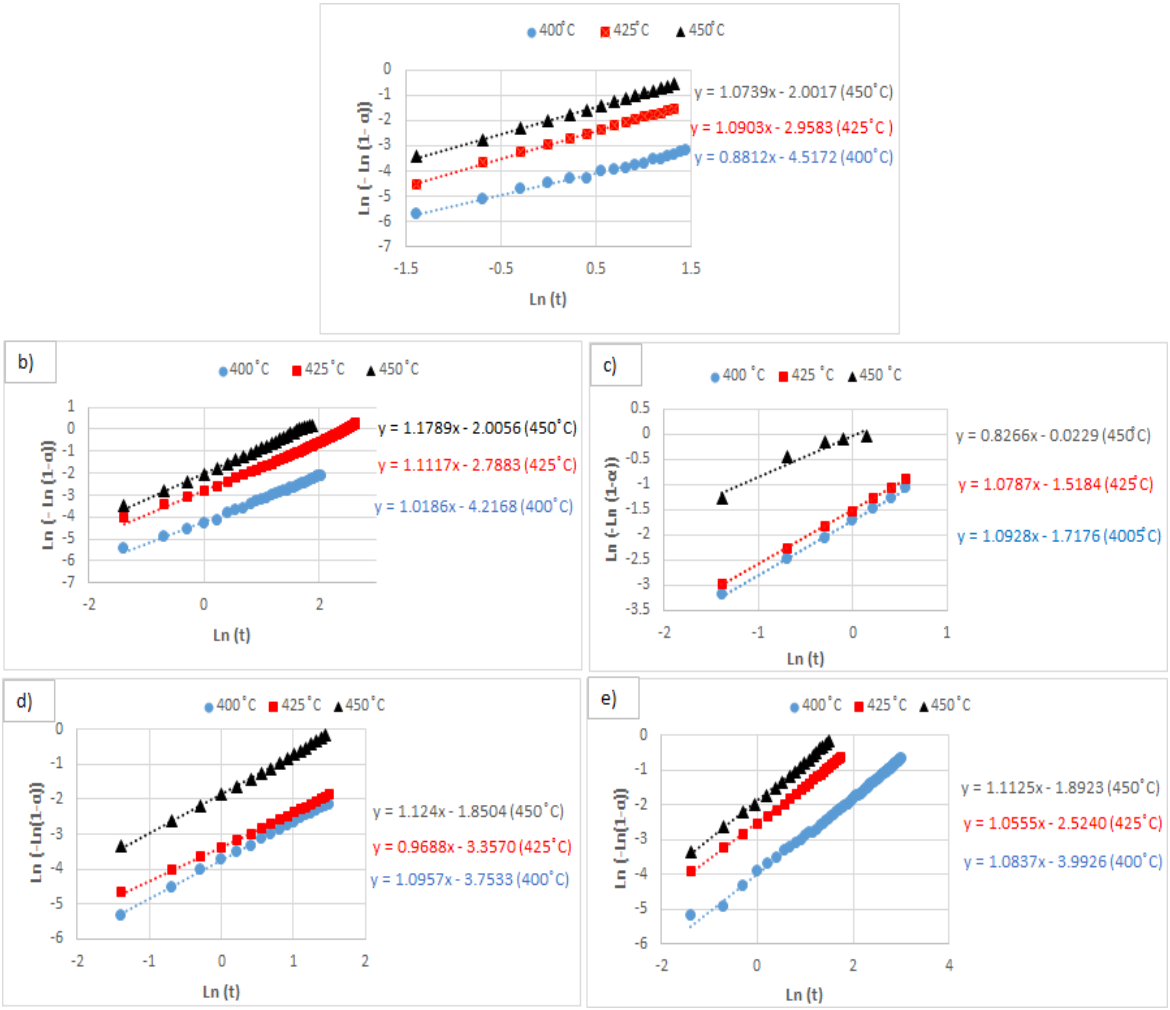

Figure 4-9. JMAK graph of Ln(-Ln(1-α)) vs. Ln(t). a) Non activated/unmilled mixture. Mixtures after b) 30 min of BM (13.8 kJ/g), c) 60 min of BM (27.6 kJ/g), d) 90 min of BM (41.4 kJ/g) and e) 120 min of BM (55.1 kJ/g).

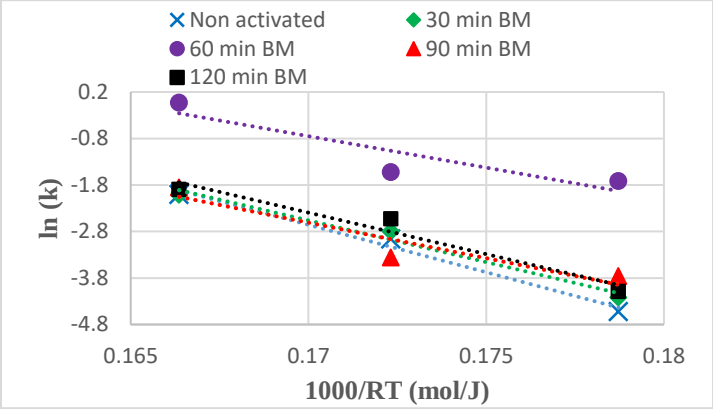

Sample	Equation	R^2
Non activated	y = -204.017 + 32.028	0.9864
30 min BM	y = -179.449x + 27.946	0.9787
60 min BM	y = -135.219x + 22.236	0.8184
90 min BM	y = -152.820x + 23.370	0.8852
120 min BM	y = -178.385x + 27.931	0.9526

Figure 4-10. ln(k) vs. 1000/RT graph for the extraction process with the reactants that are activated with different levels of milling energy input, along with the equations of the best fit passing lines.

The smaller crystallite/nanograin size provides the higher density of grain boundaries in the structure. Grain boundaries have a more open structure compared to the grain interior and facilitate the diffusion process by acting as short-circuit diffusion paths [176]. In addition, because of the higher concentrations of structural defects at the grain boundaries, atomic migration occurs faster and the surface diffusivity (D) is higher, compared to the bulk of the grains. Therefore, the diffusion rate accelerates. The higher density of dislocations near the grain boundaries is the other reason of diffusion kinetics enhancement by decreasing the

crystallite/nanograin size. Dislocation cores have a more open structure and the number of atomic bonds is lower at those sites. So, the vacancies can move more easily at the dislocation cores and enhance the kinetics of diffusion (concept of dislocation pipe diffusion) [176, 177].

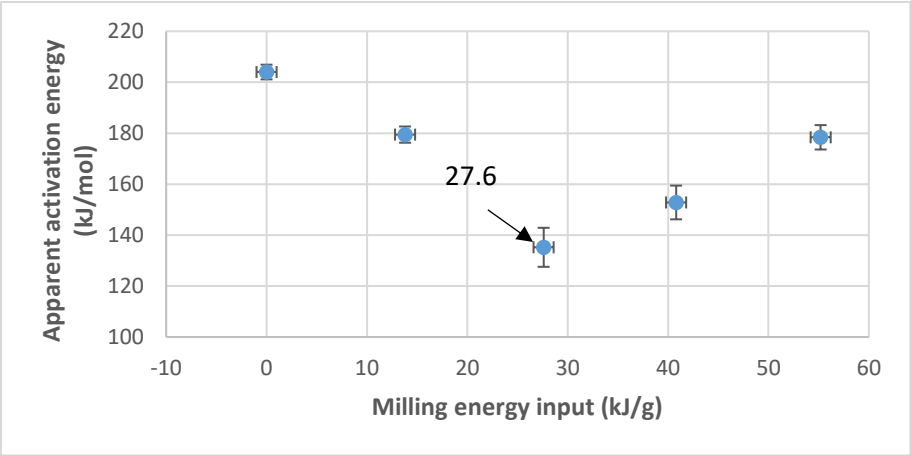

Figure 4-11. The apparent activation energy variation as a function of milling energy input.

Considering all the factors that enhance the kinetics of diffusion in grain boundaries as compared to the grain interior, the effect of crystallite/nanograin size reduction on the optimization of diffusion controlled reaction rate is evident. So, the milling energy input of 27.6 kJ/g produces the minimum crystallite size and results in the most favorable microstructure for overall extraction rate improvement. Therefore, the milling energy input of 27.6 kJ/g is the optimal quantity of milling energy, which provides the optimal crystal microstructure for diffusion controlled extraction processes and the minimum apparent activation energy for the solid-state extraction in the ÅAU process.

Regarding the feasibility of mechanical activation process, it is important to mention that, the reported milling energy in this study was mainly generated through the impact and shear energies between the balls and powders as is modelled and explained in [151]. Electrical energy was just utilized to provide the required rotational energy of milling device, which was about 0.09 kWh for the magneto-mill used in this research, based on the mill configurations

and applied milling parameters, such as a rotational speed. Implementation of fossil fuel as an electricity generator, would produce about 0.045-0.09 kg CO_2 in one-hour suggested milling time of this study (0.5-1 kg CO_2 emission per kWh electricity generation by fossil fuel), depending upon the type of applied fossil fuel. This estimated amount of CO_2 emission is insignificant and can not violate the feasibility of the process. Furthermore, the required electrical energy could be also supplied by other clean alternative sources such as hydro, hydrogen, solar and nuclear energy, rather than fossil fuel, to eliminate the extra CO_2 emission during the electricity production.

To address the cost wise feasibility of the process, the price of electricity in Ontario, Canada (the geographical location where the research was performed) was taken into consideration, which is about 18 cents per kWh at peak rate. In this sense, the total cost of electricity production for 1 h milling in this research, would be about 1.6 cents, which seems to be both feasible and practical. And finally, although, the consumed energy during pre-activation process, increases the overall amount of energy consumption in the mineral carbonation process, as is also addressed by Haug et al. [24], the latter enhancement in the rate of carbon sequestration would still remain as a great motivation for effective pre-activation researches.

4.5 Summary

In this study, we investigated the milling enhancement of the kinetics of $MgSO_4$ extraction through the solid-state reaction of ammonium sulfate and olivine, based on the ÅAU carbonation route. The ultimate objective was to evaluate an optimal amount of required milling energy input to produce the most suitable crystal structure, in order to achieve the most enhanced reaction rate in extraction process. The following outcomes are summarized to address the objectives:

1. The trend of structural parameters, including particle size, SSA, total pore volume, crystallite size and crystal strain, vs. milling energy input was investigated and the amount

of optimal energy input to achieve the best combination of structural parameters for enhancing the rate of diffusion process as a rate limiting factor during the $MgSO_4$ solid state extraction was evaluated.

2. Activation energy of extraction process was evaluated via the Arrhenius method for all extraction processes, using non-activated/unmilled and activated batches of reactants. The activation of reactants (the ammonium sulfate and olivine mixture) with the milling energy input of about 27.6 kJ/g results in the lowest amount of activation energy for solid-state $MgSO_4$ extraction. We showed earlier [156] that the controlling effect of milling energy on structural variations seem to be independent of the type of milling device. Considering this fact, the optimal quantity of milling energy input of 27.6 kJ/g was suggested to be applied for achieving the best kinetics of $MgSO_4$ extraction from solid-state olivine and ammonium sulfate reaction. This optimal amount of milling energy input caused around 34% reduction in the activation energy of $MgSO_4$ solid-state extraction.

Chapter 5

Directed Precipitation of Anhydrous Magnesite for Improved Performance of Permanent CO_2 storage

5.1 Overview

This research phase studies the indirect aqueous carbon sequestration via $Mg(OH)_2$. Anhydrous $MgCO_3$ (magnesite) from $Mg(OH)_2$ carbonation is the most desirable carbonated phase, among all the carbonate precipitates (hydrous or anhydrous) as it has the highest CO_2 storage density and great stability. However, the formation of magnesite is significantly hindered by its kinetics of precipitation in an aqueous carbonation medium. This study considers two separate strategies. First, control of carbonation parameters such as temperature and pressure, and second, enhancement of the heterogeneous precipitation using seeding material that could improve the reaction kinetics and conversion efficiency of the direct carbonation of $Mg(OH)_2$. The effects of carbonation temperature and pressure on the anhydrous precipitate concentration and consequently the efficiency of carbonation have been evaluated. The results support the fundamental role of carbonation temperature in determining the reaction direction through the formation of anhydrous precipitates, so that no trace of hydromagnesite ($Mg_5(CO_3)_4(OH)_2 \cdot 4H_2O$) is observed at 200℃. Two seeding materials, hydrophobic activated carbon and hydrophilic alumina, were used and the influence of the surface chemistry of varying seeding sites (hydrophobic vs. hydrophilic seeds) was elaborated. At the carbonation temperature of 100℃ and 150℃, a heterogeneous precipitation using hydrophilic alumina results in lower concentrations of anhydrous magnesite in precipitated compounds, even as compared to the seedless solution, owing to the hydrophilic properties of alumina. In contrast, in all considered cases, activated carbon improves the rate of carbonation and formation of anhydrous precipitates. The usage of activated carbon as heterogeneous nucleation sites in an aqueous medium results in a magnesite concentration of around 60% and

the corresponding carbonation conversion of about 72% under the controlled condition of 200℃ and 30 bar CO_2 pressure.

5.2 Introduction

Mineral carbonation-based-CCS (MC-CCS) processes are generally implemented respectively in either direct or indirect approaches upon the separation or combination of two critical stages of extraction and carbonation, in either dry or aqueous mediums [6, 83-85]. Although MC-CCS is thermodynamically favorable, its slow kinetics greatly hinders its use. Various kinetic improvement methods have been suggested to speed up the overall rate of carbon sequestration, such as pre-activation techniques (e.g., the author's previously explored mechanical pre-activation [156]), and optimization of carbonation parameters, as is considered in this phase of research.

Among these suggested MC-CCS routes, aqueous indirect carbonation has received significant industrial attention, as it combines the benefits of improved kinetics in aqueous approaches and the process controllability of indirect carbonation [23]. Among the different types of divalent cation bearing feedstock used in MC-CCS, Mg-bearing materials are the most preferred resources, due to their great abundancy, high theoretical CO_2 storage capacity, and noticeable absorbent element content [3, 6, 75].

$Mg(OH)_2$ is the major reactive compound extracted from such feedstock for indirect carbon sequestration. Both extraction and carbonation of $Mg(OH)_2$ need to be kinetically improved to facilitate rapid indirect carbon sequestration. The authors studied enhancing the kinetics of extraction stage in previous research [109].The generally accepted elementary steps of the $Mg(OH)_2$ aqueous carbonation process are: dissolution of CO_2 in water (Eq.(2-4)), dissolution of $Mg(OH)_2$ material to liberate divalent cations in the solution (Eq. (5-1)), and precipitation of carbonated product (Eq.(2-6)) [6, 9, 45, 93, 94, 109, 135]. Precipitation (Eq. (2-6)) may result in the formation of water as a reaction product, depending upon the type of Mg-carbonate produced. The stoichiometry balance of Eq. (2-6) also depends also upon these products.

$$Mg(OH)_{2(s)} + 2H^{+}_{(aq)} \rightarrow Mg^{+2}_{(aq)} + 2H_2O_{(l)} \quad 5\text{-}1$$

Varying the temperature and pressure results in different hydrous and anhydrous carbonate products during aqueous carbonation of $Mg(OH)_2$ [45, 135]. In the common applicable range of a carbonation process, hydrous carbonates require a higher level of super-saturation (a higher equilibrium constant) than anhydrous magnesite, suggesting a higher thermodynamic tendency for the formation of anhydrous carbonates vs. hydrous ones. The hydrous precipitates are thermodynamically metastable. In addition, they offer a lower saturation index (SI) of precipitation than anhydrous magnesium carbonates. A saturation index (SI) is the factor which determines solution tendency to form precipitates. This factor compares the actual concentration of solutes under the term of Ion Activation Product (IAP) with thermodynamic solubility product (KSP) to predict the tendency of precipitates formation [178]. However, hydrous carbonate formation can occur more easily due to better kinetics of formation.

The formation of the anhydrous magnesite phase is strongly limited by the kinetics of the precipitation process Eq.(2-6) [134-136]. However, anhydrous carbonates are much more favorable compared to hydrous ones owing to their higher storage capability (a lower molecular weight) and thermodynamic stability. So, it is very important to stimulate the kinetics of anhydrous carbonates formation to improve a total carbonation performance. Thus, directing the precipitation toward the formation of anhydrous carbonate phases is desirable, and is referred to as “directed precipitation” in this work.

A number of researchers have investigated the kinetics and mechanism of magnesite ($MgCO_3$) precipitation during aqueous carbonation of $Mg(OH)_2$ Their main focus has been on predicting most likely carbonate precipitates to be formed as a function of applied conditions such as temperature and pressure [37-41, 44].

The enhancement of precipitation kinetics was studied in [42-45]. For example, the effect of heterogeneous nucleation on precipitation of calcium carbonate in an aqueous solution was studied by Chevalier et al. [42], considering two different hydrophobic and hydrophilic

nucleation sites. Similarly, Swanson et al. [45], studied the effect of seeding precipitation on the aqueous carbonation of $Mg(OH)_2$ using magnesite and alumina seeds. They attributed the effect of their seeding materials to the crystal orientation of the seeds and magnesite precipitates during precipitation, but ignored other critical factors such as their surface properties [45].

More thorough investigation is required to determine the effects of temperature and pressure on the magnesite content of precipitated carbonates and the corresponding influence on the efficiency of carbonation. To fill this gap, the first phase of this study thoroughly explored the effects of temperature and pressure on the most sensitive, quantitative factors associated with anhydrous magnesite formation (magnesite content and carbonation conversion percentage) in order to understand the path of directed carbonation of $Mg(OH)_2$ toward favorable anhydrous carbonates.

In the second phase, a heterogeneous precipitation through seeding to enhance the rate of magnesite formation, was studied. Two different seeding materials with varying wettability properties were used with the objective of enhancing the kinetics of precipitation using the general effect of heterogeneous nucleation sites. The possible effects of different precipitation sites with varying surface chemistry and wettability properties on the water content of precipitated carbonates were examined.

In summary, the main objectives of this study are as follows:

1. Quantitative evaluation of the effect of carbonation temperature and pressure on the directed precipitation of $MgCO_3$ during the aqueous carbonation of $Mg(OH)_2$, by investigating the variation in the magnesite concentration and the total extent of carbonation conversion.
2. Assessment of the general effect of heterogeneous nucleation on the kinetics enhancement of the anhydrous magnesite formation, under varying temperature and pressure conditions.

3. The study of possible effects of dissimilar surface properties of heterogeneous nucleation sites on directed precipitation, under different temperature and pressure conditions, during aqueous carbonation.

5.3 Experimental

Magnesium hydroxide ($Mg(OH)_2$) powders (Alfa Aesar 1039-42-8; 95-100% assay) were used in this research as a Mg-bearing source during aqueous carbonation. In each carbonation test, 3 g of $Mg(OH)_2$ was added to 100 cc distilled water (a concentration of around 0.5 molar).

Carbonation reactions were performed in a 4650 Parr high-temperature, high-pressure reaction vessel. The vessel was evacuated and purged with CO_2 gas prior to setting the desired carbonation pressure and temperature. In all cases, the reactor was heated from room temperature to the desired carbonation temperature, at a rate of about 10 $deg.min^{-1}$, and then was kept under adjusted constant temperature for 60 min. In all cases the carbonation pressure was adjusted to the desired value through opening the valve connected to inlet CO_2 bottle. Figure 5-1 shows a schematic of the carbonation setup. A combination of reaction temperatures and pressures was selected based on the saturated water thermodynamic table [179], such as to ensure that the solvent water would not evaporate under applied conditions and the gas phase remained pure CO_2. Carbonation temperatures of 100, 150 and 200℃ and CO_2 pressure of 10, 20, 25 and 30 bar were tested.

The experimental occur under either seedless or seeding conditions. The alpha alumina (Al_2O_3) particles (Alfa Aesar 1344-21-1; 99.9% assay; <1.0 μm APS; 2-4 m^2/g SSA) were used as hydrophilic seeding materials. Activated carbon powders (MTI TF-B-520; 5 μm APS; 2000 m^2/g SSA) were applied as hydrophobic seeding sources. To supply an equal surface area of heterogeneous nucleation sites during carbonation, 1.0 g of alumina or 1.5 mg of activated carbon powders was added to the carbonation solution.

After carbonation process, the reactor was cooled to room temperature, and the carbonation solution, including the carbonated precipitates, was filtered using 2.5 μm pore size filtering

papers (Whatman 1442-055; grade 42). To evaporate adsorbed moisture from the powders, the recovered precipitates were oven dried for two hours at 200℃, after filtration.

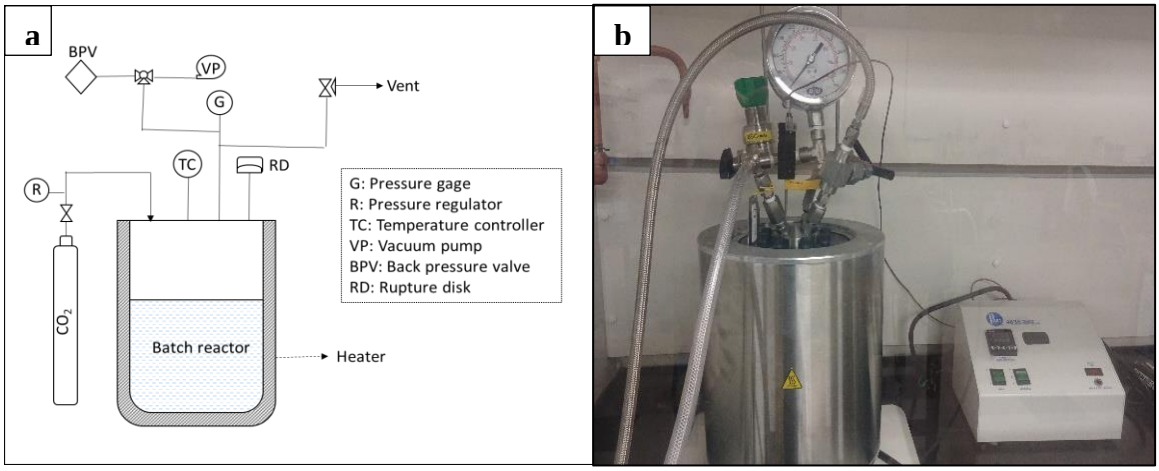

Figure 5-1. $Mg(OH)_2$ aqueous carbonation apparatus. a) Schematic overview (the drawing is not on scale), b) Actual carbonation reactor.

Thermal analyses were performed in a combined DSC/TGA thermal analyzer device (NETZSCH STA 449F3A-0918-M Jupiter), under argon atmosphere. An alumina crucible was used as a sample container. In all cases, the specimens were heated from room temperature to 750 °C at a rate of 10 deg.min-1. SEM micrographs were obtained via the secondary electron detector of LEO 1550 Zeiss SEM at 10 kV. To promote the conductivity of samples for SEM imaging, samples were gold coated prior to SEM analysis using a UHV spotter system for 139 seconds, with a current of 20 mA. XRD phase analysis was performed using an INEL XRG 3000 Powder Diffractometer, via monochromic Cu Kα1 radiation with the wavelength of 0.15406 nm, generated by the accelerating voltage and current of 30 kV and 30 mA, respectively.

5.4 Results and Discussion

5.4.1 Effect of Temperature and Pressure on Directed Magnesite Precipitation in Seedless Aqueous Carbonation of $Mg(OH)_2$

The effects of temperature and pressure on the kinetics of magnesite formation, as a potential favorable anhydrous carbonation product during $Mg(OH)_2$ carbonation, were characterized. Seedless $Mg(OH)_2$ aqueous carbonation was evaluated at temperatures of 100, 150 and 200℃. Pressure was adjusted to 10, 20, 25 and 30 bar. The carbonation products were then filtered, dried and analyzed to track the presence and relative concentration of brucite ($Mg(OH)_2$), hydromagnesite ($Mg_5(CO_3)_4(OH)_2 \cdot 4H_2O$) and magnesite ($Mg(CO_3)$). These phases are the typical products of aqueous carbonation of $Mg(OH)_2$ in the applied range of temperatures and pressures in this research, in accordance with the available literature data that were evaluated from a standpoint of the thermodynamic stability of possible carbonated precipitates [37, 40, 45, 135, 136]. Figure 5-2 presents the SEM micrograph of carbonated products (magnesite and hydromagnesite), showing the rhombohedral structure of magnesite (Figure 5-2-a) vs. the sheet like morphology of hydromagnesite (Figure 5-2-b). In the initial stage, carbonation products were analyzed using XRD method for qualitative evaluation of possibly formed crystalline carbonation precipitates. Figure 5-3 shows the XRD patterns of precipitated phases, at the varying applied temperature and pressure conditions. Comparing the XRD patterns illustrated in Figure 5-3, it seems that temperature exerts a significant effect in a direct precipitation of $Mg(OH)_2$, so that no obvious diffraction peak of hydrous magnesites is observed at the carbonation cases at 200℃, and favorable anhydrous magnesite was shown to be the sole crystalline carbonated product during aqueous carbonation of $Mg(OH)_2$ under 200℃.

Knowing that an XRD method is not capable of detecting the possibly amorphous phases during carbonation, thermal analysis was performed as a complimentary technique to evaluate both crystalline and amorphous phases. Also, a quantitative investigation of the percent fraction of possible carbonation products was carried on through thermal decomposition of

dried carbonated products in a thermogravimetric (TG) apparatus under an inert argon atmosphere.

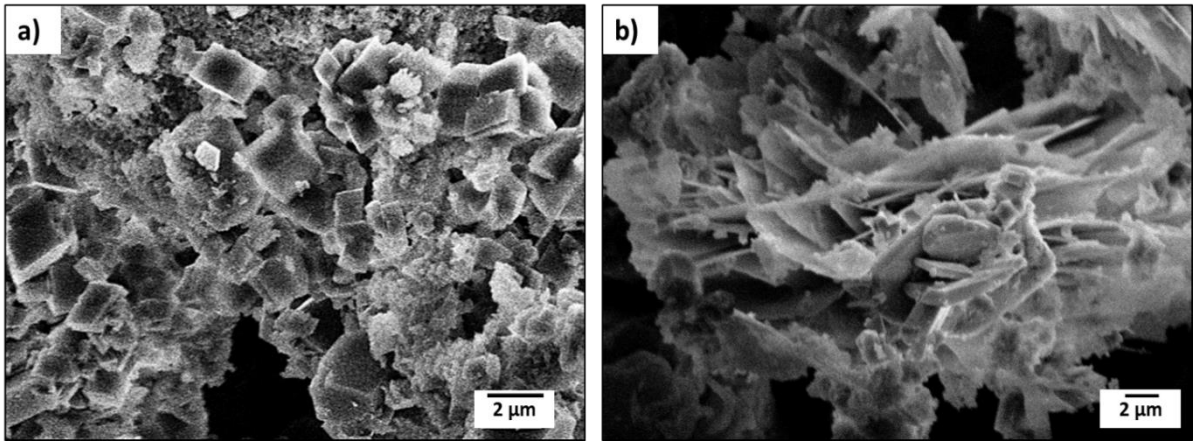

Figure 5-2. SEM micrograph of hydrous and anhydrous precipitated carbonate compounds in $Mg(OH)_2$ aqueous carbonation process. a) Magnesite ($MgCO_3$), b) hydromagnesite ($(Mg_5(CO_3)_4(OH)_2 \cdot 4H_2O)$).

Figure 5-4 presents the thermogravimetric analysis (TGA) results attributed to the decomposition of different carbonated products at a temperature range from room temperature to 750℃. Different chemical compounds are characterized by a varying temperature range of decomposition related to the specific type of chemical bonding in their structure. Hence, the mass fraction of each carbonated product (brucite, magnesite and hydromagnesite) can be calculated based on the TGA mass percentage variations at a specific temperature range, attributed to the decomposition of that particular compound. Eq. (5-2) presents the decomposition (dehydroxylation) reaction of brucite which was reported to take place at the range of around 400-450℃ [45, 140, 180].

$$Mg(OH)_{2(s)} \rightarrow MgO_{(s)} + H_2O_{(g)} (\sim 400\text{-}450°C) \qquad 5\text{-}2$$

Hollingbery [180] performed a comprehensive study of a decomposition mechanism of hydromagnesite through reviewing and evaluating the previously-suggested mechanisms and theories [180-185] and presented a three stage dissociation mechanism during the thermal decomposition of hydromagnesite.

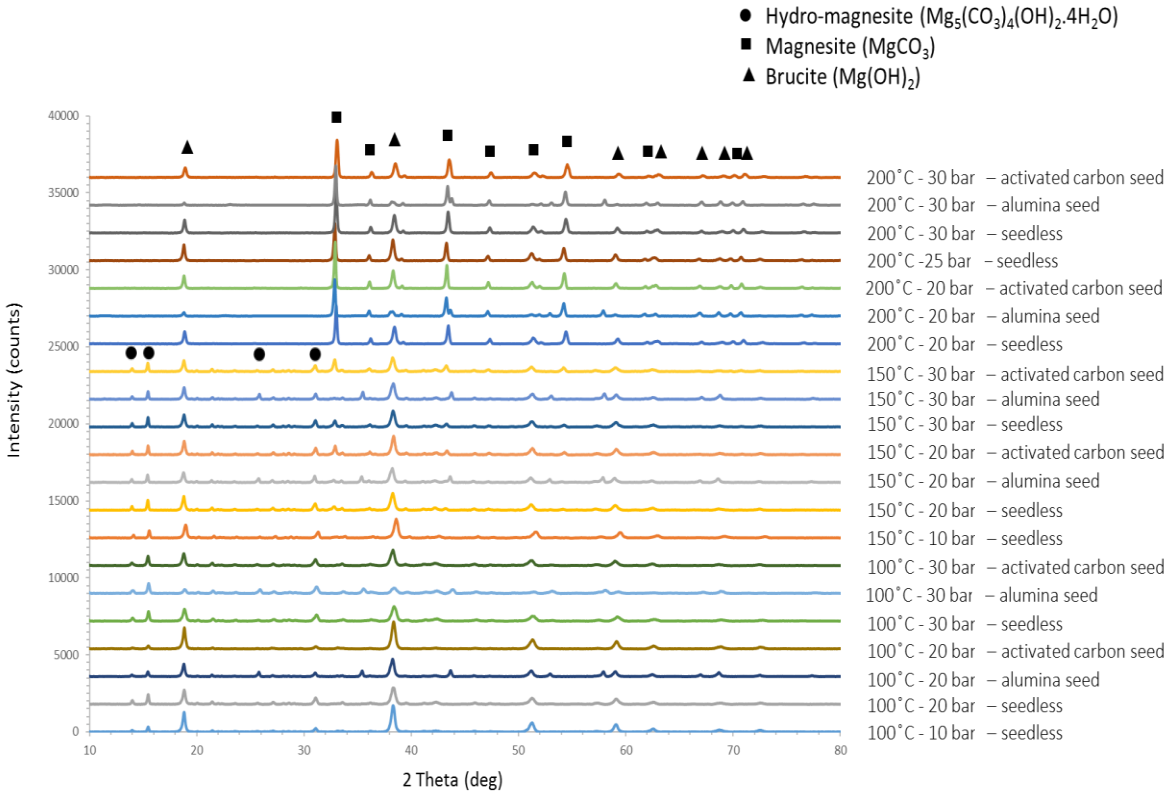

Figure 5-3. XRD patterns of precipitated phases, formed during aqueous $Mg(OH)_2$ aqueous carbonation.

Based on the proposed mechanism, hydromagnesite decomposes through three separate stages of dehydration (release of structural water) Eq. (5-3) , dehydroxylation (repealing the hydroxyl group) Eq.(5-4), and the final decarbonation stage Eq.(5-5) [37, 38, 45, 140].

$$Mg_5(CO_3)_4(OH)_2 \cdot 4H_2O_{(s)} \rightarrow Mg_5(CO_3)_4(OH)_{2(s)} + 4H_2O_{(g)} \quad (\sim 220\text{-}350°C) \qquad 5\text{-}3$$

$$Mg_5(CO_3)_4(OH)_{2(s)} \rightarrow (Mg)_4(CO_3)_{4(s)} + MgO_{(s)} + H_2O_{(g)} \quad (\sim 350\text{-}460\ °C) \qquad 5\text{-}4$$

$$(Mg)_4(CO_3)_{4(s)} \rightarrow 4MgO_{(s)} + 4CO_{2\ (g)} \quad (>515°C) \qquad 5\text{-}5$$

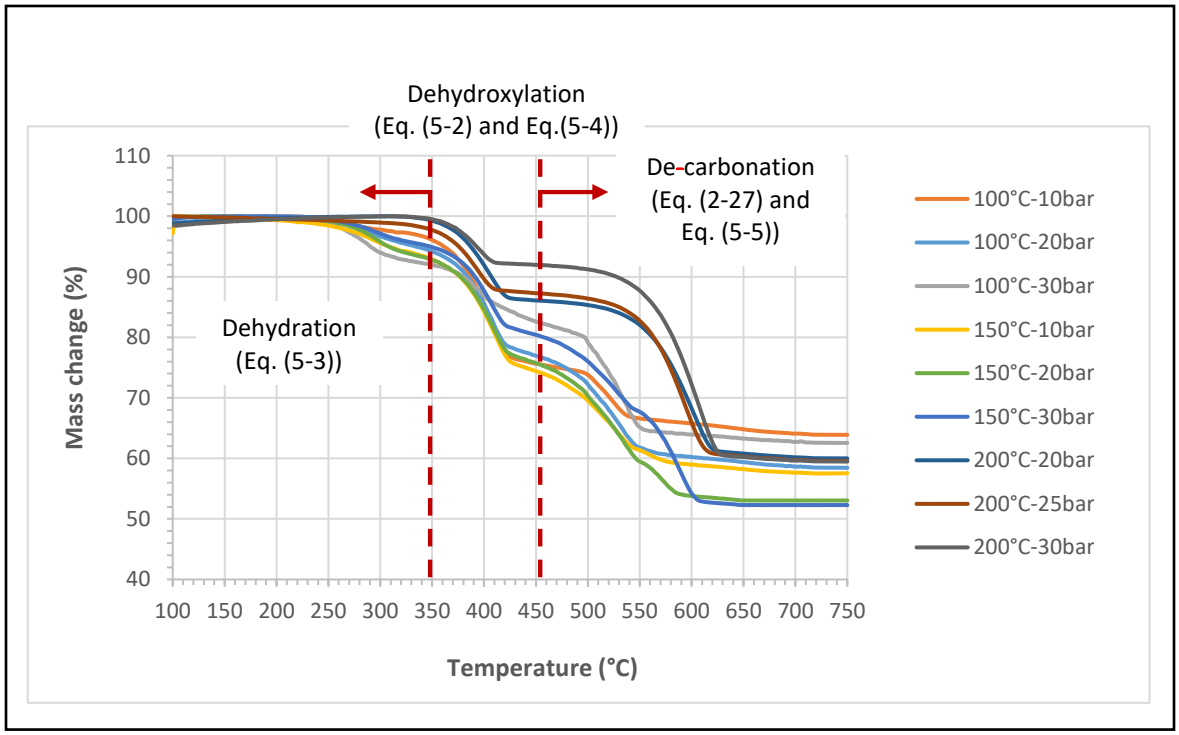

Figure 5-4. TGA thermal decomposition graph of precipitated phases, formed during aqueous carbonation of $Mg(OH)_2$.

Subsequently magnesite, as the most favorable product of $Mg(OH)_2$ aqueous carbonation, decomposes at the temperature higher than 460℃ based on Eq. (2-27). Considering the decomposition reactions and corresponding temperature ranges, TGA curves were sectioned into three separate ranges in Figure 5-4, representing the first section of hydromagnesite dehydration in the approximate range of 220-350℃, the second section of hydromagnesite and

brucite dehydroxylation in the approximate range of 350- 460℃, and the third section of hydromagnesite and magnesite decarbonation over 460℃. Since there is a clear overlap between the dehydroxylation of brucite (Eq. (5-2)) and hydro-magnesite (Eq. (5-4), as well as de-carbonation range of magnesite (Eq. (2-27)) and hydro-magnesite (Eq. (5-5)), the isolated dehydration temperature range of hydromagnesite (220-350℃) has been considered as a separate stage in estimating the mass percentage of hydromagnesite (Eq. (5-3)). The mass percentage of hydro-magnesite can be calculated using Eq. (5-6), based on the stoichiometry of the hydro-magnesite dehydration reaction (Eq. (5-3)).

$$\text{Hydromagnesite (mol \%)} = \frac{\text{TGA mass change (\%) in the range of hydromagnesite dehydration (}\sim 220\text{-}350^{\circ}\text{C)}}{\text{molar number of water(4)} \times \text{molar mass of water (18 g.mol}^{-1}\text{)}} \qquad 5\text{-}6$$

Although in a similar study by Swanson et al. [45], a thermal decomposition range of over 460°C has been specifically addressed to magnesite decarbonation, the present authors believe that considering the previously suggested mechanisms and dissociation models of hydromagnesite [37, 38, 45, 140, 186], there would be a strong overlap between the decarbonation range of magnesite and hydromagnesite. Hence, this temperature range would not result in a concentration of pure magnesite and the initial dehydration range of hydromagnesite has been addressed as a unique decomposition range when calculating the hydromagnesite concentration in a magnesite- brucite- hydromagnesite mixture as given by Eq.(5-6).

Since the decarbonation of both magnesite (Eq. (2-27)) and hydro-magnesite (Eq. (5-5)) is possible at the thermal range of over 460℃ (at the third stage, shown in Figure 5-4), the corresponding mass reduction owing to a decomposition at this temperature range has been attributed to the combined decarbonation of magnesite and hydromagnesite compounds. The pure concentration of magnesite can then be estimated upon deduction of the hydromagnesite portion which can be calculated based on Eq. (5-6). Subsequently, considering the stoichiometry of hydromagnesite decomposition reactions (Eq. (5-3) to Eq. (5-5)), the

contribution of mass reduction as a result of hydromagnesite decarbonation can be calculated and deduced in the thermal range of over 460 ℃, to estimate the net concentration of the magnesite phase (Eq. (5-7)). Hydromagnesite mol % was calculated using Eq.(5-6). Obviously, the balanced value over 100 presents the molar percentage of brucite in the analyzed compound. It needs to be mentioned here that the ranges of mass change variation in TGA graphs were set and justified based on the corresponding TGA first derivative curve (dTGA) for an accurate mass change period selection in each section.

$$\text{Magnesite (mol \%)} = \frac{\text{TGA mass change (\%) in the thermal range of over 460°C}}{\text{molar mass of } CO_{2(g)}\ (44\ \text{g.mol}^{-1})} - (\text{hydromagnesite (mol \\%)} \times 4) \qquad 5\text{-}7$$

A ternary diagram presented in Figure 5-5 is plotted based on the relative molar percentage of each component, under different applied conditions. As shown in Figure 5-5, no hydromagnesite phase forms under 200℃, and anhydrous magnesite is the only carbonated product formed at the highest temperature of 200 ℃. This result was also confirmed by the XRD diffraction patterns (Figure 5-3), which shows no evidence of crystalline hydromagnesite diffraction peaks for 200 ℃ carbonation cases.

Also, as shown in Figure 5-5, the molar percentage of the magnesite compound, as the intended carbonated phase in the directed carbonation of $Mg(OH)_2$, increases as a function of both temperature and pressure. As shown in Figure 5-6, the magnesite molar percentage (M%), which was analyzed based on the thermal decomposition in TGA curves as explained earlier, increases as a function of both temperature and pressure. However, the effect of temperature increase on the increment of M% is more profound than that of the pressure.

To further clarify the effect of temperature and pressure on the magnesite percentage value, the mechanism of carbonate precipitate formation during the $Mg(OH)_2$ carbonation process must be taken into consideration. The mechanisms of the formation of magnesite in aqueous carbonation solutions have been addressed and evaluated in the literature [3, 44, 45, 134-136]. According to the suggested mechanism, magnesite mainly precipitates through the

transformation of pre-formed hydrous carbonates such as hydromagnesite [39, 40, 45, 134, 135, 187]. The transition stage of intermediate hydromagnesite to magnesite transformation was considered as a bottle neck stage in the magnesite precipitation process.

At high temperatures, the liberation of water molecules from hydromagnesite structure is facilitated, the transition of pre-formed hydromagnesite to magnesite is enhanced and magnesite precipitation is enhanced [44]. This mechanism could reasonably explain why during a certain precipitation period (60 min), the extent of precipitated magnesite increases as a function of temperature. Therefore, no trace of hydromagnesite has been recorded in either XRD (Figure 5-3) or TGA (Figure 5-4).

In regard with the reported zero concentration of hydromagnesite at 200℃, it needs to be emphasized that, although XRD method is solely capable of crystalline phase detection, the possibility of the presence of amorphous hydromagnesite phase is negligible, considering the outcome of thermogravimetric analysis which is capable of detecting both amorphous and crystalline phases. The extent of magnesite precipitation also increases as a function of pressure as is also recorded in previous studies [37, 39, 135]. However, as presented in Figure 5-6, the effect of pressure on increasing the magnesite content is more noticeable at higher temperatures. This observation may be attributed to the fact that the rate of dissolution of CO_2 gas in the aqueous solution as a first stage of $Mg(OH)_2$ carbonation (Eq. (2-4)), decreases with a temperature increase. Hence, at high temperatures, a CO_2 pressure increase can have a greater effect through promoting CO_2 concentration in the solution.

In the next stage, the effect of temperature and pressure parameters on the total value of conversion percentage was studied. The carbonation conversion percentage is defined as the amount of CO_2 which is stored in the material relative to the maximum theoretical capacity of a considered material to store CO_2 [6, 77].

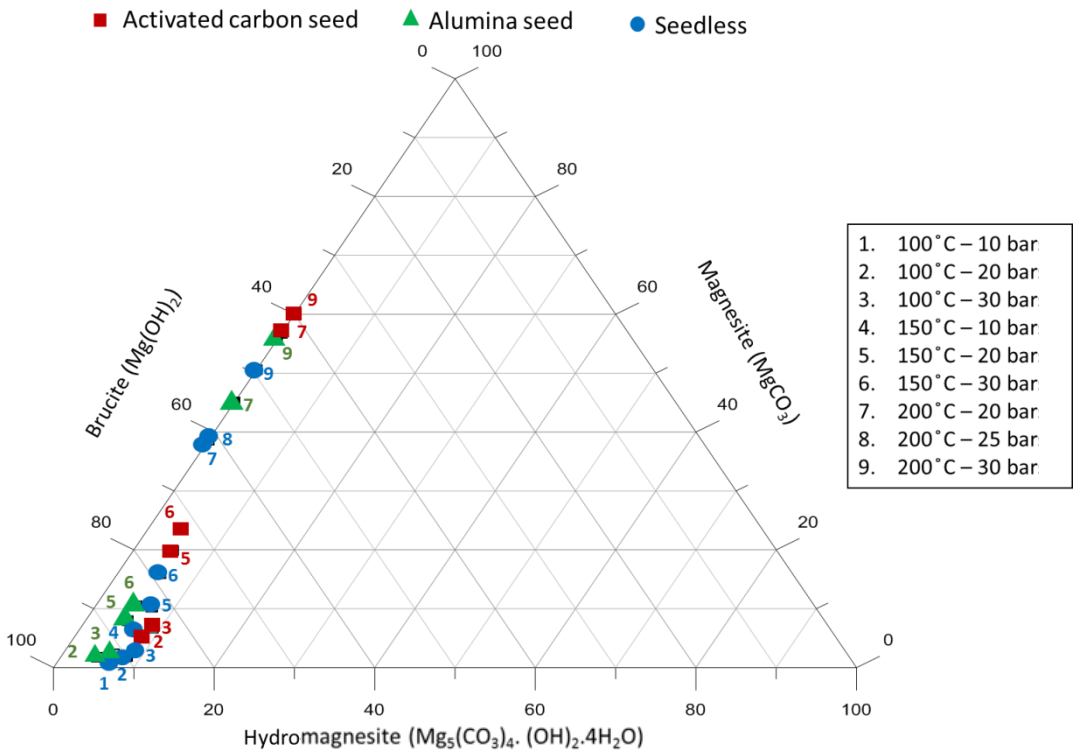

Figure 5-5. Phase diagram, representing the relative concentration of brucite ($Mg(OH)_2$), magnesite ($MgCO_3$) and hydromagnesite ($Mg_5(CO_3)_4.(OH)_2.4H_2O$) in the precipitated phases, formed during aqueous carbonation of $Mg(OH)_2$.

In order to calculate the extent of conversion percentage under each condition, the mass ratio of actual CO_2 released during TGA thermal decomposition to the maximum theoretically possible CO_2 release was calculated. The maximum theoretically possible CO_2 release was considered as the amount of CO_2 gas that could be released during TGA thermal decomposition, if the total product of $Mg(OH)_2$ carbonation is anhydrous magnesite. Magnesite was chosen as a reference material, with the maximum possible CO_2 release in thermal decomposition, having the highest Mg to C ratio and lowest molecular weight. It results in the highest density of CO_2 storage, among all the other possible products of carbonation in proposed $Mg(OH)_2$ carbonation [77]. With this definition, the total amount of carbonation conversion percentage can be calculated from Eq. (5-8).

$$\text{Carbonation conversion (\%)} = \frac{(\text{Hydromagnesite mol\%} \times 4) + (\text{Magnesite mol\%})}{100} \qquad 5\text{-}8$$

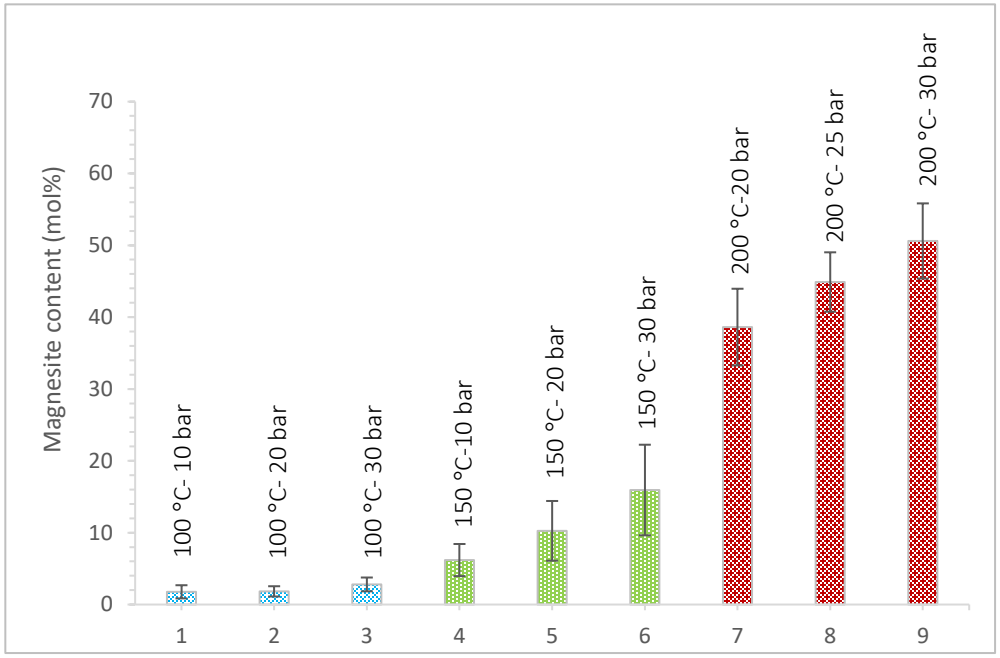

Figure 5-6. Magnesite molar concentration variation as a function of carbonation temperature and pressure, in precipitates formed during seedless aqueous carbonation of $Mg(OH)_2$.

Figure 5-7 shows the trend of $Mg(OH)_2$ carbonation conversion percentage as a function of temperature and pressure. The trend of conversion percentage variation as a function of temperature and pressure is very close to that presented for the molar percentage of magnesite in Figure 5-6. The similarity between in Figure 5-7 and Figure 5-6, points out towards the important role of the directed precipitation of anhydrous magnesite on improving carbonation efficiency. Adding the great thermodynamic stability of magnesite to the scenario, the importance of directed precipitation is even more significant.

5.4.2 Effect of Heterogeneous Seeding on Directed Precipitation of Anhydrous Magnesite under Varied Temperature and Pressure Conditions, During Aqueous Carbonation of $Mg(OH)_2$

Because the kinetics of magnesite formation is the most important barrier to the directed precipitation of $MgCO_3$ [45], heterogeneous nucleation was proposed and implemented in this phase of research. As is well-known from the theory of precipitation processes, heterogeneous nucleation is capable of enhancing the total kinetics of precipitation, through reducing the activation energy barrier of nucleation [42, 43, 45, 53, 188-191]. This reduction has been proven and explained through considering the geometry of nuclei and the changes in the acting interfacial surfaces. Heterogeneous nucleation can successfully add a negative energy contribution term (as a result of the destruction of the seed to liquid interface), to the general terms of free energy variation during nucleation process and enhance the kinetics of nucleation stage [53, 189, 190]. Knowing that heterogeneous seeding is fairly capable of enhancing the rate of precipitation in $Mg(OH)_2$ aqueous carbonation, seeding sites were added to the solution with the goal of possible enhancement of directed precipitation. The effect of dissimilar heterogeneous sites on kinetics of magnesium carbonate ($MgCO_3$) formation was evaluated. Alumina (Al_2O_3) and activated carbon seeds were examined as hydrophilic and hydrophobic precipitation sites, respectively. The total surface area of these seeding materials was kept constant in order to eliminate the effect of precipitation site availability. The effect of different seeds' surface properties on the carbonation conversion percentage and magnesite content was evaluated under varying temperature and pressure conditions to track the performance of seeding sites as a function of carbonation conditions. Aqueous carbonation of $Mg(OH)_2$ was performed at temperatures of 100, 150 and 200℃ under the CO_2 pressures of 20 and 30 bar. At each condition, seedless and heterogeneous precipitation was tested and compared.

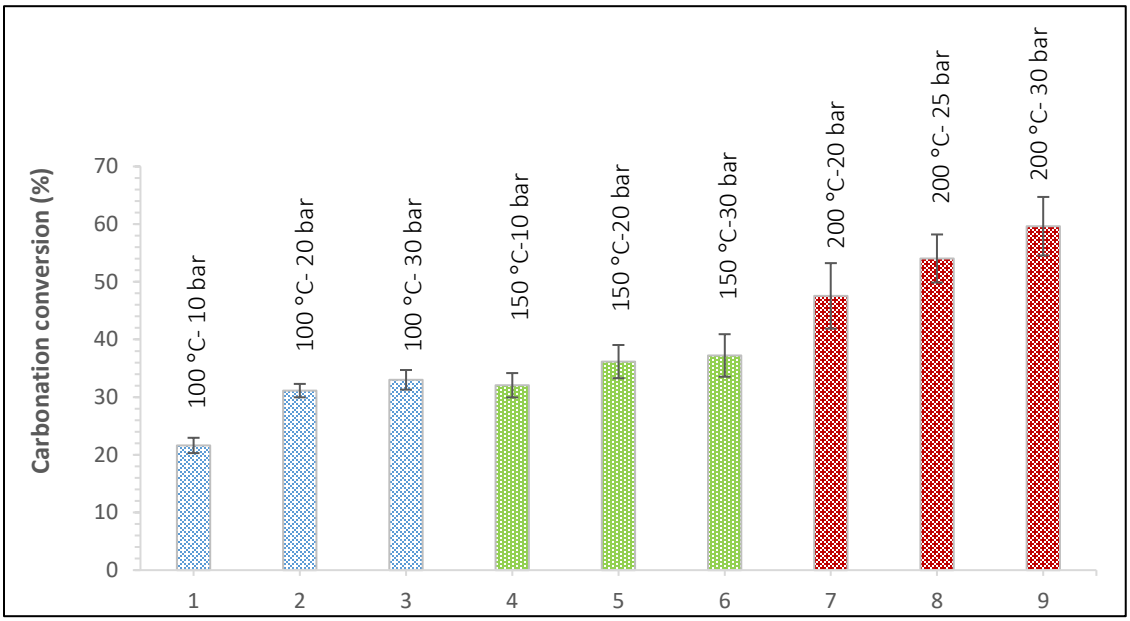

Figure 5-7. Carbonation conversion percentage variation as a function of carbonation temperature and pressure in precipitates formed during seedless aqueous carbonation of $Mg(OH)_2$.

In the first stage, crystalline carbonated products were analyzed using XRD method. The results are included in Figure 5-3. Similar to the previous research stage explained in section. (5.4.1), the brucite ($Mg(OH)_2$), hydromagnesite ($Mg_5(CO_3)_4(OH)_2{\cdot}4H_2O$) and magnesite ($Mg(CO_3)$) phases were identified in diffraction patterns to evaluate the qualitative effect of the preferred nucleation process on the type of precipitated phases. Based on the XRD results in Figure 5-3, the crystalline hydromagnesite phase was not found at high temperature condition (200℃). Again, TGA was performed as a complement to XRD analysis, to compensate for the weakness of XRD method in analyzing the possible amorphous carbonation products.

Figure 5-8 shows the TGA thermal decomposition plots of the carbonation products which were utilized to calculate the total conversion percentage of carbonation process, as well as the molar concentration of the possible hydromagnesite, magnesite and brucite phases, based on

the method explained in section (5.4.1). The ternary diagram presented in Figure 5-5 includes the data corresponding to heterogeneous carbonation as well as those recorded under seedless condition. Similar to the results of seedless precipitation, the effect of temperature increase on directing the $Mg(OH)_2$ carbonation process through the formation of anhydrous magnesium carbonate (magnesite) is clearly shown. The molar percentage of magnesite increases with increasing temperature. Thus, hydromagnesite content is not significant at the high temperature of 200 ℃, neither as an amorphous phase monitored with TGA (Figure 5-9) nor as a crystalline phase detected by XRD (Figure 5-3). The noticeable effect of temperature on the formation of $MgCO_3$ can be explained based on the previously discussed mechanism of magnesite formation, from the intermediate hydromagnesite phase, since high temperature speeds up the rate of hydromagnesite to magnesite transition through facilitating the liberation of water molecules [44]. Comparing the data points attributed to the activated carbon and alumina seeds in the ternary carbonation diagram presented in Figure 5-5, under similar temperature and pressure conditions, the magnesite molar concentration is higher for activated carbon.

Figure 5-9 shows that the magnesite concentration increases as a function of temperature and pressure in both seeding conditions, owing to the enhanced kinetics of hydromagnesite to magnesite transition or promoting the dissolution of CO_2 in aqueous solution as a first stage of carbonation (Eq. (2-4)). The trend in Figure 5-9 shows that the concentration of anhydrous magnesite phase is higher using activated carbon carbonation, compared to both alumina and seedless carbonations under similar applied temperature and pressure conditions. This result may be attributed, firstly, to the role of activated carbon as a heterogeneous site of nucleation, which decreases the energy barrier to nucleation [42, 43, 45, 53, 188-191]. On the other hand, unlike the alumina seed, activated carbon shows a water repelling effect, known as hydrophobic property, and so tends to repel water molecules. Because of this intrinsic hydrophobic property of activated carbon, the kinetics of the water-repellent process during hydromagnesite to magnesite transition can be enhanced, resulting in a higher concentration of magnesite precipitation, compared to hydrophilic alumina seeds.

Interestingly, the amount of magnesite concentration is the lowest with the alumina seeding, even lower than that for a seedless carbonation under 100 and 150℃, despite that heterogeneous seeding nucleation sites should, at least, in theory, enhance the kinetics of nucleation. This interesting finding can be explained considering the polar structure and hydrophilic property of alumina seeds which result in the hydrogen bond formation on the surface of alumina when it comes into contact with water [188, 192-195]. This, in turn, impedes the liberation of water molecules during the transition of hydromagnesite into magnesite phase and totally reduces the rate of magnesite phase formation, causing a reduction of magnesite quantity during carbonation.

In contrast to the 100 and 150 ℃ cases, at the applied carbonation temperature of 200 ℃ and a pressure of 20 bar (Figure 5-9), the concentration of magnesite phase is higher for the alumina seeding compared to the seedless carbonation, indicating clearly the dominant effect of high temperature and pressure on the hydromagnesite to magnesite transition through enhanced water liberation [188, 192-195]. However, at 200°C and a high pressure of 30 bar the magnesite content (Figure 5-9) reaches, within the experimental error, nearly the same quantity for the alumina (bar # 18 in Figure 5-9) and activated carbon (bar # 17 in Figure 5-9) seeding. Apparently, the effects of high temperature and pressure overcome the transition barrier and the influence of heterogeneous seeding, either hydrophobic or hydrophilic, becomes less important although the activated carbon seeding still results in the highest magnesite content in Figure 5-9 (bar # 17).

The total conversion percentage of the carbonation process was calculated based on the thermal method explained in section (5.4.1). The results are presented in Figure 5-10, and show a very similar trend to that of the magnesite molar percentage (Figure 5-9). This result shows a primary effect of anhydrous phase formation on the total efficiency of the carbonation process as discussed earlier.

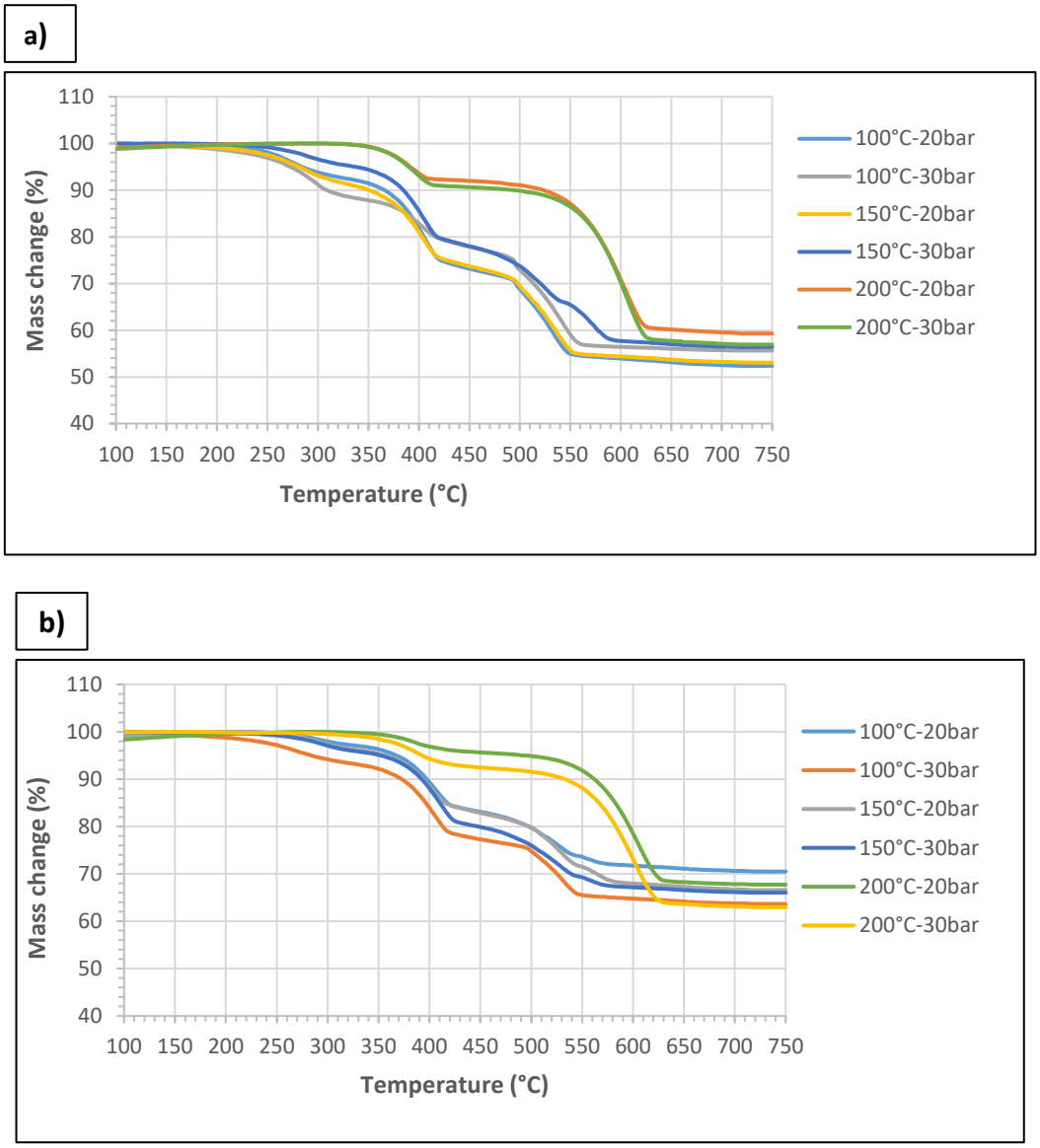

Figure 5-8. TGA thermal decomposition graph of precipitated phases, formed during aqueous carbonation of $Mg(OH)_2$ in heterogeneous carbonation using different seeding sites. a) Activated carbon and b) alumina.

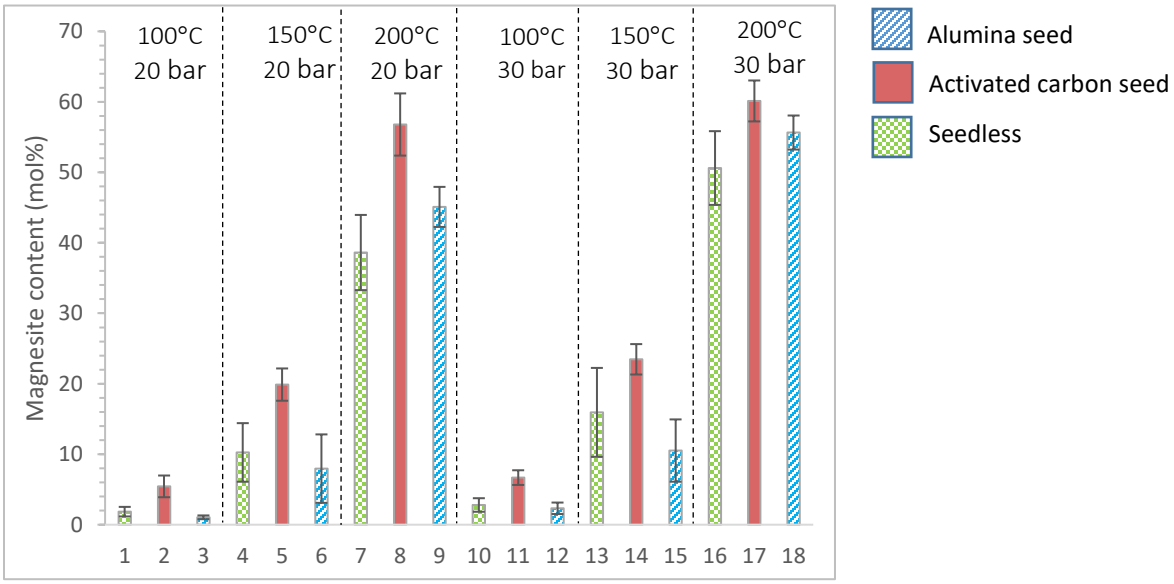

Figure 5-9. Magnesite molar concentration under varying carbonation temperature and pressure conditions, in precipitates formed during aqueous carbonation of $Mg(OH)_2$, under heterogeneous and seedless carbonation conditions.

Quantitative assessment of the outcomes of this research shows that simultaneously controlling the applied temperature and pressure and the effective implementation of seeds can increase the efficiency of carbonation for a specific period of time. It is found that under the carbonation conditions of 200℃, CO_2 pressure of 30 bar and with activated carbon seeding, the molar percentage of favorable anhydrous magnesite phase in the carbonation products reaches about 60% (Figure 5-9), with the corresponding carbonation conversion of about 72% (Figure 5-10).

Furthermore, the proposed carbonation approach has shown a successful outcome, even under moderate temperature conditions of 100 and 150℃. The molar percentage of magnesite in Figure 5-10 shows an increase of about 200% under the controlled conditions of 100℃ and CO_2 pressure of 20 bar and about 23%, at 150℃ and CO_2 pressure of 30 bar, using the activated carbon seeding, compared to similar conditions under seedless precipitation.

By comparison, in similar research on aqueous carbonation of $Mg(OH)_2$, Swanson et al. [45], reported the maximum magnesite concentration of about 98% which was achieved in one hour of carbonation at the carbonation temperature of 150℃ and CO_2 pressure of 15 atm, through injecting magnesite sites in the solution. Their reported concentration is much larger than 60% obtained in this work (150℃, about 30 bar CO_2 and with activated carbon seeds) (Figure 5-10). One reason for a larger concentration in [45] might be that their reactor was equipped with stirrer device which could facilitate the kinetics of mass transfer which was not employed in the present work. However, there is also a possibility that Swanson et al. [45] overestimated their results by not taking into account a separation issue between the quantity of the magnesite phase formed as an anhydrous precipitate during carbonation and the pre-injected magnesite seeds added to the solution intentionally, to form a preferred site of nucleation. The whole amount of mass change during decomposition of products in the decarbonation range of magnesite was attributed in [45] to the precipitated magnesite decomposition, neglecting whether the decomposed magnesite in that region was the product of carbonation or was a pre-injected seed. Furthermore, the portion of magnesite formed during thermal analysis as a consequence of previously decomposed hydromagnesite (through sequenced dehydration (Eq.(5-5)) and dehydroxylation (Eq. (5-4)) was not differentiated from magnesite formed during carbonation. In other words, the overlap in thermal decomposition range between the third stage of hydromagnesite decomposition (Eq.(5-5)) and the magnesite decarbonation (Eq. (2-27)) has not been considered by Swanson et al. [45]. Hence, the whole TGA mass change during decarbonation was ascribed to precipitated anhydrous magnesite. Attributing the whole mass change reduction in the thermal range of decarbonation to magnesite as a carbonation product might have been the cause of noticeable differences between the results of this research and those reported in [45].

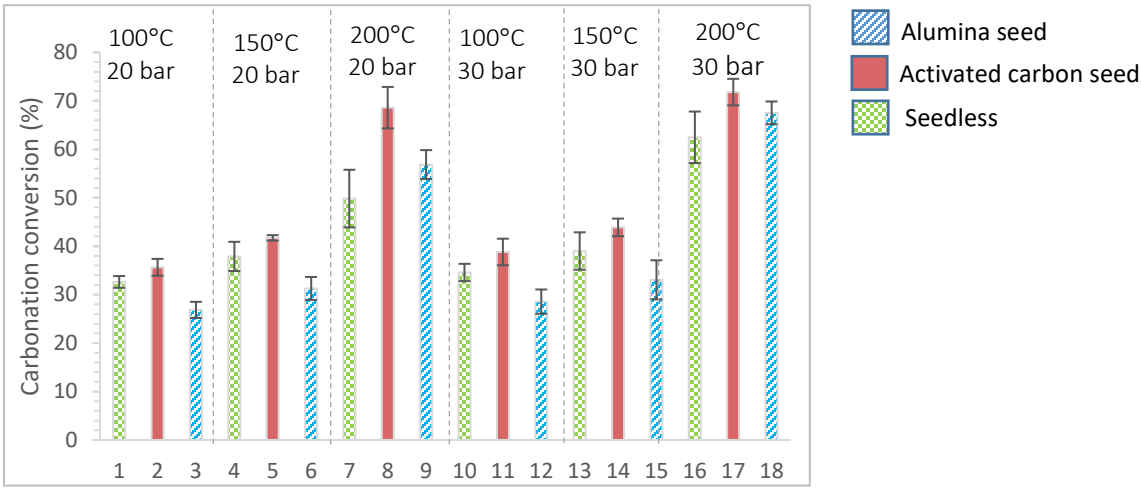

Figure 5-10. Carbonation conversion percentage under varying carbonation temperature and pressure conditions, in precipitates formed during aqueous carbonation of $Mg(OH)_2$, under heterogeneous and seedless carbonation conditions.

5.5 Summary

Directed precipitation of anhydrous magnesium carbonate ($MgCO_3$)/magnesite was evaluated and studied in this work. Although the formation of magnesite is thermodynamically favorable, the slow rate of precipitation is a limiting factor. Kinetics of precipitate nucleation and anhydrous magnesite formation (transition of hydromagnesite to magnesite) are enhanced through controlling the carbonation parameters and approaching heterogeneous carbonation.

Controlling the carbonation temperature and pressure during seedless carbonation of $Mg(OH)_2$ was the initial approach to enhance the kinetics of magnesite formation. In addition, implementation of seeding (heterogeneous) nucleation sites, including alumina and activated carbon, has been suggested, in order to accelerate the kinetics of anhydrous magnesite precipitation. The research outcomes are summarized as follows:

1. The effect of temperature on the increment of magnesite phase concentration in the final product of the carbonation process is noticeable. The enhancing effect of temperature on

the directed carbonation of $Mg(OH)_2$ is mostly attributed to the facilitating effect of temperature on water liberation during hydromagnesite to magnesite transition.

2. The role of preferred precipitation sites (heterogeneous seeding) on the directed precipitation of anhydrous magnesium carbonate and carbonation conversion percentage is significant. However, the influence of heterogeneous precipitation on directed precipitation is found to be dependent upon the nature of the precipitation sites.
3. The effect of heterogeneous nucleation sites (seeding materials) on the directed precipitation of magnesite is related to the surface chemistry of seeds. Thus, hydrophobic activated carbon enhances the kinetics of directed precipitation more efficiently than hydrophilic alumina. This observation is explained by the mechanism of magnesite formation through the transition of initially formed hydromagnesite to magnesite and their dissimilar behavior in aqueous solution. A hydrophilic polar compound alumina, has a great tendency to form a hydrogen bond with water molecules in an aqueous solution which delays the liberation of water molecules as a critical stage of hydromagnesite to magnesite transition. In contrast, hydrophobic activated carbon accelerates the kinetics of hydromagnesite to magnesite transition as a result of its intrinsic water repelling effect.
4. This approach shows that the simultaneous controlling of carbonation parameters accompanied by the implementation of heterogeneous sites succeeds in forming up to 60% magnesite molar concentration and a total conversion percentage of about 72%. Also, using activated carbon precipitation sites, even at the moderate thermal condition of 100 and 150℃, the magnesite molar concentration was increased by 200% and 23%, respectively, as compared to seedless condition.

Chapter 6
Summary and Future Work

6.1 Research Summary

The outcomes of the current Ph.D. thesis are summarized in three sections, based on the main research phases that are covered in chapters three to five.

6.1.1 Phase One- Investigation of Milling Energy Input on Structural Variation of Processed Olivine Powders for CO_2 Sequestration

6.1.1.1 Summary

In an attempt to find a correlation between structural parameters and milling energy input, the modified structural properties of olivine powders were found to be directly controlled by the amount of injected milling energy input. Based on the outcomes of this phase of study, the optimal value of pre-activation milling energy input, resulting in the most appropriate micro-structural properties for the purpose of permanent CO_2 storage, is about 55 kJ/g.

The trend of micro-structural parameter variation as a function of milling energy input, supplied by the high energy magneto ball mill in this research, was compared with previously reported trends which were gained with other types of milling devices. Addressing the similarity of recorded trends observed by different milling devices, the achieved amount of optimal milling energy input (about 55 kJ/g) was claimed to be a unique value, regardless of the type of implemented milling device.

6.1.1.2 Limitations and Suggestions

In this phase of research, the optimal amount of milling energy input is suggested, which ends up with the most suggested microstructure for CO_2 storage purposes.

A quantitative energy balance and economy efficiency analysis of the process must be evaluated. This should be done in order to evaluate the practical feasibility of the suggested pre-activation energy level, when integrated to a whole structure of mineral carbonation system. Different CO_2 emitters and varied sources of energy could be tried and compared, in order to suggest a feasible carbonation system, integrating the suggested level of pre-activation energy.

6.1.2 Phase Two- Optimizing Milling Energy for The Enhancement of Solid State Magnesium Sulfate ($MgSO_4$) Thermal Extraction for Permanent CO_2 Storage

6.1.2.1 Summary

A study on the kinetic enhancement of ÁAU solid-state extraction approach for $Mg(OH)_2$ production was performed as the second stage of the current Ph.D. work. The kinetics of solid-state extraction was enhanced via the pre-mechanical activation of reactant materials, including ammonium sulfate and olivine.

The pre-activation energy level of 27.6 kJ/g was found to be capable of forming the most suitable microstructure for the mineral carbonation process. Also, the suggested optimal pre-activation milling energy input was found to reduce the activation energy of solid-state extraction process, up to 34%.

Again, referring to the previous claim in section (6.1.1.1), about the generality of optimal milling energy input, regardless of milling device, the calculated amount of optimal pre-activation milling energy input, could be generalized to every mechanical pre-activation process, regardless of the device that is utilized for pre-activation purposes.

6.1.2.2 Limitations and Suggestions

Similar to the previous suggestion in section (6.1.1.2), the optimized level of energy that is calculated for the purpose of enhancing the kinetics of aforementioned solid-state reaction, is

calculated based on materials properties. Hence, a quantitative energy balance and economy efficiency analysis of the process must be investigated. Different CO_2 emitters and energy producers needs to be assessed, to estimate the practical feasibility of estimated pre-activation energy level.

The suggested methodology for the calculation of optimal pre-activation milling energy level could be examined and expanded to other carbonation feedstock and extraction techniques, upon application and industrial requirements.

6.1.3 Phase Three- Directed precipitation of anhydrous magnesite for improved performance of permanent CO_2 storage

6.1.3.1 Summary

This study was aiming to direct the process of $Mg(OH)_2$ aqueous mineral carbonation, through the formation of anhydrous Mg-carbonates.

The results of temperature and pressure control confirmed that temperature has a more noticeable effect on the formation of anhydrous Mg-carbonates, as compared to pressure. Therefore, anhydrous magnesite was found to be the sole precipitated carbonate under high temperature condition of 200 ºC during the one-hour carbonation process, ran at CO_2 pressure range of 10 to 30 bars. So, utilization of high temperature carbonation conditions was shown to enhance the process of directed anhydrous carbonation, and this effect was found to occur independent of carbonation pressure in the studied pressure range.

On the other hand, implementation of heterogeneous precipitation condition was shown to control the process of directed mineral carbonation. The efficiency of the heterogeneous approach was attributed to the type and surficial properties of implemented seeding materials. In this regard, the comparison of the behavior of hydrophilic alumina seeds and hydrophobic activated carbon confirmed the superior performance of activated carbon to end up with anhydrous precipitates. This behavior was mostly ascribed to the water repellant property of hydrophobic activated carbon, which stimulates the formation of favorable anhydrous

carbonates. Hence, the carbonation efficiency of $Mg(OH)_2$ aqueous carbonation process improved to about 72%, through implementation of activated carbon precipitation sites, under 200 ºC and CO_2 pressure of 30 bars.

6.1.3.2 Limitation and Suggestions

This study compares the efficiency of carbonation processes, under the implementation of two different seeding materials. The amount of SSA, as one of the most determinant parameters in mineral carbonation was designed to be kept constant and the hydrophobicity and surficial properties were discussed logically in accordance to the previously offered mechanisms of precipitates' formation. However, still there might be other surficial and structural differences between the implemented seeds that could be responsible for the different reported behaviors and performances. In this research the difference in behavior and performance of implemented seeding materials was mostly attributed to surface properties and specifically, to the hydrophobicity of considered materials. Hence, comprehensive investigation of the other possible causes of difference, in addition to surficial effect would be remained essential in order to come up with the most appropriate seeds, where the kinetics of precipitation is a limiting barrier.

Also, the carbonation apparatus used in this research phase was not equipped with mechanical agitation system. This practical limitation can lead to mass transfer kinetics barrier. This experimental barrier is also suggested to be addressed in future works.

List of Publications

Publications Referring to the Topic of Current Ph.D. Thesis

- ***Atashin, S.***, Wen, J.Z., Varin. R.A. (2016). Optimizing milling energy for enhancement of solid-state magnesium sulfate ($MgSO_4$) thermal extraction for permanent CO_2 storage, RSC Advances, 6: 68860 - 68869.
- ***Atashin, S.***, Kandasamy, J., Gökalpand, I., Wen, J.Z., Varin. R.A. (2016). Evaluation of the effect of steam concentration in flue gas, on carbonation of magnesium hydroxide for mineral CO_2 sequestration. Proceedings of 2016 8th International Conference on Chemical, Biological and Environmental Engineering (ICBEE 2016), Toronto, Ontario, Canada, September 24-26.
- ***Atashin, S.***, Wen, J.Z., Varin. R.A. (2015). Investigation of milling energy input on structural variation of processed olivine powders for CO_2 sequestration. Journal of Alloys and Compounds, 618:555-561.

Presentations Referring to the Topic of Current Ph.D. Thesis

- ***Atashin, S.***, Raj, A.,Wen, J.Z., Varin. R.A. (2015). Investigation of carbonation properties of magnesium hydroxide through thermal analysis. Canadian Material Science Canada 2015 (CMSC 2015), Halifax, Nova scotia, Canada, April 2015.
- ***Atashin, S.***, Power, I. (2014). Accelerating carbon mineralization in mine waste. Carbon Management Canada (CMC 2014), Banf, Alberta, Canada, May 2014.

Publications Referring to Collaborative Projects During Ph.D. Program

- Sui, H., ***Atashin, S.***, Wen, J.Z. (2016). Thermo-chemical and energetic properties of layered nano-thermite composites, Thermochemica Acta, 642: 17-24.

- J. Kang, J., ***Atashin, S.,*** Wen, J.Z., (2016). Frequency and temperature dependent electrochemical characteristics of electrodes made of commercialized activated carbon, graphene and single-walled carbon nanotubes, Carbon.
- Sui, H., ***Atashin, S.***, Wen, J.Z. (2016). Layer by layer nano-energetic composites fabricated via electrophoretic deposition. Proceedings of Combustion Institute – Canadian Section, University of Waterloo, Waterloo, Ontario, Canada, May 2016.
- Saceleanu, F., ***Atashin, S.***, Wen, J.Z. (2016). Roles of diffusion mechanism during oxidation of aluminum micro/nanoparticles. Proceedings of Combustion Institute – Canadian Section, University of Waterloo, Waterloo, Ontario, Canada, May 2016.
- Rawlins, J., Kang, J., ***Atashin, S.***, Wen, J.Z. (2014). Fabrication and characterization of micro-structure Al/CuO thermite foils. Proceedings of Combustion Institute – Canadian Section, University of Windsor, Windsor, Ontario, Canada, May 2014.

References

[1] Energy and climate change-world energy outlook-special briefing for COP21, International Energy Agency, France, 2015.

[2] Bea, S.A., S.A. Wilson, K.U. Mayer, G.M. Dipple, I.M. Power, P. Gamazo, Reactive transport modeling of natural carbon sequestration in ultramafic mine tailings, Vadose Zone Journal, 11 (2011).

[3] Carnevale, D.C., Carbon sequestration potential of the coast range ophliolite in california, in: Environmental and Earth Sciences, University of Rhodeisland, USA, 2013.

[4] Gislason, S.R., D. Wolff-Boenisch, A. Stefansson, E.H. Oelkers, E. Gunnlaugsson, H. Sigurdardottir, B. Sigfusson, W.S. Broecker, J.M. Matter, M. Stute, G. Axelsson, T. Fridriksson, Mineral sequestration of carbon dioxide in basalt: A pre-injection overview of the carbfix project, International Journal of Greenhouse Gas Control, 4 (2010) 537-545.

[5] McKelvy, M.J., A.V.G. Chizmeshya, J. Diefenbacher, H. Béarat, G. Wolf, Exploration of the role of heat activation in enhancing serpentine carbon sequestration reactions, Environmental Science & Technology, 38 (2004) 6897-6903.

[6] Olajire, A.A., A review of mineral carbonation technology in sequestration of CO_2, Journal of Petroleum Science and Engineering, 109 (2013) 364-392.

[7] Olivier, J.G.J., G. Janssens-Maenhout, M. Muntean, J.A.H.W. Peters, Trends in global CO_2 emissions-2015 report, PBL Netherlands Environmental Assessment Agency, No:JRC98184, Netherland, 2015.

[8] Werner, M., M. Verduyn, G. van Mossel, M. Mazzotti, Direct flue gas CO_2 mineralization using activated serpentine: Exploring the reaction kinetics by experiments and population balance modelling, Energy Procedia, 4 (2011) 2043-2049.

[9] Huijgen, W.J.J., R.N.J. Comans, Carbon dioxide sequestration by mineral carbonation, literature review, ECN-Clean Fossil Fuels Environmental Risk Assessment, Checked by: H.T.J. Reijers, Netherland, 2003.

[10] Kirsch, K., CO_2-induced metal release from sandstones: Implications for geologic carbon sequestration, in: Hydrologic Science and Engineering, Faculty and the board of Trustees, Colorado School of Mines, USA, 2013.
[11] Koukouzas, N., V. Gemeni, H.J. Ziock, Sequestration of CO_2 in magnesium silicates, in western macedonia, Greece, International Journal of Mineral Processing, 93 (2009) 179-186.
[12] Kwon, S., Mineralization for CO_2 sequestration using olivine sorbent in the presence of water vapor school of civil and environmental engineering, in: School of Civil and Environmental Engineering, Georgia Institute of Technology, 2011.
[13] Nduagu, E., T. Bjorklof, J. Fugerlund, E. Makila, J. Salonen, H. Geerlings, R. Zevenhoven, Production of magnesium hydroxide from magnesium silicate for the purpose of CO_2 mineralization-part 2: Mg extraction modeling and application to different Mg silicate rocks, Minerals Engineering, 30 (2012) 87-94.
[14] Sabouni, R., Carbon dioxide adsorption by metal organic frameworks (synthesis, testing and modeling), in: Chemical and Biochemical Engineering, University of Western Ontario, Canada, 2013.
[15] Boden, T.A., G. Marland, R.J. Andres, Global fossil-fuel CO_2 emissions, in, Carbon Dioxide Information Analysis Center, US Department of Energy (DOE), Oak Ridge national library, Tennessee, USA, 2010.
[16] Carbon dioxide: Projected emissions and concentrations, in, Intergovernmental Panel on Climate Change (IPCC), Department of Energy and Climate Change, 2014. (Last attempt: November 2016) http://www.ipcc-data.org/observ/ddc_co2.html
[17] Projections of future changes in climate-IPCC fourth assessment report, Climate change 2007: The physical science basis, 2007. (Last attempt: November 2016) https://www.ipcc.ch/publications_and_data/ar4/wg1/en/spmsspm-projections-of.html
[18] Trends in atmospheric carbon dioxide, in: Recent monthly average mauna Loa CO_2, US Department of Commerce-National Oceanic and Atmospheric Administration-Earth System Research Laboratory-Global Monitoring Division-NOAA Research, 2016. (Last attempt: November 2016) http://www.esrl.noaa.gov/gmd/ccgg/trends/

[19] Fricker, K.J., A.-H.A. Park, Effect of H_2O on $Mg(OH)_2$ carbonation pathways for combined CO_2 capture and storage, Chemical Engineering Science, 100 (2013) 332-341.
[20] Daval, D., O. Sissmann, N. Menguy, G.D. Saldi, F. Guyot, I. Martinez, J. Corvisier, B. Garcia, I. Machouk, K.G. Knauss, R. Hellmann, Influence of amorphous silica layer formation on the dissolution rate of olivine at 90°C and elevated P CO_2, Chemical Geology, 284 (2011) 193-209.
[21] Geerlings, H., R. Zevenhoven, CO_2 mineralization-bridge between storage and utilization of CO_2, Annual review of chemical and biomolecular engineering, 103 (2013) 103-117.
[22] Zevenhoven, R., J. Fagerlund, J.K. Songok, CO_2 mineral sequestration: Developments toward large-scale application, Greenhouse Gases: Science and Technology, 1 (2011) 48-57.
[23] Haug, T.A., Dissolution and carbonation of mechanically activated olivine- investigating CO_2 sequestration possibilities, in: Faculty of Engineering Science and Technology, Department of Geology and Mineral Resources Engineering, NTNU-Trykk, Norwegian University of Science and Technology, Trondheim, Norway, 2010.
[24] Haug, T.A., R.A. Kleiv, I.A. Munz, Investigating dissolution of mechanically activated olivine for carbonation purposes, Applied Geochemistry, 25 (2010) 1547-1563.
[25] Rimstidt, J.D., S.L. Brantley, A.A. Olsen, Systematic review of forsterite dissolution rate data, Geochimica et Cosmochimica Acta, 99 (2012) 159-178.
[26] Hariharan, S.B., M. Werner, D. Zingaretti, R. Baciocchi, M. Mazzotti, Dissolution of activated serpentine for direct flue-gas mineralization, Energy Procedia, 37 (2013) 5938-5944.
[27] Sanna, A., M. Uibu, G. Caramanna, R. Kuusik, M.M. Maroto-Valer, A review of mineral carbonation technologies to sequester CO_2, Chemical Society Reviews, (2014).
[28] Verduyn, M., H. Geerlings, G. van Mossela, S. Vijayakumari, Review of the various CO_2 mineralisation product forms, Energy Procedia 4, 4 (2011) 2885-2892.
[29] Al-Fattah, S.M., M.F. Barghouty, G. Bureau, B.O. Dabbousi, S. Fillacier, P.L. Thiez, C. McQuale, G. Munier, J.R. Andot, Carbon capture and storage; technologies, policies, economics and implementation strategies, CRC Press, Netherlands, 2012.

[30] Gysi, A.P., A. Stefánsson, Mineralogical aspects of CO_2 sequestration during hydrothermal basalt alteration -an experimental study at 75 to 250°C and elevated P_{CO2}, Chemical Geology, 306–307 (2012) 146-159.

[31] van Noort, R., C.J. Spiers, M.R. Drury, M.T. Kandianis, Peridotite dissolution and carbonation rates at fracture surfaces under conditions relevant for in situ mineralization of CO_2, Geochimica et Cosmochimica Acta, 106 (2013) 1-24.

[32] Nduagu, E., Mineral carbonation: Preparation of magnesium hydroxide ($Mg(OH)_2$) from serpentinite rock, in, Åbo Akademi University, Finland, 2008.

[33] Nduagu, E., Production of $Mg(OH)_2$ from Mg-silicate rock for CO_2 mineral sequestration, in: Thermal and Flow Engineering Laboratory, Department of Chemical Engineering, Division for Natural Sciences and Technology, Åbo Akademi University, Turku, Finland 2012.

[34] Nduagu, E., J. Bergerson, R. Zevenhoven, Life cycle assessment of CO_2 sequestration in magnesium silicate rock-a comparative study, Energy conversion and manageent, 55 (2012) 116-126.

[35] Nduagu, E., I. Romao, J. Fugerlund, R. Zevenhoven, Performance assessment of producing $Mg(OH)_2$ for CO_2 mineral sequestration, Applied Energy, 106 (2013) 116-126.

[36] Nduagu, E.I., J. Highfield, J. Chen, R. Zevenhoven, Mechanisms of serpentine - amonium sulfate reactions: Toward higher efficiencies in flux recovery and Mg extraction for CO_2 mineral sequestration, RSC Advances, 4 (2014) 64494-64505.

[37] Botha, A., C.A. St rydom, Preparation of a magnesium hydroxy carbonate from magnesium hydroxide, Hydrometallurgy, 62 (2001) 175– 183.

[38] Davies, P.J., B. Bubela, The transaction of nesquehonite into hydromagnesite, Chemical Geology, 12 (1973) 289-300.

[39] Harrison, A.L., I.M. Power, G.M. Dipple, Accelerated carbonation of brucite in mine tailings for carbon sequestration, Environmental Science & Technology, 47 (2013) 126−134.

[40] Xiong , Y., A.S. Lord, Experimental investigations of the reaction path in the $MgO–CO_2–H_2O$ system in solutions with various ionic strengths, and their applications to nuclear waste isolation, Applied Geochemistry, 23 (2008) 1634–1659.

[41] Zhao, L., L. Sang, J. Chen, J. Ji, H.H. Teng, Aqueous carbonation of natural brucite: Relevance to CO_2 sequestration, Environmental Science & Technology, 77 (2010) 406–411.
[42] Chevalier, N.R., Do surface wetting properties affect calcium carbonate heterogeneous nucleation and adhesion?, The Journal of Physical Chemistry, 118 (2014) 17600−17607.
[43] Donnet, M., P. Bowen, N. Jongen, H. Hofmann Use of seeds to control precipitation of calcium carbonate and determination of seed nature Langmuir, 21 (2005) 100-108.
[44] Sheila, D., P.R. Khangaonkar, Precipitation of magnesium carbonate, Hydrometallurgy, 22 (1989) 249-258
[45] Swanson, E., K. Fricker, M. Sun, A. Park, Directed precipitation of hydrated and anhydrous magnesium carbonates for carbon storage, Phys Chem Chem Phys., 16 (2014) 23440-23450.
[46] Kaldi, J.G., M. Gibson-Poole, T.H.D. Payenberg, Geological input to selection and evaluation of CO_2 geosequestration sites, M. Grobe, J.C. Pashin, L.R. Dodge (Eds.) Carbon dioxide sequestration in geological media - State of the science, The American association of petroleum geologists, USA, 2009, pp. 5-16.
[47] Climate change: Review of greenhouse gases, Climate change, Emission, United States Environmental Protection Agency (EPA), USA, 2016. (Last attempt: November 2016) https://www3.epa.gov/climatechange/ghgemissions/gases.html
[48] Jarvis, K., R.W. Carpenter, T. Windman, Y. Kim, R. Nunez, F. Alawneh, Reaction mechanisms for enhancing mineral sequestration of CO_2, Environmental Science & Technology, 43 (2009) 6314-6319.
[49] IEA statistics, CO_2 emissions from fuel combustion highlights, International Energy Agency, 9 rue de la Fédération, 75739 Paris Cedex 15, France, 2012 (Last attempt: November 2016) www.iea.org.
[50] Geologic storage and monitoring of CO_2: A uk research strategy, UK CCSRC Community Network, 2010. (Last attempt: November 2016) http://www.geos.ed.ac.uk/ccs/Meetings/storage-7july2010/.

[51] Grobe, M., J.C. Pashin, L.R. Dodge, Carbon dioxide sequestration in geological media - state of the science, The American association of petroleum geologists, USA, 2009.
[52] O'Connor, W.K., G.E. Rush, Applications of mineral carbonation to geological sequestration of CO_2, 30^{th} International Technical Conference on Coal Utilization & Fuel Systems, Clearwater, Florida, 2005.
[53] Porter, D.A., K. Easterling, M.Y. Sherif, Phase transformations in metals and alloys, 3 ed., CRC Press, USA, 2009.
[54] Power, I.M., A.L. Harrison, G.M. Dipple, S.A. Wilson, P.B. Kelemen, M. Hitch, G. Southam, Carbon mineralization: From natural analogues to engineered systems, Reviews in Mineralogy and Geochemistry, 77 (2013) 305-360.
[55] Reeves, S.R., An overview of CO_2-ECBM and sequestration in coal seams, in: Grobe, M., J.C. Pashin, L.R. Dodge (Eds.) Carbon dioxide sequestration in geological media - state of the science, The American association of petroleum geologists, USA, 2009, pp. 17-32.
[56] Carbon capture & storage: Governement of Canada. (Last attempt: November 2016). http://www.nrcan.gc.ca/energy/coal/carbon-capture-storage/4295
[57] What is CCS?: in, Carbon Capture and Storage Association (CCS), 2016. (Last attempt: November 2016) http://www.ccsassociation.org/what-is-ccs/
[58] Carbon capture & storage - CCS101: The Carbon Capture and Storage Information Source, 2016. (Last attempt: November 2016) http://ccs101.ca/
[59] Quick facts on CO_2 capture & storage in canada: Natural Resources canada, Government of Canada. (Last attempt: November 2016). http://www.nrcan.gc.ca/energy/coal/carbon-capture-storage/4297
[60] Boot-Handford, M.E., J.C. Abanades, E.J. Anthony, M.J. Blunt, S. Brandani, N. Mac Dowell, J.R. Fern´andez, M.C. Ferrari, R. Gross, J.P. Hallett, R.S. Haszeldine, P. Heptonstall, A. Lyngfelt, Z. Makuch, E. Mangano, R.T.J. Porter, M. Pourkashanian, G.T. Rochelle, N. Shah, Y. J.G., P.S. Fennell, Carbon capture and storage update, Energy and Environmental Science, 7 (2014) 130-189.

[61] Boschi, C., A. Dini, L. Dallai, G. G. Ruggieri, G. Gianelli, Enhanced CO_2-mineral sequestration by cyclic hydraulic fracturing and Si-rich fluid infiltration into serpentinites at malentrata (tuscany, italy), Chemical Geology, 265 (2009) 209-226.

[62] Seifritz, W., CO_2 disposal by means of silicates, Nature, (1990) 345, 486.

[63] Dunsmore, H.E., A geological perspective on global warming and the possibility of carbon dioxide removal as calcium carbonate mineral, Energy Conversion and Management 33 (1992) 565-572.

[64] Kojima, T., A. Nagamine, N. Ueno, S. Uemiya, Absorption and fixation of carbon dioxide by rock weathering, Energy Conversion and Management, 38, Supplement (1997) S461-S466.

[65] Gunter, W.D., P. E.H., T.J. McCann, Aquifer disposal of CO_2 rich gases: Reaction design for added capacity, Energy Conversion and Management, 34 (1993) 941-948.

[66] Lackner, K.S., C.H. Wendt, D.P. Butt, E.L. Joyce Jr, D.H. Sharp, Carbon dioxide disposal in carbonate minerals, Energy, 20 (1995) 1153-1170.

[67] Goldberg, P., Z.Y. Chen, W.K. O'Connor, R.P. Walters, H. Ziock, CO_2 mineral sequestration studies in US, National Energy Technology Laboratory, Pittsburgh, PA, USA, 2001.

[68] O'Connor, W.K., P.C. Turner, R.P. Walters, Carbon dioxide sequestration by ex-situ mineral carbonation, Second Annual Dixy Lee Ray Memorial Symposium, American Society of Mechanical Engineers, Washington D. C., 1999.

[69]CO_2 utilization focus area: US Department of Energy. (Last attempt: November 2016) http://www.netl.doe.gov/research/coal/carbon-storage/research-and-development/co2-utilization

[70] Cue´ llar-Franca, R.M., A. Azapagic, Carbon capture, storage and utilisation technologies: A critical analysis and comparison of their life cycle environmental impacts, Journal of CO_2 Utilization, 9 (2015) 85-102.

[71] Metz, B., O. Davidson, H.D. Coninck, M. Loos, L. Meyer, Carbon oxide capture and storage, IPCC Special Report on Carbon dioxide Capture and, Cambridge university press, UK, 2005.

[72] Zevenhoven, R., J. Kohlmann, A.B. Mukherjee, Direct dry mineral carbonation for CO_2 emissions reduction in finland, 27th International Technical Conference on Coal Utilization & Fuel Systems Clearwater, USA, March 4-7, 2002.

[73] Maroto-Valer, M.M., Developments and innovation in carbon dioxide (CO_2) capture and storage technology / edited by m. Mercedes Woodhead Publishing, Cambridge, 2010.

[74] Lackner, K.S., H.J. Ziock, From low to no emission, Modern Power Systems, 20 (2000) 31-32.

[75] Rollason, R.J., J.M.C. Plane, A kinetic study of the reactions of MgO with H_2O, CO_2 and O_2: Implications for magnesium chemistry in the mesosphere, Physical Chemistry Chemical Physics, 3 (2001) 4733-4740.

[76] Kohlmann, J., R. Zevenhoven, The removal of CO_2 from flue gas using magnesium silicates in finland, in: 11th International conference on coal science (ICCS-11), San Francisco, 2001.

[77] Gadikota, G., E.J. Swanson, H. Zhao, A.-H.A. Park, Experimental design and data analysis for accurate estimation of reaction kinetics and conversion for carbon mineralization, Industrial & Engineering Chemistry Research, 53 (2014) 6664-6676.

[78] Carbon sequestration: Mineral carbonation in peridotite for CO_2 capture and storage (CCS), Lamont Doherty Earth Observatory, Research education news and events people marine OPS , Columbia university, Earth institute. (Last attempt: November 2016) https://www.ldeo.columbia.edu/gpg/projects/carbon-sequestration

[79] Rockley, S.A., Carbon capture and storage, Elsevier, UK, 2010.

[80] Kwon, S., M. Fan, H.F.M. DaCosta, A.G. Russell, Factors affecting the direct mineralization of CO_2 with olivine, Journal of Environmental Sciences, 23 (2011) 1233-1239.

[81] Lackner, K.S., Carbonate chemistry for sequestering fossil carbon, Annual Review of Environment and Resources, 27 (2002) 193-232.

[82] Fegley, B., R. Osborne, Practical chemical thermodynamics for geoscientists, Academic Press, USA, 2012.

[83] Aresta, M., Carbon dioxide as chemical feedstock, Wiley-VCH Verlag GmbH & Co. KGaA, Weinheim, Germany, 2010.

[84] Zevenhoven, R., S. Teir, Long-term storage of CO_2 as magnesium carbonate in finland, 3rd annual conference on carbon capture and sequestration, Alexandria, 2004.

[85] Zevenhoven, R., S. Teir, S. Eloneva, Heat optimisation of a staged gas–solid mineral carbonation process for long-term CO_2 storage, Energy, 33 (2008) 362-370.

[86] Hangx, S.J.T., C.J. Spiers, Coastal spreading of olivine to control atmospheric CO_2 concentrations: A critical analysis of viability, International Journal of Greenhouse Gas Control, 3 (2009) 757-767.

[87] Lackner, K.S., D.P. Butt, C.H. Wendt, Progress on binding CO_2 in mineral substrates, Energy Conversion and Management, 38, Supplement (1997) S259-S264.

[88] Montes-Hernandez, G., R. Chiriac, F. Toche, F. Renard, Gas–solid carbonation of $Ca(OH)_2$ and cao particles under non-isothermal and isothermal conditions by using a thermogravimetric analyzer: Implications for CO_2 capture, International Journal of Greenhouse Gas Control, 11 (2012) 172-180.

[89] Zevenhoven, R., J. Fagerlund, Mineral sequestration for ccs in finland and abroad, World renewable energy congress, Sweden, 2011.

[90] Zevenhoven, R., J. Fagerlund, E. Nduagu, I. Romão, B. Jie, J. Highfield, Carbon storage by mineralisation (csm): Serpentinite rock carbonation via $Mg(OH)_2$ reaction intermediate without CO_2 pre-separation, Energy Procedia, 37 (2013) 5945-5954.

[91] Zevenhoven, R., I. Kavaliauskaite, Mineral carbonation for long-term CO_2 storage: An exergy analysis, International Journal of Thermodynamics, 7 (2004) 23-31.

[92] Zevenhoven, R., J. Kohlmann, CO_2 sequestration by magnesium silicate mineral carbonation in finland , Second nordic mini symposium on carbon dioxide capture and storage, Göteborg, 2001.

[93] Fauth, D.J., P. Goldberg, J.P. Knoer, Y. Soong, W.K. O'Connor, D.C. Dahlin, D.N. Nilson, R.P. Walters, Carbon dioxide storage as mineral carbonates, , Deviation of Fuel Chemical, American Chemical Society, 45 (4), (2000), 708-712.

[94] Garcia, B., V. Beaumont, E. Perfetti, V. Rouchon, D. Blanchet, P. Oger, G. Dromart, A.Y. Huc, F. Haeseler, Experiments and geochemical modelling of CO_2 sequestration by olivine: Potential, quantification, Applied Geochemistry, 25 (2010) 1383-1396.

[95] Julcour, C., F. Bourgeois, B. Bonfils, A. Benhamed, F. Guyot, F. Bodénan, C. Petiot, E.C. Gaucher, Ex situ mineral carbonation for CO_2 mitigation: Evaluation of mining waste resources, aqueous carbonation processability and life cycle assessment (carmex project), Chemical Engineering Journal, 262 (2015) 716-726.

[96] Olsson, J., N. Bovet, E. Makovicky, K. Bechgaard, Z. Balogh, S.L.S. Stipp, Olivine reactivity with CO_2 and H_2O on a microscale: Implications for carbon sequestration, Geochimica et Cosmochimica Acta, 77 (2012) 86-97.

[97] Schuiling, R.D., O. Tickell, Olivine against climate change and ocean acidification.(Last attempt: November 2016)
http://www.innovationconcepts.eu/res/literatuurSchuiling/olivineagainstclimatechange23.pdf

[98] Brown, G.E., D.K. Bird, T. Kendelewicz, K. Maher, W. Mao, N. Johnson, R.J. Rosenbauer, M. Park, P.G.D. Real, Geological sequestration of CO_2: Mechanisms and kinetics of CO_2 reactions in mafic and ultramafic rock formations. http://web.stanford.edu/~gebjr/09%20GCEP%20Progress%20Report%20(Brown%20et%20al.2).pdf

[99] Putnis, A., An introduction to mineral sciences, Cambridge University Press, UK, 1992.

[100] Voormeij, D.A., G.J. Simandl, Geological and mineral CO_2 sequestration options: A technical review, Geological fieldwork, 2002.

[101] Larachi, F., J.P. Gravel, B.P.A. Grandjean, G. Beaudoin, Role of steam, hydrogen and pretreatment in chrysotile gas–solid carbonation: Opportunities for pre-combustion CO_2 capture, International Journal of Greenhouse Gas Control, 6 (2012) 69-76.

[102] Marini, L., Development in geochemistry 11, Geological sequestration of carbon dioxide; thermodynamics, kinetics and reaction path modelling, Elsevier, UK, 2007, pp. 15-26.

[103] Mascetta, J.A., M.C. Kernion, Barron's e-z chemistry, Barron's, USA, 2009.

[104] Bard, A.J., Chemical equilibrium, Harper & Row, USA, 1966.
[105] Fagerlund, J., J. Highfield, R. Zevenhoven, Kinetics studies on wet and dry gas-solid carbonation of MgO and $Mg(OH)_2$ for CO_2 sequestration, RSC Advances, 2 (2012) 10380-10393.
[106] Bearat, H., M.J. McKelvy, A.V. Chizmeshya, D. Gormley, R. Nunez, R.W. Carpenter, K. Squires, G.H. Wolf, Carbon sequestration via aqueous olivine mineral carbonation: Role of passivating layer formation, Environmental Science & Technology, 40 (2006) 4802-4808.
[107] Lackner, K.S., D.P. Butt, C.H. Wendt, Binding carbon dioxide in mineral form: A critical step towards a zero-emission coal power plant, DOE Office of Scientific and Technical Information (OSTI), USA, 1998.
[108] Bobicki, E.R., Q. Liu, Z. Xu, H. Zeng, Carbon capture and storage using alkaline industrial wastes, Progress in Energy and Combustion Science 38 (2012) 302-320.
[109] Atashin, S., J.Z. Wen, R.A. Varin, Optimizing milling energy for enhancement of solid-state magnesium sulfate ($MgSO_4$) thermal extraction for permanent CO_2 storage, RSC Advances, 6 (2016).
[110] Highfield, J., H. Lim, J. Fagerlund, R. Zevenhoven, Activation of serpentine for CO_2 mineralization by flux extraction of soluble magnesium salts using ammonium sulfate, RSC Advances, 2 (2012) 6535-6541.
[111] Fagerlund, J., S. Teir, E. Nduagu, R. Zevenhoven, Carbonation of magnesium silicate mineral using a pressurised gas/solid process, Energy Procedia, 1 (2009) 4907-4914.
[112] Saldi, G.D., D. Daval, G. Morvan, K.G. Knauss, The role of Fe and redox conditions in olivine carbonation rates: An experimental study of the rate limiting reactions at 90 and 150°c in open and closed systems, Geochimica et Cosmochimica Acta, 118 (2013) 157-183.
[113] O'Connor, W.K., D.C. Dahlin, D.N. Nilson, G.E. Rush, R.P. Walters, P.C. Turner, CO_2 storage in solid form: A study of direct mineral carbonation, 5^{th} International Conference on Greenhouse GasTechnologies, Cairns, Australia, 2000.

[114] Kerisit, S., J.H. Weare, A.R. Felmy, Structure and dynamics of forsterite–SC CO_2/H_2O interfaces as a function of water content, Geochimica et Cosmochimica Acta, 84 (2012) 137-151.

[115] Kwak, J.H., J.Z. Hu, R.V.F. Turcu, K.M. Rosso, E.S. Ilton, C. Wang, J.A. Sears, M.H. Engelhard, A.R. Felmy, D.W. Hoyt, The role of H_2O in the carbonation of forsterite in supercritical CO_2, International Journal of Greenhouse Gas Control, 5 (2011) 1081-1092.

[116] Thompson, C.J., J.S. Loring, K.M. Rosso, Z. Wang, Comparative reactivity study of forsterite and antigorite in wet supercritical CO_2 by in situ infrared spectroscopy, International Journal of Greenhouse Gas Control, 18 (2013) 246-255.

[117] Béarat, H., M.J. McKelvy, A.V.G. Chizmeshya, R. Sharma, R.W. Carpenter, Magnesium hydroxide dehydroxylation/carbonation reaction processes: Implications for carbon dioxide mineral sequestration, Journal of the American Ceramic Society, 85 (2002) 742-748.

[118] Shih, S., C. Ho, Y. Song, J. Lin, Kinetics of the reaction of $Ca(OH)_2$ with CO_2 at low temperature, Industrial & Engineering Chemistry Research, 38 (1999) 1316-1322.

[119] Wu, S.F., T.H. Beum, J.I. Yang, J.N. Kim, Properties of Ca-base CO_2 sorbent using $Ca(OH)_2$ as precursor, Industrial & Engineering Chemistry Research, 46 (2007) 7896-7899.

[120] Butt, D.P., K.S. Lackner, C.H. Wendt, S.D. Conzone, H. Kung, Y.C. Lu, J.K. Bremser, Kinetics of thermal dehydroxylation and carbonation of magnesium hydroxide, Journal of the American Ceramic Society 7(1996) 1892–1898.

[121] Butt, D.P., K.S. Lackner, C.H. Wendt, V. R., L. PILED, Y. Park, T. Holesinger, D.M. Harradine, K. Nomura, The kinetics of binding carbon dioxide in magnesium carbonate, in, Proceedings of the 23rd international technical conference on coal utilization and fuel systems, USA, March 9–13, 1998.

[122] Kato, Y., N. Yamashita, K. Kobayashi, Y. Yoshizawa, Kinetic study of the hydration of magnesium oxide for a chemical heat pump, Applied Thermal Engineering, 16 (1996) 853-862.

[123] L'Vov, B.V., A.V. Novichikhin, A.O. Dyakov, Mechanism of thermal decomposition of magnesium hydroxide, Thermochimica Acta, 315 (1998) 135-143.

[124] Assima, G.P., F. Larachi, J. Molson, G. Beaudoin, Accurate and direct quantification of native brucite in serpentine ores—new methodology and implications for CO_2 sequestration by mining residues, Thermochimica Acta, 566 (2013) 281-291.

[125] Gerdemann, S.J., D.C. Dahlin, W.K. O'Connor, L.R. Penner, Carbon dioxide sequestration by aqueous mneral carbonation of magnesium silicate minerals, 2nd Annual Conference on Carbon Sequestration, Alexandria, Virginia, 2003.

[126] O'Connor, W.K., D.N. Nilson, R.P. Walters, P.C. Turner, Carbon dioxide sequestration by direct mineral carbonation with carbonic acid, Proceedings of the 25th International Technical Conf. On Coal Utilization & Fuel Systems, Coal Technology Assoc., Clear Water, Florida, 2000.

[127] Pokrovsky, O.S., J. Schott, Kinetics and mechanism of forsterite dissolution at 25°C and pH from 1 to 12, Geochimica et Cosmochimica Acta, 64 (2000) 3313-3325.

[128] O'Connor, W.K., D.C. Dahlin, D.N. Nilson, S.J. Gerdemann, G.E. Rush, L.R. Penner, R.P. Walters, P.C. Turner, Continuing studies on direct aqueous mineral carbonation for CO_2 sequestration, 27th International Technical Conf. on Coal Utilization & Fuel Systems, Clear Water, Florida, 2002.

[129] Wolff-Boenisch, D., S.R. Gislason, E.H. Oelkers, The effect of crystallinity on dissolution rates and CO_2 consumption capacity of silicates, Geochimica et Cosmochimica Acta, 70 (2006) 858-870.

[130] Fabian, M., M. Shopska, D. Paneva, G. Kadinov, N. Kostova, E. Turianicová, J. Briančin, I. Mitov, R.A. Kleiv, P. Baláž, The influence of attrition milling on carbon dioxide sequestration on magnesium–iron silicate, Minerals Engineering, 23 (2010) 616-620.

[131] Sandvik, K.L., R.A. Kleiv, T.A. Haug, Mechanically activated minerals as a sink for CO_2, Advanced Powder Technology, 22 (2011) 416-421.

[132] Fauth, D.J., J.P. Baltrus, J.P. Knoer, Y. Soong, B.H. Howard, W.J. Graham, M.M. Maroto-Valer, J.M. Andresen, Conversion of silicate minerals with carbon dioxide producing environmentally benig nandstable carbonates, Journal of the American Chemical Society, Division of Fuel Chemistry, 46 (2001) 278-279.

[133] Verduyn, M., H. Boerrigter, R. Oudwater, G.A.F. van Mossel, A novel process concept for CO_2, mineralization; technical opportunities and challenges, transport and storage, 5th Trondheim Conference on CO_2 Capture, Trondheim, 2009.

[134] Hänchen, M., V. Prigiobbe, R. Baciocchi, M. Mazzotti, Precipitation in the mg-carbonate system—effects of temperature and CO_2 pressure, Chemical Engineering Science, 63 (2008) 1012–1028.

[135] Montes-Hernandez, G., F. Renarda, R. Chiriac, N. Findling, F. Toche, Rapid precipitation of magnesite micro-crystals from $Mg(OH)_2$-H_2O- CO_2 slurry enhanced by naoh and a heat-ageing step (from 20 to 90ºc), Crystal Growth & Design, 12 (2012) 5233–5240.

[136] Schaef, H.T., C.F. Windisch Jr., B.P. McGrail, P.F. Martin, K.M. Rosso, Brucite ($Mg(OH)_2$) carbonation in wet supercritical CO_2: An in situ high pressure X-ray diffraction study, Geochimica et Cosmochimica Acta, 75 (2011) 7458–7471.

[137] Riviere, J.C., M. Sverre, Handbook of surface and interface analysis: Methods for problem-solving, Second Edition ed., CRC Press, USA, 2009.

[138] Vajtai, R., Springer handbook of nanomaterials, Springer-Verlag Berlin Heidelberg, USA, 2013.

[139] Aliofkhazraei, M., Handbook of mechanical nanostructuring,Wiley, 2015.

[140] Földvári, M., Handbook of thermogravimetric system of minerals and its use in geological practice, Occasional papers of the geological institute of hungary,, Geological Institute of Hungary, Hungary, 2011.

[141] Kleiv, R.A., M. Thornhill, Mechanical activation of olivine, Minerals Engineering, 19 (2006) 340-347.

[142] Turianicová, E., P. Baláž, Ľ. Tuček, A. Zorkovská, V. Zeleňák, Z. Németh, A. Šatka, J. Kováč, A comparison of the reactivity of activated and non-activated olivine with CO_2, International Journal of Mineral Processing, 123 (2013) 73-77.

[143] Patents: , CA2066740, EP0494899, AU643949 (Ed.).

[144] Calka, A., A.P. Radlinski, Universal high performance ball-milling device and its application for mechanical alloying, Materials Science and Engineering: A, 134 (1991) 1350-1353.
[145] Varin, A.R., T. Czujko, Z.S. Wronski, Nanomaterials for solid state hydrogen storage, Springer Science and Business Media, New York, USA, 2009.
[146] Materials data inc. (Last attempt: November 2016) http://www.materialsdata.com/
[147] Chantler, C.T., N.A. Rae, C.Q. Tran, Accurate determination and correction of the lattice parameter of lab6 (standard reference material 660) relative to that of Si (640b), Journal of Applied Crystallography, 40 (2007) 232-240.
[148] Pourghahramani, P., E. Forssberg, Microstructure characterization of mechanically activated hematite using xrd line broadening, International Journal of Mineral Processing, 79 (2006) 106-119.
[149] Balzar, D., K.S. Constan, Voigt-function model in diffraction line-broadening analysis, Microstructure Analysis From Diffraction, International Union of Crystallography, 1999.
[150] Summers, C.A., D.C. Dahlin, G.E. Rush, W.K. O'Connor, S.J. Gerdemann, Grinding method to enhance the reactivity of olivine, SME Annual Meeting and Exhibit, Denver, Colorado, 2004.
[151] Parviz, R., R.A. Varin, Combined effects of molar ratio and ball milling energy on the phase transformations and mechanical dehydrogenation in the lithium amide-magnesium hydride ($LiNH_2 + nMgH_2$)(n = 0.5–2.0) nanocomposites, International Journal of Hydrogen Energy, 38 (2013) 8313-8327.
[152] Baláž, P., E. Turianicová, M. Fabián, R.A. Kleiv, J. Briančin, A. Obut, Structural changes in olivine $(Mg, Fe)_2SiO_4$ mechanically activated in high-energy mills, International Journal of Mineral Processing, 88 (2008) 1-6.
[153] Lowell, S., J.E. Shields, M. Thomas, F. Thommes, Characterization of porous solids and powders: Surface area, pore size and density, Kluwer Academic Publishers, USA, 2004.
[154] Klug, H.P., L. Alexander, X-ray diffraction procedures for polycrystalline and amorphous materials, John Wiley & Sons, New York, 1974.

[155] Varin, R.A., J. Bystrzycki, A. Calka, Effect of annealing on the microstructure, ordering and microhardness of ball milled cubic ($L1_2$) titanium trialuminide intermetallic powder, Intermetallics, 7 (1999) 785-796.

[156] Atashin, S., J.Z. Wen, R.A. Varin, Investigation of milling energy input on structural variations of processed olivine powders for CO_2 sequestration, Journal of Alloys and Compounds, 618 (2015) 555-561.

[157] Criado, J.M., A. Ortega, C. Real, E. Torres De Torres, Re-examination of the kinetics of the thermal dehydroxilation of kaolinite, Clay Minerals, 19 (1984) 653-661.

[158] Hancock, J.D., J.H. Sharp, Method of comparing solid-state kinetic data and its application to the decomposition of kaolinite, Journal of the American Ceramic Society, 55 (1972) 74-77.

[159] Augis, J.A., J.E. Bennett, Calculation of the avrami parameters for heterogeneous solid state reactions using a modification of the kissinger method, Journal of thermal analysis, 13 (1978) 283-292.

[160] Redfern, S.A.T., The kinetics of dehydroxilation of kaolinite, Clay Minerals, 22 (1987) 447-456.

[161] Saniger, J.M., H. Hu, Kinetic studies of the dehydration process for polyacrylic acid-metal oxide compounds, Materials Letters, 15 (1992) 113-117.

[162] López Ortiz, A., M.A. Escobedo Bretado, V. Guzmán Velderrain, M. Meléndez Zaragoza, J. Salinas Gutiérrez, D. Lardizábal Gutiérrez, V. Collins-Martínez, Experimental and modeling kinetic study of the CO_2 absorption by Li_4SiO_4, International Journal of Hydrogen Energy, 39 (2014) 16656-16666.

[163] Carl Koch, L.O.k., M. Seal, S. Veprek, , Structural nanocrystalline materials: Fundamentals and applications, Cambridge University Press, UK, 2007.

[164] Fecht, H.J., E. Hellstern, Z. Fu, W.L. Johnson Nanocrystalline metals prepared by high-energy ball milling Metallurgical Transactions A, 21A (1990) 2333-2337.

[165] Bai, Q., D.L. Kohlstedt, High-temperature dislocation creep of olivine single crystals, 2. Dislocation structures, Tectonophysics, 206 (1992) 1-29.

[166] Farla, R.J.M., H. Kokkonen, J.D. Fitz Gerald, A. Barnhoorn, U.H. Faul, J. Jackson, Dislocation recovery in fine-grained polycrystalline olivine, Physics and Chemistry of Minerals, 38 (2010) 363-377.

[167] Karato, S., M. Ogawa, High-pressure recovery of olivine: Implications for creep mechanisms and creep activation volume, Physics of the Earth and Planetary Interiors, 28 (1982) 102-117.

[168] Drury, M.R., J.L. Urai, Deformation-related recrystallization processes, Tectonophysics, 112 (1990) 235-253.

[169] Groza, J.R., J.F. Shackelford, Materials processing handbook, CRC Press, USA, 2007.

[170] Vainshtein, B.K., V.M. Friedkin, V.L. Indenbom, Structure of crystals, Springer, Russia, 1995.

[171] Abbaschian, R., L. Abbaschian, R.E. Reed-Hill, Physical metallurgy principles, 4 ed., CENGAGE, Stanford, USA, 2009.

[172] Bozzolo, N., A. Agnoli, N. Souai, M. Bernacki, R.E. Loge, Strain induced abnormal grain growth in nickel base superalloys, 5th International Conference on Recrystallization and Grain Growth, Sydney, Australia, 2013, pp. 321-324.

[173] Paggi, G.A.A., R. Donnini, Strain induced grain boundary migration effects on grain growth of an austenitic stainless steel during static and metadynamic recrystallization, Materials Characterization, 107 (2015) 174-181.

[174] Khawam, A., D.R. Flanagan, Solid-state kinetic models: Basics and mathematical fundamentals, Journal of Physical Chemistry B, 110 (2006) 17315-17328.

[175] Chromik, R.R., W.K. Neils, E.J. Cotts, Thermodynamic and kinetic study of solid state reaction in the Cu-Si system, Journal of Applied Physics, 86 (1999) 4273-4281.

[176] Ovid'ko, I.A., A.B. ReÏzis, Grain-boundary dislocation climb and diffusion in nanocrystalline solids, Physics of the Solid State, 43 (2001) 35-38.

[177] Hirscher, M., Handbook of hydrogen storage: New materials for future energy storage, Wiley-VCH, Stuttgart, Germany, 2010.

[178] Mineral saturation index: A Dictionary of Earth Sciences, Encyclopedia.com. (Last attempt: November 2016) http://www.encyclopedia.com/science/dictionaries-thesauruses-pictures-and-press-releases/mineral-saturation-index.

[179] Gaskell, D.R., Introduction to the thermodynamics of materials, 5 ed., CRC Press, USA, 2008.

[180] Hollingbery, L.A., T.R. Hull, Brucite ($Mg(OH)_2$), hudromagnesite ($Mg_5(CO_3)_4(OH)_2{\cdot}4H_2O$) and magnesite ($Mg(CO_3)$), Thermochimica Acta, 509 (2010) 1-11.

[181] Padeste, C., O. H.R, A. Relier, The thermal behaviour of pure and nickel-doped hydromagnesite in different atmosphers, Mat. Res. Bull, 26 (1991) 1263-1268.

[182] Sawada, Y., K. Uematsu, N. Mizutani, M. Kato, Thermal decomposition of hydromagnesite $4MgCO_3{\cdot}Mg(OH)_2{\cdot}4H_2O$, Journal of Inorganic and Nuclear Chemistry, 40 (1978) 979-982.

[183] Sawada, Y., J. Yamaguchi, O. Sakurai, K. Uematsu, N. Mizutani, M. Kato, Thermogravimetric study on decomposition of hydromagnesite $4MgCO_3.Mg(OH)_2.4H_2O$, Thermochimica Acta, 32 (1979) 127-140.

[184] Sawada, Y., J. Yamaguchi, O. Sakurai, K. Uematsu, N. Mizutani, M. Kato, Isothermal differential scanning calorimetry on an exothermic phenomenon during thermal decomposition of hydromagnesite $4\ MgCO_3 \cdot Mg(OH)_2 \cdot 4\ H_2O$, Thermochimica Acta, 34 (1979) 233-237.

[185] Todor, D.N., Thermal analysis of minerals, Abacus Press, England, 1976.

[186] Robie, R.A., B.S. Hemingway, The enthalpies of formation of nesquehonite, $MgCO_3.H_2O$, and hydromagnesite $5MgO.4CO_2.5H_2O$, Journal of research-U.S. department of the interior, 1 (1973) 543-549.

[187] Chu Zhang, P., H.L. Anderson, J.W. Kelly, J.L. Krumhansl, H.W. Papenguth, Kinetics and mechanisms of formation of magnesite from hydromagnesite in brine in: Applied Geochemistry, 2000.

[188] Lefe`vre, G., M. Duc, P. Lepeut, R. Caplain, M. Fe´doroff, Hydration of γ-alumina in water and its effects on surface reactivity, Langmuir, 18 (2002) 7530-7537.

[189] Tadros, T.F., J.B. Rosenholm, Colloid stability: The role of surface forces, Wiley, USA, 2011.

[190] Tanford, C., Interfacial free energy and the hydrophobic effect, Proc. Natl. Acad. Sci., USA, 1979, pp. 4175-4176.

[191] Nesse, W., D, Introduction to mineralogy, Second ed., Oxford university press, Newyork, 2010.

[192] Akao, M., S. Iwai, The hydrogen bonding of hydromagnesite, Acta Crystallographica, B33 (1977) 1273-1275.

[193] Akao, M., F. Marumo, S. Iwai, The crystal structure of hydromagnesite, Acta Crystallographica.B3, 267 (1974) 2670-2672.

[194] Azimi, G., R. Dhiman, H.M. Kwon, A.T. Paxson, K.K. Varanasi, Hydrophobicity of rare-earth oxide ceramics, Nature Materials, 12 (2013) 315–320.

[195] KC, H., W.F. Schneider, A. Curioni, W. Andreoni, The chemistry of water on alumina surfaces: Reaction dynamics from first principles, Science, 282 (1998) 265-268.

[196] Kinetics of Phase Growth: single-component or composition-invariant transformation. (Last attempt: November 2016) http://www.eng.utah.edu/~lzang/images/lecture-15.pdf

Appendix A

Particle Size Measurement from SEM Micrographs

Particle size is measured using SEM micrographs, obtained by secondary electron detector. The SEM magnification is adjusted to assure that the image shot contains reasonable statistical population for measurement. The SEM images are then analyzed using image analyzer software for size measurement. Image J, version 1.47 V, developed at the National Institutes of Health, USA, [146] is used in current research for the particle size analysis. The diameter size of each particle is measured using image analyzer software in different directions, to find an approximate equivalent spherical diameter size of the considered powder. And finally, the arithmetic average of measured lengths is considered as mean particle size (Eq. (A-1)), and is reported with valid standard deviation. Figure A-1 represents the schematic procedure of particle size measurement, using SEM micrographs.

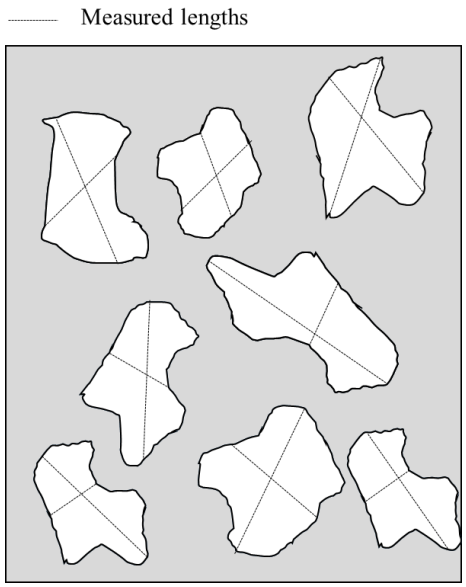

Figure A-1 Schematic overview of particle size measurement using SEM micrographs.

$$D = \frac{1}{n}\sum_{i=1}^{n} L_i$$

n is total number of measured lengths, L is measured length and D is mean particle size.

Appendix B

The Johnson-Mehl- Avrami- Kohnogorov (JMAK) Kinetics Model

B.1 Assumptions

The kinetics of the phase transformation process can be modelled using the JMAK kinetics model, considering the following assumptions:

1. Nucleation starts randomly in the bulk and at the surface
2. The sample size is much greater than any individual transformed region
3. Nucleation growth occurs homogeneously.
4. Nucleation rate is constant [145].

B.2 Kinetics of Phase Transformation

Assuming phase α is transferring to β under isothermal condition, radial length of growth nuclei can be written as Eq. (B-1).

$$r(t) = r_0 + vt \qquad \text{B-1}$$

r_0 is initial radius of nuclei, v is radial growth velocity (length/time), and t is growth time.

Assuming n as number of nuclei per unit volume, the number of nuclei that are isolated at time t can be shown as Eq. (B-2).

$$n(t) = n[1 - x(t)] \qquad \text{B-2}$$

Where, x(t) is volume fraction transformation.

At time t, the volume fraction for the growth of an isolated nuclei from radius r to r+dr is as Eq. (B-3).

$$d\,x(t) = n(t).\,dv = 4\pi n v^3 r^2 dt\,[1- x(t)] \quad \text{B-3}$$

Knowing that r(t) = vt and dr = v dt, x(t) can be rewritten as Eq. (B-4) and Eq. (B-5).

$$\frac{d\,x(t)}{1-x(t)} = 4\pi n v^3 t^2 dt \quad \text{B-4}$$

$$x(t) = 1-\exp\left[-\frac{4\pi n v^3 t^3}{3}\right] \quad \text{B-5}$$

Assuming the time constant (τ) is $[\frac{3}{4\pi n v^3}]^{1/3}$, x(t) will be as Eq.(B-6).

$$x(t)= 1-\exp\left[\frac{-t}{\tau}\right]^{1/m} \quad \text{B-6}$$

Taking m as the Avrami order and kinetics constant (k) as 1/τ, the JMAK kinetics model is derived as Eq. (B-7) [196].

$$x(t)= 1-\exp\left[-(kt)^m\right] \quad \text{B-7}$$

Appendix C

Evaluation of The Effect of Steam Concentration in Flue Gas, on Carbonation of Magnesium Hydroxide for Mineral CO_2 Sequestration[14]

C.1 Overview

In order to improve the efficiency of indirect carbonation processes, $Mg(OH)_2$ carbonation needs to be well-controlled, and the energy release should be quantified. Carbonation efficiency of $Mg(OH)_2$ can be greatly enhanced by water steam. In this study, an investigation on the effects of steam concentration on $Mg(OH)_2$ carbonation was performed, and the determinant effect of $Mg(OH)_2$ dehydroxylation was discussed. Carbonation reactions were evaluated in the isothermal conditions of 200℃, 250℃ and 325℃, under the atmosphere of an Ar-CO_2-H_2O mixture. H_2O concentrations of 0, 10 and 15% were tested, and the effective concentration range of H_2O was suggested based on the proposed carbonation mechanisms. The results clearly supported the enhancing effect of water steam on the kinetics of $Mg(OH)_2$ dry carbonation process. However, the exact effect of water steam on kinetics of $Mg(OH)_2$ dry carbonation is strongly dependant upon the dehydroxylation ability of $Mg(OH)_2$ powders. Finally, with the careful consideration of water steam effect on dehydroxylation and carbonation of $Mg(OH)_2$, the concentration of 10% water steam is determined as an optimal concentration among those tried, resulting in the enhanced kinetics of $Mg(OH)_2$ dry carbonation.

[14] The content of this chapter is published as:

Atashin, S., Kandasamy, J., Gökalpand, I., Wen, J.Z., Varin. R.A. (2016). Evaluation of the effect of steam concentration in flue gas, on carbonation of magnesium hydroxide for mineral CO_2 sequestration. Proceedings of 2016 8th International Conference on Chemical, Biological and Environmental Engineering (ICBEE 2016), Toronto, Ontario, Canada, September 24-26.

C.2 Experimental

Magnesium hydroxide ($Mg(OH)_2$) powder, produced by Fluka analytical (purity > 99%) and supplied by Sigma Aldrich (Germany), was utilized. The carbonation process and thermogravimetry analysis were performed in a NETZSCH STA 429 thermal analyzer coupled with a water vapor generation furnace. To evaluate the effects of water steam concentration on the carbonation process of $Mg(OH)_2$, carbonation was run under three different gas mixture concentrations, namely, (100%CO_2), (80%CO_2-10%H_2O-10%Ar) and (80%CO_2-15%H_2O-5%Ar). The total gas pressure was 1atm, and isothermal conditions of 200, 250 and 325℃ were applied for the duration of 600 min.

C. 3 Results and Discussion

The Carbonation of $Mg(OH)_2$ powders was investigated under three different steam concentrations of 0, 10 and 15%, under varying isothermal conditions. Thermodynamic stability was considered prior to any kinetic investigation, to predict the possible carbonation products. Thermodynamics stability was evaluated using Geochemists Work Bench software (Release11.0.2, 2016), which indicated that $MgCO_3$ is the only stable phase under all applied temperature and steam concentrations.

The variation of samples' mass vs. reaction time is recorded by a TGA device. The amount of mass change during the $Mg(OH)_2$ to $MgCO_3$ carbonation process (Eq. (2-12)) was considered as the upper limit of mass change (44% mass gain). On the other hand, the maximum amount of mass loss during $Mg(OH)_2$ dehydroxylation (Eq. (5-2)) was addressed as the lower mass change limit (31% mass loss). In all cases, the amount of carbonation conversion was calculated considering these upper and lower mass change limits, using lever rule, to address carbonation contribution, during a combined dehydroxylation/carbonation process. Table C-1 presents carbonation conversions achieved under varying temperature and steam concentration conditions.

Table C-1. Carbonation conversion achieved during atmospheric pressure dry carbonation of $Mg(OH)_2$, under different temperature and steam concentration conditions.

Temperature (ºC)	200			250			325		
Steam concentration (%)	0	10	15	0	10	15	0	10	15
Carbonation conversion	26	39	39	28	35	39	36	59	44

As is presented in Table C-1, carbonation conversion increases with temperature, under pure CO_2 atmosphere. In order to evaluate the possible mechanism involved in the carbonation process of $Mg(OH)_2$, dehydroxylation of $Mg(OH)_2$ is addressed under different temperature and steam concentration conditions. In all considered temperatures, $Mg(OH)_2$ will be dehydroxylated to MgO under pure CO_2 atmosphere. Referring to the mechanism suggested by Fricker et al. [19], the carbonation and dehydroxylation processes can occur simultaneously during the carbonation of $Mg(OH)_2$ [19, 20]. Although, MgO formed as a product of $Mg(OH)_2$ dehydroxylation is known as an unreactive compound, the dehydroxylation process of $Mg(OH)_2$ is suggested to enhance the carbonation process through couple dynamic mechanism [19, 20]. The observed increase in carbonation conversion, as a function of temperature in pure CO_2 conditions, can be explainedusing the so far proposed mechanisms of $Mg(OH)_2$ carbonation by Fagerlund et al. [105], saying that the dehydroxylation of $Mg(OH)_2$ results in the outward transfer of water molecules from the inner $Mg(OH)_2$ structure to the surface. So, the carbonation reaction occurs on the surface, by surficial dissolution of Mg in the formed surficial layer, and later reacts with CO_2 [105]. The formed surficial $MgCO_3$ layer acts as a diffusion barrier and prohibits further carbonation reactions. And, dehydroxylation of $Mg(OH)_2$, and the consequent outward transfer of water steam, can be referred to as enhancing factors. These produce fresh reactive carbonation surfaces through the breakage of $MgCO_3$ barrier layer. With this hypothesis, higher temperature can enhance the kinetics of $Mg(OH)_2$

carbonation under pure CO_2 atmosphere by enhancing the dehydroxylation reaction of $Mg(OH)_2$.

As the water steam concentration increases to 10%, the carbonation conversion increases dramatically, as presented in Table C-1. The enhancing effect of water steam on the carbonation of $Mg(OH)_2$ is mostly attributed to the preparation of a denser water layer to cover the reactive compounds for Mg dissolution and subsequent carbonation [105, 118]. However, the dehydroxylation process of $Mg(OH)_2$ to MgO is still an effective process through the breakage of the $MgCO_3$ barrier layer and, hence, carbonation conversion increases as a function of temperature.

Increasing the amount of water steam to 15%, cannot promote the $Mg(OH)_2$ carbonation conversion %, as presented in Table C-1. This outcome is also observed by Kerisit et al [114] through studying the dynamics of a forsterite surface in a steam-involved carbonation process. As they proposed, the thick layer of water which forms under high steam concentrations can hinder the carbonation process by limiting CO_2 access to the surface. However, in this condition, carbonation could be still promoted by increasing temperature through enhancement of $Mg(OH)_2$ dehydroxylation and breakage of surficial $MgCO_3$. But, the effect of temperature on carbonation conversion enhancement is much lower than that of 10% steam condition since, in this case (15% steam system), the availability of CO_2 on the surface is more limiting, as compared to dehydroxylation speed.

C. 4 Summary

In this research task the effect of water steam on enhancing the carbonation process of $Mg(OH)_2$ was evaluated. The effective concentration of water steam in flue gas for $Mg(OH)_2$ carbonation was estimated through TGA analysis, and the results are discussed based on previously suggested carbonation mechanisms. As the results show, availability of external water steam can promote the carbonation conversion of $Mg(OH)_2$ through formation of external water shells for Mg dissolution. On the other hand, the considerable effect of $Mg(OH)_2$ dehydroxylation on the breakage of the$MgCO_3$ diffusion barrier layer was discussed. Finally,

the suggested amount of water steam for and enhanced $Mg(OH)_2$ carbonation process was addressed to be around 10%, among the evaluated steam concentration range.